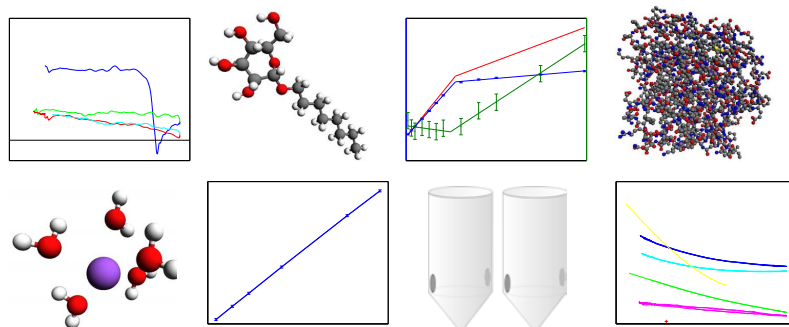


Master Thesis, s042198

Theory and application of ultrasound diagnostics of aqueous solutions

Kasper Kristensen



Supervisor:

Henrik Bruus
Department of Micro- and Nanotechnology
Technical University of Denmark

Industrial supervisor:

Thomas H. Callisen
Detergent Applications
Novozymes A/S

5 July 2010

Abstract

Ultrasonic velocimetry is an experimental technique that can be used to obtain information on various types of aqueous solutions. Since the ultrasonic velocity depends on both the density and adiabatic compressibility of the aqueous solution, ultrasonic velocimetry is often combined with densimetry to obtain information of the volumetric as well as the elastic properties of the solutes dissolved in the solution.

This thesis examines to what extent information on aqueous solutions can be obtained when ultrasonic velocimetry is applied as a stand-alone technique. In order to pursue this objective, a theoretical framework for interpreting ultrasonic velocities recorded in aqueous solutions in the limit of infinite solute dilution is presented. This framework is used to treat experimental results recorded for three different classes of aqueous solutions containing low-weight molecules, surfactants and proteins, respectively. The outcome of this treatment implies that the intermolecular interactions between solutes in aqueous solutions in general are negligible in the investigated concentration regimes but that intramolecular solute interactions are important for a correct interpretation of the ultrasonic velocity. Furthermore, it is found that the changes in ultrasonic velocity associated with the addition of solutes to water are associated to changes in both solution density and compressibility. However, when the temperature is increased, the differential ultrasonic velocities between the aqueous solutions and a water reference are found to decrease due to primarily changes in solution compressibility. For aqueous protein solutions, it is found that the differential ultrasonic velocity is primarily due to hydration. However, to account for the decrease in differential ultrasonic velocity observed for increasing temperatures for protein solutions, it is found that both hydration and intrinsic contributions are important. Moreover, experiments on Lipolase solutions imply that ultrasonic velocimetry can be used to investigate Ca^{2+} induced protein aggregation.

The experimentally recorded differential ultrasonic velocities are also attempted normalized to various parameters that scale with the size of the solutes, namely the solute molar mass, number of atoms per solute, solvent excluded surface area and solvent accessible surface area. It is found that the differential ultrasonic velocities do not scale with a single solution parameter implying that more advanced normalization procedures are required.

Resumé

Ultrasonisk velocimetri er en eksperimentel teknik, der kan bruges til at opnå information om forskellige typer af vandige opløsninger. Da ultralydshastigheden afhænger af både densitet og adiabatisk kompressibilitet af de vandige opløsninger er ultrasonisk velocimetri ofte kombineret med densimetri for at opnå information om både de volumetriske og elastiske egenskaber af de opløste substanser.

Denne afhandling undersøger hvor meget information der kan opnås om vandige opløsninger når ultrasonisk velocimetri bruges uden andre supplerende eksperimentelle teknikker. Derfor præsenteres en række teoretiske formler udledt i grænsen af uendelig fortynding af de opløste substanser. Disse formler bruges til at behandle eksperimentelle resultater målt for tre forskellige klasser af vandige opløsninger henholdsvis indeholdende lavmolekylære substanser, surfaktanter og proteiner. Det viser sig at intermolekylær vekselvirkning mellem de opløste substanser generelt kan negligeres i de undersøgte koncentrationsområder, mens intramolekylær vekselvirkning er vigtig for en korrekt fortolkning af de målte ultralydshastigheder. Derudover viser det sig at ændringer i ultralydshastigheden forekommende ved opløsning af substanser i vand kan relateres til ændringer i både opløsningens densitet og kompressibilitet. Når temperaturen stiger måles en mindre forskel mellem ultralydshastighederne i vandige opløsninger og rent vand i alle udførte forsøg. Denne mindre forskel relateres til ændring i opløsningens kompressibilitet relativt til vands kompressibilitet. For vandige proteinopløsninger er det fundet at forskelle i ultralydshastighed mellem opløsning og rent vand primært kan henføres til hydrering. Dog er det også fundet at den mindre forskel i ultralydshastighed mellem proteinopløsninger og rent vand associeret til stigende temperaturer både er på grund af hydrering og intrinsiske bidrag. Derudover viser det sig at ultrasonisk velocimetri kan bruges til at undersøge Ca^{2+} -induceret proteinaggregering.

De eksperimentelt målte forskelle i ultralydshastigheder er også forsøgt normaliseret til forskellige parametre, der skalerer med størrelsen af de opløste substanser, dvs. den molære masse af de opløste substanser, antallet af atomer pr. opløst substans, det molekulære overfladeareal samt det solvent-tilgængelige overfladeareal. Det ses at forskellene i ultralydshastighederne ikke skales med en enkelt parameter indikerende at mere avancerede normaliseringsmodeller er nødvendige.

Preface

This thesis is submitted as fulfillment of the requirements for obtaining the degree of Master of Science at the Technical University of Denmark. The content of the thesis is based on work carried out in the Theoretical Microfluidics group at the Department of Micro- and Nanotechnology (DTU Nanotech) and in the laboratories of the Detergent Applications unit at Novozymes A/S. The duration of the work was 5 months and 3 weeks in the period from January 2010 to July 2010 corresponding to a credit of 35 ECTS points.

During the course of the work, multiple persons have made skilled contributions to the thesis. First of all, I would like to thank my supervisor Henrik Bruus for being a great source of critique and advice to my work, and for helping me with several things not directly related to the project. I would also like to thank my industrial supervisor Thomas H. Callisen for helping me with numerous highly appreciated tips and tricks for the experimental work and spending a lot of time introducing me to various exciting topics of modern biophysics. Moreover, I am very thankful to Lene Bjørg Cesar for her invaluable assistance in the laboratories on Novozymes.

During most of the project period, the majority of the Theoretical Microfluidics group lived in Santa Barbara in California while I stayed in Denmark. I would like to thank Fridolin Okkels for helping me in this period with various practical issues that arises on a daily basis during the work on a master thesis. Fortunately, I also get the chance to visit Santa Barbara for a couple of weeks in May. I am very grateful for the warm hospitality shown by the emigrated part of the Theoretical Microfluidics group during my visit giving me a truly great experience in California. Furthermore, I would like to thank professor J. Thomas Gerig from the University of California, Santa Barbara for discussing the biochemical interpretations of the recorded data giving valuable inputs to the thesis.

Finally, I would like to thank my family and my girlfriend Nadia for their loving support during the project.



Kasper Kristensen
Department of Micro- and Nanotechnology
Technical University of Denmark
5 July 2010

Contents

List of figures	xiv
List of tables	xv
List of symbols	xvii
1 Introduction	1
1.1 Ultrasonic velocimetry	1
1.1.1 Ionic solvation	2
1.1.2 Surfactants	2
1.1.3 Proteins	3
1.1.4 Others	5
1.2 Objectives of the thesis	5
1.3 Outline of the thesis	6
2 Basic theory	9
2.1 Fundamental acoustic theory	9
2.1.1 Governing equations	9
2.1.2 Perturbation theory	10
2.1.3 The wave equation	11
2.1.4 The ultrasonic velocity	11
2.2 The Newton–Laplace equation	12
2.3 Ultrasonic velocimetry in ideal mixtures	12
2.4 Ultrasonic velocimetry in aqueous solutions	14
2.5 Ultrasonic absorption	16
3 Experimental setup	19
3.1 The time-harmonic solution to the wave equation	19
3.1.1 Inviscid system	19
3.1.2 Viscous system	20
3.2 The concept of acoustic resonance	21
3.3 The ResoScan System	23
3.3.1 Design	23
3.3.2 Working principle	24

3.3.3	Accuracy	25
3.3.4	Typical experimental procedure	26
4	Test experiments	29
4.1	Test experiments on Milli-Q water	29
4.1.1	Introduction to water	29
4.1.2	Relevant chemical background theory	29
4.1.3	Ultrasonic introduction	30
4.1.4	Experimental procedure	31
4.1.5	Results and discussion	31
4.1.6	Calibration of the ResoScan System	33
4.2	Compressibility of polystyrene	35
4.2.1	Experimental procedure	35
4.2.2	Results and discussion	36
4.3	Summary	38
5	Case study: Low-weight molecules	39
5.1	Relevant chemical introduction	39
5.2	Ultrasonic introduction	40
5.3	Experimental procedure	41
5.4	Results	42
5.5	Discussion	44
5.5.1	The additive assumption	44
5.5.2	Density or compressibility	44
5.5.3	Hydration	47
5.6	Summary	48
6	Case study: Surfactants	49
6.1	Relevant chemical introduction	49
6.2	Ultrasonic introduction	51
6.2.1	Mathematical model	51
6.3	Experimental procedure	55
6.4	Results	56
6.5	Discussion	58
6.5.1	The additive assumption	58
6.5.2	Density or compressibility	59
6.6	Summary	60
7	Case study: Proteins	63
7.1	Relevant chemical introduction	63
7.2	Ultrasonic introduction	65
7.2.1	Mathematical model	65
7.3	Experimental procedure	67
7.4	Results	68

7.5	Discussion	72
7.5.1	The additive assumption	72
7.5.2	Density or compressibility	73
7.5.3	Intrinsic contributions or hydration	74
7.5.4	The protein surface	75
7.5.5	The effect of adding salt to protein solutions	76
7.6	Summary	77
8	Comparison across model systems	79
8.1	Calculations	79
8.2	Results	82
8.3	Discussion	83
8.3.1	Normalization of differential ultrasonic velocities	83
8.4	Summary	84
9	Conclusion and outlook	85
9.1	Conclusion	85
9.2	Outlook	86
A	Derivation of equations	87
A.1	Governing equations	87
A.1.1	The Navier–Stokes equation	87
A.1.2	The equation of continuity	88
A.2	Ultrasonic velocimetry on aqueous solutions	88
A.2.1	The partial molar volume	88
A.2.2	The ultrasonic velocity in aqueous solutions	89
A.2.3	Multicomponent Systems	90
B	Calibration of the ResoScan System	91
B.1	300 mK per min scan rate	91
B.2	500 mK per min scan rate	93

List of Figures

1.1	Schematic overview of the experimental work conducted of this thesis	6
3.1	Sketch of a double-actuated one-dimensional acoustic slab	21
3.2	The ResoScan System	24
4.1	Ball-and-stick model of water molecule	30
4.2	Ultrasonic velocities recorded in Milli-Q water as a function of temperature	31
4.3	Comparison of data from the ResoScan System to literature data	32
4.4	Differential ultrasonic velocities for MQ water in both cavities vs. temperature	34
4.5	Outcome of correction and smoothening scheme	35
4.6	Relative differential ultrasonic velocities for polystyrene samples	37
5.1	Hydration of Na^+ and Cl^-	40
5.2	Differential ultrasonic velocity of NaCl in Milli-Q water and buffer	42
5.3	Differential ultrasonic velocities vs. temperature for low-weight molecules .	43
5.4	Density and compressibility contributions in NaCl and CaCl_2 solutions . . .	46
6.1	Ball-and-stick diagram of octyl glucoside and sodium dodecyl sulfate	50
6.2	Differential ultrasonic velocities for OG and SDS vs. concentration	56
6.3	Differential ultrasonic velocities for OG vs. temperature	58
7.1	Ball-and-stick diagram of an amino acid and Lipolase	64
7.2	Differential ultrasonic properties for varying Lipolase concentration in buffer	69
7.3	Differential ultrasonic velocities for Lipolase for varying NaCl and CaCl_2 concentrations	70
7.4	Differential ultrasonic velocities vs. temperature for Lipolase with and with- out NaCl and CaCl_2	71
7.5	First derivative of differential ultrasonic velocities vs. temperature for Lipo- lase with and without NaCl and CaCl_2	72
7.6	Density and compressibility contributions in protein solutions	74
7.7	Intrinsic and hydration contributions in proteins solutions	75
7.8	Calculation of protein surface characteristics from ultrasonic velocity	76
8.1	Definitions of solvent accessible surface and solvent excluded surface	80
8.2	Normalized relative molar increments in ultrasonic velocity	82

B.1	Calibration of temperature scan of 300 mK min^{-1} scan rate	91
B.2	Calibration of temperature scan of 500 mK min^{-1} scan rate	92

List of Tables

1.1	Overview of experimental conditions	7
6.1	Parameters used in surfactant calculations	54
6.2	Molar masses used in surfactant calculations	55
7.1	Parameters used in protein calculations	66
7.2	Densimetric and ultrasonic data for myoglobin	73
8.1	Parameters used to normalize the relative increments in ultrasonic velocity	81

List of symbols

Symbol	Description	Unit
∇	Nabla or gradient vector operator	m^{-1}
∇^2	Laplace operator	m^{-2}
\equiv	Equal to by definition	
\approx	Approximately equal to	
\sim	On the order of magnitude	
\propto	Proportional to	
$\mathcal{O}(x^n)$	Terms on the order of x^n and higher	
\times	Cross product	
\cdot	Dot product	
$\partial/\partial x$	Partial derivative with respect to x	$[x]^{-1}$
B_M	Temperature-dependent compressibility parameter	$\text{cm}^3 \text{mol}^{-1} \text{bar}^{-1} \text{\AA}^{-3}$
B_c	Compressibility contribution from charged solvent accessible surface area	$\text{cm}^3 \text{mol}^{-1} \text{bar}^{-1} \text{\AA}^{-2}$
B_n	Compressibility contribution from nonpolar solvent accessible surface area	$\text{cm}^3 \text{mol}^{-1} \text{bar}^{-1} \text{\AA}^{-2}$
B_p	Compressibility contribution from polar solvent accessible surface area	$\text{cm}^3 \text{mol}^{-1} \text{bar}^{-1} \text{\AA}^{-2}$
c	Specific concentration	mg mL^{-1} or g cm^{-3}
C	Molar concentration	mol L^{-1} or mol cm^{-3}
C_{at}	Atomic molar concentration	mol cm^{-3}
C_M	Temperature-dependent expansion factor	
C_{cp}	Volume contribution from polar and charged solvent accessible surface area	$\text{cm}^3 \text{mol}^{-1} \text{\AA}^{-2}$
C_n	Volume contribution from nonpolar solvent accessible surface area	$\text{cm}^3 \text{mol}^{-1} \text{\AA}^{-2}$
E_{tot}	Total energy of acoustic resonator	J

Continued on next page

Symbol	Description	Unit
ΔE	Energy loss per resonator oscillation cycle	J
f	Frequency	s^{-1}
f_N	Resonance frequency of the N th resonance	s^{-1}
Δf_{3dB}	Full width half maximum of resonance peak	s^{-1}
k	Complex wave number	m^{-1}
k_0	Real wave number	m^{-1}
\mathbf{k}_0	Real wave vector	m^{-1}
K_S	Adiabatic compressibility	$m^3 Pa^{-1}$
ϕK_S°	Apparent molar adiabatic compressibility	$cm^3 bar^{-1} mol^{-1}$
K_S°	Partial molar adiabatic compressibility	$cm^3 bar^{-1} mol^{-1}$
K_h	Hydration contribution to partial molar adiabatic compressibility	$cm^3 bar^{-1} mol^{-1}$
K_M	Intrinsic contribution to partial molar adiabatic compressibility	$cm^3 bar^{-1} mol^{-1}$
k_S°	Partial specific adiabatic compressibility	$cm^3 bar^{-1} g^{-1}$
m	Mass	kg
M	Molar mass	$g mol^{-1}$
n	Moles of solute	mole
N_{at}	Number of atoms per solute	
p	Pressure	Pa or bar
Q	Q-factor	
\mathbf{r}, r	Position	m
S	Entropy	$J K^{-1}$
S_c	Charged solvent accessible surface area	\AA^{-2}
S_n	Nonpolar solvent accessible surface area	\AA^{-2}
S_p	Polar solvent accessible surface area	\AA^{-2}
S_{ses}	Solvent excluded surface area	\AA^{-2}
S_{sas}	Solvent accessible surface area	\AA^{-2}
t	Time	s
T	Temperature	K or $^\circ C$
\mathbf{U}, U	Speed of sound or ultrasonic velocity	$m s^{-1}$
U_0	Ultrasonic velocity in reference sample	$m s^{-1}$
$[u]$	Relative specific increment in ultrasonic velocity	$cm^3 g^{-1}$
ΔU	Difference in ultrasonic velocity between reference and sample or between the two resonator cavities	$m s^{-1}$
$[U]$	Relative molar increment in ultrasonic velocity	$cm^3 mol^{-1}$
$[U]_{at}$	Relative atomic increment in ultrasonic velocity	$cm^3 mol^{-1}$
$[U]_{ses}$	Relative molar increment in ultrasonic velocity normalized to the solvent excluded surface area	$cm^3 mol^{-1} \text{\AA}^{-2}$
$[U]_{sas}$	Relative molar increment in ultrasonic velocity normalized to the solvent accessible surface area	$cm^3 mol^{-1} \text{\AA}^{-2}$

Continued on next page

Symbol	Description	Unit
$[U]_h$	Hydration contribution to the relative molar increment in ultrasonic velocity	$\text{cm}^3 \text{mol}^{-1}$
$[U]_M$	Intrinsic contribution to the relative molar increment in ultrasonic velocity	$\text{cm}^3 \text{mol}^{-1}$
$[U]_{\beta_S}$	Compressibility contribution to the relative molar increment in ultrasonic velocity	$\text{cm}^3 \text{mol}^{-1}$
$[U]_{\rho}$	Density contribution to the relative molar increment in ultrasonic velocity	$\text{cm}^3 \text{mol}^{-1}$
V	Volume	m^3 or cm^3
V_0	Volume of reference sample	m^3 or cm^3
ϕV	Apparent molar volume	$\text{cm}^3 \text{mol}^{-1}$
V°	Partial molar volume	$\text{cm}^3 \text{mol}^{-1}$
V_h	Hydration contribution to partial molar volume	$\text{cm}^3 \text{mol}^{-1}$
V_M	Intrinsic molar volume	$\text{cm}^3 \text{mol}^{-1}$
V_W	van der Waals volume	\AA^3
v°	Partial specific volume	$\text{m}^3 \text{g}^{-1}$
v_M	Intrinsic specific volume	$\text{m}^3 \text{g}^{-1}$
\mathbf{v}	Fluid velocity	m s^{-1}
α	Attenuation coefficient	m^{-1}
β	Ratio between compressional bulk viscosity and dynamic viscosity	
β_S	Adiabatic compressibility coefficient	Pa^{-1} or bar^{-1}
β_{S0}	Adiabatic compressibility coefficient of reference sample	Pa^{-1} or bar^{-1}
β_M	Intrinsic adiabatic compressibility coefficient	bar^{-1}
$\Delta\beta_S$	Difference in adiabatic compressibility coefficient between reference and sample	bar^{-1}
γ	Dimensionless damping parameter	
η	Dynamic viscosity	Pa s
λ	Wavelength	μm
λ_0	Real value wavelength	μm
ρ	Mass density	kg m^{-3} or g cm^{-3}
ρ_0	Mass density of reference sample	kg m^{-3} or g cm^{-3}
$\Delta\rho$	Difference in mass density between reference and sample	g cm^{-3}
ω	Angular frequency	s^{-1}

Chapter 1

Introduction

Many physical experimental techniques are known to give information about the properties of molecules dissolved in aqueous solutions. Examples of such techniques include nuclear magnetic resonance spectroscopy, dynamic light scattering, fluorescent imaging and calorimetric methods. All of these experimental techniques give information about different observables associated with the studied model systems and all have their individual strengths and weaknesses. This master thesis is primarily concerned with another example of such a physical experimental technique, namely ultrasonic velocimetry and its applicability on various types of aqueous solutions. To give the reader an introduction to the many applications of ultrasonic velocimetry on aqueous solutions, this chapter contains a short literature review on the topic in Section 1.1. This review does not give any mathematically rigid or theoretically complete introduction to ultrasonic velocimetry (such an introduction will follow in Chapter 2) nor is it meant to be comprehensive. Rather, the review is meant to give the reader a feeling of the many possible hypotheses and conclusions that may arise when applying ultrasonic velocimetry to aqueous solutions, either when using the technique as a stand-alone method or in combination with other experimental techniques, to motivate the relevance and importance of working with this technique. After this review, the chapter is rounded off by stating the objectives in Section 1.2 and outlining the contents of the thesis in Section 1.3.

1.1 Ultrasonic velocimetry

An acoustic wave is a longitudinal wave propagating through a given medium with accompanying variations in the pressure, density and velocity fields of that medium [3]. Ultrasonic waves are acoustic waves propagating with a frequency above 20 kHz. In ultrasonic velocimetry, the propagation velocity of the ultrasonic wave, called the ultrasonic velocity, is typically measured applying wave frequencies in the frequency range between 5 to 10 MHz. The ultrasonic velocity, U , in a given medium depends on the mass density, ρ , and the adiabatic compressibility, β_S , of that medium through a simple mathematical

relation called the Newton–Laplace equation

$$U = \frac{1}{\sqrt{\rho\beta_S}}. \quad (1.1)$$

The ultrasonic velocity is thus capable of providing volumetric and elastic information on solutes in aqueous solution [16]. This information can be used to gain important information about the microscopic structure of solutes dissolved in aqueous solutions and the water hydrating the solutes [16, 53]. Ultrasonic velocimetry on aqueous solutions is often combined with densimetry to acquire exact values of both the mass density and the adiabatic compressibility of the solution allowing for a more complete volumetric and elastic characterization of the solution and the dissolved solutes. However, ultrasonic velocimetry on aqueous solutions is also used frequently together with a wealth of other experimental techniques potentially allowing for an even more complete characterization of the solution and the dissolved solutes.

Comparing to other experimental methods, a large number of advantages are associated with ultrasonic velocimetry. Thus the technique is capable of conducting fast and exact measurements of relative accuracy $\sim 10^{-5}$ yielding a typical minimal detectable solute concentration on the order of 0.1 mg mL^{-1} for proteins and even smaller for other types of solutes. The technique is also capable of measuring up to high concentrations and conducting the measurements in a wide temperature range. Furthermore, ultrasonic velocimetry is nondestructive, does not require any kind of chemical modifications of the studied samples, and can be used to study samples that are optically opaque [46]. Finally, only small samples are required for ultrasonic velocimetry making it a feasible technique to investigate biological samples [16].

1.1.1 Ionic solvation

Understanding the mechanisms underlying ionic solvation in water is an important topic in modern chemistry and physics. Several investigators have thus treated this problem using a number of different experimental techniques, including ultrasonic velocimetry. Onori *et al.* used ultrasonic velocimetry and densimetry to investigate the hydration of ions in aqueous sodium chloride solutions [47], and a number of other aqueous alkali halide solutions [48]. Making a number of assumptions about the properties of hydrated ions, they obtained estimates for the hydration numbers of the salts and quantitative information about the volumetric properties of the hydrated ions. Ultrasonic velocimetry combined with several other experimental techniques was also employed recently in a number of papers by Afanasiev *et al.* to investigate ionic hydration [2]. Although their approach to the problem is much more mathematically rigid and complex than the approach by Onori *et al.*, no new conclusions on the physics of ion solvation however seem to appear from their study.

1.1.2 Surfactants

Ultrasonic velocimetry has also been used to examine amphiphilic compounds in aqueous solution. Ultrasonic velocimetry can hence be used as a stand-alone technique for de-

termining critical concentrations of self-assembly phenomena associated with these compounds, i.e. the critical micelle concentration for surfactants in solution may be associated with a sharp inflection point in the ultrasonic velocity. Ultrasonic velocimetry was used by Junquera *et al.* [32] to determine the dependence of the critical micelle concentration of sodium dodecyl sulfate on temperature, and of Durackova *et al.* [23] to determine the dependence of the critical micelle concentration of sodium dodecyl sulfate and dodecylbenzene sulfonic acid sodium salt on temperature and electrolyte cosolvent concentration.

Ultrasonic velocimetry has also been combined with densimetric techniques to obtain quantitative information about the volumetric properties of surfactants in solution. Using results from these two experimental techniques and a relatively simple physical model, Galán *et al.* [27] were capable of obtaining information about the volumetric properties of tetradecylmethylammonium nitrate in solution in monomer and micelle state. As previously mentioned, quantitative determination of the volumetric and elastic properties of solutes may help reveal important knowledge on their microscopic characteristics when compared to the volumetric and elastic properties of other well-known substances. Such a direct comparison was done in a study by Kudryashov *et al.* [36] implying that the structure of the hydrophobic core of alkyltrimethylammonium bromide micelles is similar to that of bilayer lipid membranes and pure hydrocarbon liquids implying that the microscopic structure of all of these hydrocarbon compounds resemble each other.

Ultrasonic velocimetry can of course also be combined with a number of other experimental techniques to obtain information about more complex problems associated with aqueous solutions containing amphiphilic compounds. Castro *et al.* [13] conducted a study on the complex cosolvent effects of ethanol on the micellization of two types of polyoxyethylene block copolymers. In this study, ultrasonic velocimetry was combined with surface tension methods, dynamic and static light scattering, transmission electron microscopy, fluorescence techniques and densimetry. Ultrasonic velocimetry and densimetry was used to show that the adiabatic compressibility increased as the ethanol concentration increased strengthening the conclusion of the study that the addition of ethanol causes a swelling of the hydrophobic moiety of the polyoxyethylene block copolymers micelle structures.

1.1.3 Proteins

Protein science has drawn the attention of a vast number of scientists with many different backgrounds. A large number of experimental techniques have been used to elucidate the mechanisms of protein function and stability, and ultrasonic velocimetry is no exception. For example, ultrasonic velocimetry can be used as a stand-alone technique for considering enzyme activity [69]. However it is more common to determine volumetric and elastic properties of proteins in aqueous solution using ultrasonic velocimetry combined with densimetry as this may reveal important information about the dynamics and function of proteins, e.g. the binding of ligands to enzymes may cause an induced fit mechanism causing a more tight internal packing of the atoms in the enzyme interior which is reflected by a smaller value of the adiabatic compressibility [29].

Ultrasonic velocimetry, together with densimetry, has especially been used to study protein denaturation occurring due to variations in e.g. temperature, pressure, pH or

other experimental conditions. Taulier and Chalikian published a review [61] identifying what appears to be general trends in the volumetric and elastic observables associated with protein denaturation establishing a generic framework for interpreting volumetric and elastic data of protein denaturation. Taulier and Chalikian have also been involved in a number of case studies on protein denaturation applying ultrasonic velocimetry and densimetry together with a number of other experimental techniques. Using ultrasonic velocimetry, densimetry, fluorescence anisotropy and circular dichroism, they have thus attempted to characterize the pH-dependent conformational transitions in β -lactoglobulin [60]. Ultrasonic velocimetry and densimetry contributes to this characterization by allowing estimates of changes in hydration and intrinsic packing of β -lactoglobulin during these pH-dependent conformational transitions. Another specific case study conducted by Taulier *et al.* concerns conformational transitions of apomyoglobin [62]. In this study, the authors considered a number of conformational changes induced by NaCl, NaCTA and altered pH. By applying a simple physical model taken from the above-mentioned review [61], the authors were then capable of estimating the degree of unfolding for each denatured conformation.

A number of other authors have also treated protein denaturation using ultrasonic velocimetry combined with other experimental techniques. El Kadi *et al.* considered the unfolding and refolding of bovine serum albumin as a function of pH [24]. This study applied densimetry and circular dichroism as additional remedies to ultrasonic velocimetry. It was found that the compressibility changes associated with a decreasing pH could be associated with the physiological function of serum albumin as a transporter for various types of molecules like metabolites or hormones. A study by Sasahara *et al.* treated the effect of guanidinium chloride, a well-known protein denaturant, on hen egg white lysozyme using ultrasonic velocimetry, densimetry, circular dichroism and UV spectroscopy [54]. Analysis of the recorded data implied that lysozyme in this case denatured to a partially unfolded conformation.

Ultrasonic velocity has also been used to characterize protein aggregation. A recent study by Ochenduszko and Buckin thus considered the heat-induced aggregation of β -lactoglobulin using ultrasonic spectroscopy [46]. In ultrasonic spectroscopy, the ultrasonic velocity and the ultrasonic absorption is measured for varying wave frequency. This approach was capable of capturing the aggregation process of β -lactoglobulin as well as denaturation preceding the aggregation for varying pH. Ultrasonic spectroscopy has also been used by Corredig *et al.* [21] to study aggregation of whey protein isolate again both mapping thermally induced aggregation as well as preceding protein denaturation. In a study by Wang *et al.*, irreversible aggregation of α -lactalbumin was studied by ultrasonic velocimetry, reverse phase HPLC and differential scanning calorimetry [72]. The authors used ultrasonic velocimetry to determine the degree of irreversible aggregation of α -lactalbumin and showed a good correlation to the results recorded using reverse phase HPLC and differential scanning calorimetry. Finally, ultrasound measurements have been used to shed light on amyloidogenesis in a number of studies by Smirnovas *et al.* [57, 58, 59]. Amyloidogenesis is a type of protein aggregation implicated in a number of neurodegenerative diseases such as Alzheimers disease or Parkinsons disease. Ultrasonic velocimetry and densimetry was used in combination with a number of other experimental techniques

to yield information about the protein dynamics of the aggregation process by determining the changes in the volumetric and elastic variables occurring during the aggregation processes.

1.1.4 Others

Ultrasonic velocimetry has also been used to obtain information about other types of aqueous model systems, e.g. systems containing nucleic acids. Hence in a number of studies, Buckin applied ultrasonic velocimetry and densimetry to examine the properties of hydration of nucleic bases [9]. Another more recent study by Han and Chalikian used ultrasonic velocimetry, densimetry and circular dichroism to study the effects of ethidium bromide binding to DNA and RNA [30]. Their study showed altered hydration properties of DNA and RNA as a results of the ligand binding.

Finally, two studies by Taulier and Chalikian probed the interaction between 1-adamantanecarboxylic acid and β -cyclodextrin [63] and the interaction between 1-adamantanecarboxylic acid and γ -cyclodextrin [64] using ultrasonic velocimetry and densimetry. Using a one-to-one stoichiometric model to represent the chemical binding the authors hypothesized that the interaction between 1-adamantanecarboxylic acid and β -cyclodextrin is due to interaction between hydrophobic residues whereas interaction between 1-adamantanecarboxylic acid and γ -cyclodextrin causes an intermolecular void space.

1.2 Objectives of the thesis

It should now be clear to the reader that ultrasonic velocimetry has been used to study a wide number of aqueous model systems resulting in multiple interesting results and hypotheses. It is also clear that the majority of the information on aqueous solutions obtained by ultrasonic velocimetry is obtained in combination with other experimental techniques, especially densimetric techniques. The laboratories of the industrial collaborator to this thesis, Novozymes, contain experimental equipment capable of accurately measuring the ultrasonic velocity and ultrasonic absorption but do not contain densimetric equipment. This motivates the main objective of this thesis. Hence the main objective is to explore the possibilities of using the ultrasound equipment on Novozymes, named the ResoScan System, as stand-alone experimental equipment for obtaining important information on various types of aqueous model systems with special emphasis put on the use of ultrasonic velocimetry as a stand-alone method for acquiring this information. Thus although the ultrasonic absorption also can give important information, it is in this thesis only treated as a supplementary quantity to the ultrasonic velocities.

The objective of the thesis is pursued through a combined experimental and theoretical approach to three case studies on different aqueous model systems containing solutes ranging from simple salt, over surfactants, to complex protein structures. The model systems are chosen so that they are relevant to the purposes of the Detergent Applications unit on Novozymes. The aim of the experimental work on the three case studies is to build the practical hands-on experimental experience needed for Novozymes to use the ResoScan System in future work as well as to record data to be used in the theoretical

work. The aim of the theoretical work on the three case studies is to discuss the possible extent of the physical and chemical interpretation of the recorded ultrasonic data as well as to test the validity of various simplifying assumptions that can be used to ease this interpretation.

1.3 Outline of the thesis

This section outlines the contents of the thesis. However, before presenting the overview of the contents of the individual chapters of the thesis, an overview of the conducted experimental work is given. To understand this overview, the reader should know that the ResoScan System contains two ultrasonic resonator cells capable of measuring the ultrasonic properties of samples injected into each of these cells. Each experiment conducted using the ResoScan System thus contains information on the absolute ultrasonic properties of the two samples as well as information on the relative difference between the two samples. This approach is advantageous as relative differences between samples are measured more accurately than absolute quantities, i.e. the approach allows for an exact characterization of solutes added to an aqueous solvent. A schematic overview of the experimental work of the thesis is given in Fig. 1.1. The highlighted boxes represent the model systems used in this thesis and the lines between these boxes indicate that the relative difference between the two model systems has been examined. The conditions under

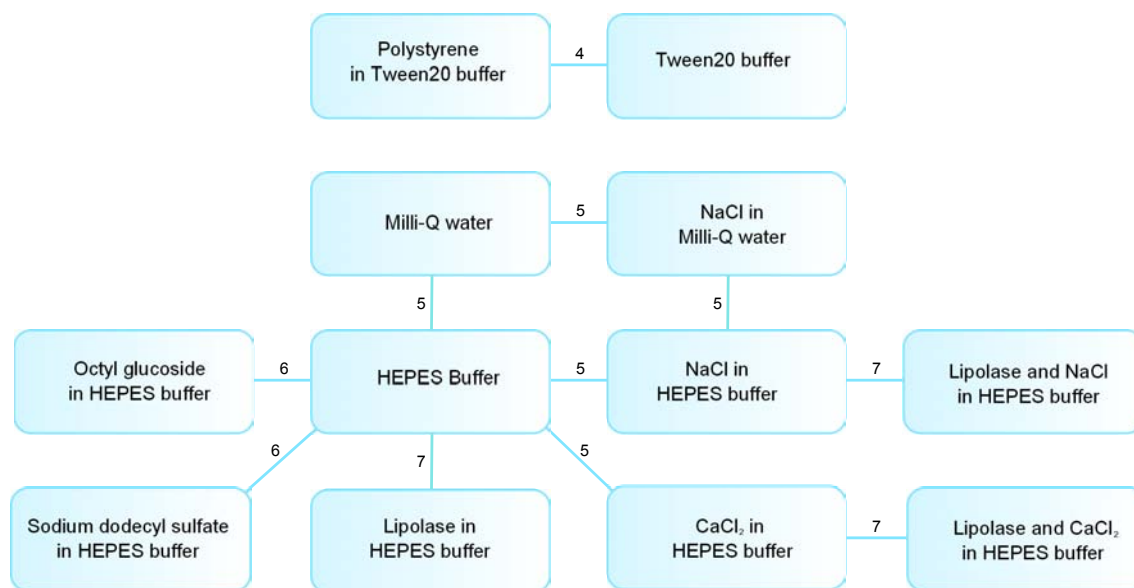


Figure 1.1: Schematic overview of the experimental work conducted in this thesis. The boxes represent the model systems used in the thesis. Lines between boxes indicate that the relative differences between these two model systems have been investigated. The numbers at each line indicate the chapter presenting the results of the experiments.

which the experiments have been conducted are outlined in Table 1.1. Hence the various

classes of aqueous solutions are investigated systematically both varying temperature and solute concentration. Fig. 1.1 and Table 1.1 are now used in the following presentation of

Cell 1	Cell 2	T [°C]	c_a [mg mL ⁻¹]	c_b [mg mL ⁻¹]
Milli-Q water	Milli-Q water	5 – 85		
Tween20 buffer	Polystyrene in Tween20 buffer	25	0 – 10	
Milli-Q water	NaCl in Milli-Q water	5 – 85 25	2.34 0 – 5.84	
Milli-Q water	HEPES buffer	5-85		
HEPES buffer	NaCl in HEPES buffer	5 – 85	3.51	
NaCl in Milli-Q water	NaCl in HEPES buffer	5 – 85 25	2.34 0-5.84	
HEPES buffer	CaCl ₂ in HEPES buffer	5 – 85	6.66	
HEPES buffer	OG in HEPES buffer	5 – 85 5 – 85 25	3.51 29.24 0 – 29.24	
HEPES buffer	SDS in HEPES buffer	25	0 – 7.21	
HEPES buffer	Lipolase in HEPES buffer	25 5 – 85	0 – 1.90 1.78	
NaCl in HEPES buffer	NaCl and Lipolase in HEPES buffer	25 5 – 85	0 – 3.51 3.51	1.90 – 1.26* 1.26
CaCl ₂ in HEPES buffer	CaCl ₂ and Lipolase in HEPES buffer	25 5 – 85	0 – 5.46 5.46	1.90 – 1.28* 1.28

Table 1.1: Overview of the conditions under which the experimental work of the thesis have been performed. All concentrations are recalculated to specific concentrations given in units of mg mL⁻¹ to make them directly comparable. c_a represents the specific concentration in cases where only one molecular compound is dissolved while c_b represents the specific concentration of Lipolase in the case of two dissolved molecular compounds. OG and SDS are short for the two types of surfactants octyl glucoside and sodium dodecyl sulfate, respectively. *These variations in these concentrations happen since the addition of salt into these samples causes a dilution of the Lipolase samples.

the contents of the individual chapters of the thesis:

Chapter 2 introduces the theoretical framework underlying ultrasonic velocimetry. Basic acoustic theory for propagation of sound waves in fluids is presented and the fundamental Newton-Laplace relation for the ultrasonic velocity in a homogenous medium is derived. Theory on the effects affecting the ultrasonic velocity in both ideal and non-ideal solutions is presented. An introduction to ultrasonic absorption is also given at the end of the chapter.

Chapters 3 and 4 is concerned with the experimental setup of the thesis, namely the ResoScan System. Hence an introduction to the principles of acoustic resonators is given and the specifications of the ResoScan System are discussed. The ResoScan System is then tested and calibrated using pure Milli-Q water, see Table 1.1. Chapter 4 is rounded off by discussing experiments attempting to calculate the adiabatic compressibility of polystyrene microbeads, see Fig. 1.1 and Table 1.1.

Chapters 5, 6 and 7 comprise the collection of case studies on the applicability of the ResoScan System, and especially the recorded ultrasonic velocities, to characterize three different classes of aqueous solutions containing low-weight molecules, surfactants and proteins, respectively, see Fig. 1.1 and Table 1.1. The composition of all of the three chapters is similar to provide a systematic introduction to this applicability. Thus all of the chapters is commenced with an introduction to the relevant chemical background theory of the model systems under investigation. This background theory is then used to discuss the molecular contributions that influence the ultrasonic velocity of aqueous solutions. In Chapters 6 and 7 this discussion is conducted through mathematical models. Next, the procedure of the experimental work is outlined and the results of this work are presented. Finally, the experimental results are discussed to elucidate important topics associated with the applicability of ultrasonic velocimetry to characterize the aqueous solutions, i.e. assumptions permitted in the treatment of the various types of aqueous solutions are identified, and the physical and chemical interpretation that is possible based on the ultrasonic velocity alone is discussed.

Chapter 8 compares the recorded ultrasonic velocities across the different model systems used in the thesis. To allow for a direct comparison of the various molecular effects playing a role in the different model systems, ultrasonic velocities are normalized to a number of parameters including the solute molar mass, number of atoms per solute, solute solvent accessible surface area and solute solvent excluded surface area. The outcome of this normalization procedure is discussed

Chapter 9 concludes the thesis and outline the scope of future work on this subject.

The figures in this thesis are produced using MATLAB and two open source programs, namely Inkscape [74] and Avogadro [73].

Chapter 2

Basic theory

In order to conduct a thorough analysis on the applicability of the ResoScan System, and especially ultrasonic velocimetry, as a stand-alone technique for characterizing aqueous solutions, it is necessary to have a sound theoretical framework for the interpretation of the recorded ultrasonic data. This chapter is meant to present such a framework.

2.1 Fundamental acoustic theory

This first section is primarily based on the master theses by Barnkob [3] and Skafte-Pedersen [56].

2.1.1 Governing equations

Fundamental acoustic theory is based on three governing equations. This section introduces these equations assuming that thermal effects can be neglected [3, 56]. Note that the three governing equations are concerned with continuous and homogenous fluids. Hence the theoretical framework derived for ultrasonic velocimetry in this chapter based on the governing equations is only applicable to cases where the considered sample can be treated as continuous and homogenous.

The first of the governing equations to be presented is the Navier–Stokes equation. The Navier–Stokes equation is found in a number of different formulations and emerges when applying Newton’s second law to a particle comoving with an ambient fluid flow [37]. This thesis will apply a formulation that assumes that the considered fluid is Newtonian and compressible and that gravity can be neglected

$$\rho \left(\frac{\partial \mathbf{v}}{\partial t} + (\mathbf{v} \cdot \nabla) \mathbf{v} \right) = -\nabla p + \eta \nabla^2 \mathbf{v} + \beta \eta \nabla (\nabla \cdot \mathbf{v}), \quad (2.1)$$

where $\rho = \rho(\mathbf{r}, t)$ is the density field of the fluid, $\mathbf{v} = \mathbf{v}(\mathbf{r}, t)$ is the velocity field of the fluid, $p = p(\mathbf{r}, t)$ is the pressure field of the fluid, η is the dynamic viscosity of the fluid and β is the ratio between the compressional bulk viscosity and the dynamic viscosity [3]. Since the local acceleration $\partial \mathbf{v} / \partial t$ is dominant for rapidly varying velocity fields and the advective

acceleration $(\mathbf{v} \cdot \nabla)\mathbf{v}$ is dominant for velocity fields with strong spatial variations [37], the advective term can be neglected in the Navier–Stokes equation in the case of acoustic applications. The Navier–Stokes equation then reduces to

$$\rho \frac{\partial \mathbf{v}}{\partial t} = -\nabla p + \eta \nabla^2 \mathbf{v} + \beta \eta \nabla(\nabla \cdot \mathbf{v}). \quad (2.2)$$

The second governing equation is the equation of continuity. This equation describes the condition for conservation of mass and is given by [37]

$$\frac{\partial \rho}{\partial t} + \nabla \cdot (\rho \mathbf{v}) = 0. \quad (2.3)$$

The final governing equation needed to present fundamental acoustic theory is a thermodynamic equation of state relating the pressure to the density. Such an equation is for example well-known in the case of an ideal fluid. In this thesis it is written on a general form given by

$$p = p(\rho). \quad (2.4)$$

A full derivation of the governing equations of acoustics is given in Appendix A.

2.1.2 Perturbation theory

Since the variations in pressure, density and velocity fields accompanying the propagation of an acoustic wave only entail small perturbations of the equilibrium state, the propagation of acoustic waves in a continuous fluid can be understood by first-order perturbation theory [3, 56]. Hence the pressure, density and velocity fields are written as first-order perturbation expansions

$$p = p_0 + p_1, \quad (2.5a)$$

$$\rho = \rho_0 + \rho_1, \quad (2.5b)$$

$$\mathbf{v} = \mathbf{v}_0 + \mathbf{v}_1, \quad (2.5c)$$

where p_0 , ρ_0 and \mathbf{v}_0 represent the fields of a fluid at rest and p_1 , ρ_1 and \mathbf{v}_1 represent the first-order perturbations including the relevant perturbation parameter. For a fluid at rest p_0 and ρ_0 are constant and $\mathbf{v}_0 = \mathbf{0}$.

The thermodynamic equation of state can be used to find a relation between p_1 and ρ_1 . Hence conducting a first order expansion of Eq. (2.4) around $p_0 = p(\rho_0)$ yields

$$p = p_0 + \left(\frac{\partial p}{\partial \rho} \right)_S \rho_1, \quad (2.6)$$

so that

$$p_1 = \left(\frac{\partial p}{\partial \rho} \right)_S \rho_1. \quad (2.7)$$

Note that the derivative is taken to be isentropic since the variations in pressure, density and velocity accompanying the propagation of an acoustic wave are so rapid that a negligible amount of heat is exchanged internally in the medium.

2.1.3 The wave equation

The governing equations and the first-order perturbation equations presented in the above can be used to derive the acoustic wave equation. Consider first the case of a fluid with zero viscosity. Inserting the first-order perturbation equations, given by Eq. (2.5), into the governing equations, given by Eqs. (2.2), (2.3) and (2.4), neglecting the viscous terms in Eq. (2.2) and using Eq. (2.7) and the fact that the spatial and temporal derivatives of p_0 and ρ_0 vanishes yield the first-order equations

$$\rho_0 \frac{\partial \mathbf{v}_1}{\partial t} = - \left(\frac{\partial p}{\partial \rho} \right)_S \nabla \rho_1, \quad (2.8a)$$

$$\frac{\partial \rho_1}{\partial t} = -\rho_0 \nabla \cdot \mathbf{v}_1. \quad (2.8b)$$

Taking the divergence of Eq. (2.8a) and the temporal derivative of Eq. (2.8b) and combining the two resulting equations yields the acoustic wave equation for the density

$$\frac{\partial^2 \rho_1}{\partial t^2} = \left(\frac{\partial p}{\partial \rho} \right)_S \nabla^2 \rho_1. \quad (2.9)$$

This equation can also be written for pressure using Eq. (2.7)

$$\frac{\partial^2 p_1}{\partial t^2} = \left(\frac{\partial p}{\partial \rho} \right)_S \nabla^2 p_1. \quad (2.10)$$

A wave equation can also be derived for a fluid with non-zero viscosity. Using an approach similar to the derivation of the inviscid wave equation for the pressure yields the viscous wave equation for the pressure [3]

$$\frac{\partial^2 p_1}{\partial t^2} = \left(\frac{\partial p}{\partial \rho} \right)_S \nabla^2 p_1 + \frac{\eta [1 + \beta]}{\rho_0} \nabla^2 \left(\frac{\partial p_1}{\partial t} \right), \quad (2.11)$$

where the new term compared to the inviscid wave equation appears due to viscosity.

2.1.4 The ultrasonic velocity

To find an expression for the speed of sound consider an acoustic pressure wave propagating with velocity \mathbf{U}

$$p_1 = p_1(\mathbf{r} - \mathbf{U}t). \quad (2.12)$$

Inserting this form of the pressure into the inviscid pressure wave equation, given by Eq. (2.10), and writing out the time derivative on the left hand side and the gradient on the right hand side then yields

$$|\mathbf{U}| = U = \sqrt{\left(\frac{\partial p}{\partial \rho} \right)_S}. \quad (2.13)$$

Hence a relation for speed of sound is obtained. This relation is also valid in the ultrasonic frequency regime [66]. Note that even though Eq. (2.13) was derived based on the assumption that the wave propagates through an inviscid medium, the relation can also be applied to aqueous systems as the effect of the viscosity is negligible.

2.2 The Newton–Laplace equation

As mentioned previously, the Newton–Laplace equation is the fundamental equation of ultrasonic velocimetry. To derive the Newton–Laplace equation consider the definition of the adiabatic compressibility coefficient [7]

$$\beta_S = -\frac{1}{V} \left(\frac{\partial V}{\partial p} \right)_S, \quad (2.14)$$

where V represents a volume. The volume can be replaced by the density using the chain rule and the fact that $V \propto \rho^{-1}$ [7]

$$\beta_S = \frac{1}{\rho} \left(\frac{\partial \rho}{\partial p} \right)_S. \quad (2.15)$$

Combining this expression with the expression for the ultrasonic velocity in Eq. (2.13) and rearranging then yields the Newton–Laplace equation

$$U = \frac{1}{\sqrt{\rho\beta_S}}. \quad (2.16)$$

The Newton–Laplace equation can be used to interpret ultrasonic velocities recorded in various types of chemical mixtures as long as the mixtures can be described as homogeneous and continuous media. In order for this to be true the wavelength of the ultrasonic wave has to be much longer than the characteristic molecular length scales of the mixture. In aqueous specimens, the ultrasonic velocity at room temperature is approximately 1500 m s^{-1} . Since the ultrasonic frequencies, f , applied in this thesis is approximately 7.8 MHz, the wavelength is approximately $\lambda = Uf^{-1} \approx 200 \text{ }\mu\text{m}$ causing ultrasonic velocimetry to be applicable to virtually all types of aqueous solutions.

2.3 Ultrasonic velocimetry in ideal mixtures

This section considers the results of applying the Newton–Laplace equation to the simple case of an ideal mixture. An ideal mixture is a chemical mixture where there is no interaction between the substances in the mixture. An adequate theoretical description of the recorded ultrasonic velocities of an ideal chemical mixture can thus be attained solely considering the intrinsic properties of the individual components of the mixture. Note that the theory presented in this section neglects a number of effects e.g. related to viscosity, thermal effects and acoustic scattering [7]. This section is mainly based on a text by Bruus [7].

Consider an ideal mixture where the two components of the mixture are denoted by subscript 0 and 1. The density of the mixture can be found using that the masses and volumes of an ideal mixture are additive. Hence the density of an ideal mixture consisting of the two components with masses m_0 and m_1 and volumes V_0 and V_1 can be written as

$$\rho_{\text{mix}} = \frac{m_0 + m_1}{V_0 + V_1}, \quad (2.17)$$

Introducing the volume fraction $x = V_1/V_{\text{mix}}$ the equation can be rewritten to

$$\rho_{\text{mix}} = (1 - x)\rho_0 + x\rho_1, \quad (2.18)$$

where ρ_0 and ρ_1 are the densities of the individual components of the mixture.

A similar expression can be obtained for the adiabatic compressibility coefficient of the mixture. Consider the definition of the adiabatic compressibility coefficient given by Eq. (2.14) applied on the entire homogenous mixture

$$\left(\frac{\partial V_{\text{mix}}}{\partial p}\right)_S = -V_{\text{mix}}\beta_{S\text{mix}}. \quad (2.19)$$

The definition of the adiabatic compressibility coefficient can also be applied on each of the two components of the mixture

$$\left(\frac{\partial V_{\text{mix}}}{\partial p}\right)_S = \left(\frac{\partial(V_0 + V_1)}{\partial p}\right)_S = -(V_0\beta_{S0} + V_1\beta_{S1}). \quad (2.20)$$

Combining Eq. (2.19) and Eq. (2.20) and dividing by V_{mix} , the following expression is found for the adiabatic compressibility coefficient

$$\beta_{S\text{mix}} = (1 - x)\beta_{S0} + x\beta_{S1}. \quad (2.21)$$

An expression for the ultrasonic velocity in the ideal binary mixture is then found by inserting Eq. (2.18) and Eq. (2.21) in Eq. (2.16)

$$U_{\text{mix}} = \left([(1 - x)\rho_0 + x\rho_1] [(1 - x)\beta_{S0} + x\beta_{S1}] \right)^{-\frac{1}{2}}. \quad (2.22)$$

Since the experimental equipment of the thesis is capable of measuring differences between a sample and a reference, it would be nice to also have an equation that can be used to calculate such differences. Consider the case of a reference consisting of material 0 with ultrasonic velocity U_0 and a sample where a given amount of the material 1 is added to material 0 with ultrasonic velocity U_{mix} . In this case, equation Eq. (2.22) can be rewritten to

$$\frac{\Delta U}{U_0} = \frac{U_{\text{mix}} - U_0}{U_0} = \left([1 + (\tilde{\rho} - 1)x] [1 + (\tilde{\beta}_S - 1)x] \right)^{-\frac{1}{2}} - 1, \quad (2.23)$$

where $\tilde{\rho} = \rho_1/\rho_0$ and $\tilde{\beta}_S = \beta_{S1}/\beta_{S0}$ and where the left hand side of Eq. (2.23) represents the relative increment in ultrasonic velocity between the reference and the sample.

The assumption of an ideal mixture may be valid in particle suspensions where the surface-to-volume ratio of the particles is high leaving the effect of the interaction between the particles and the solvent to become negligible. Thus the theory just presented will be applied in Section 4.2 to show how the compressibility of suspended polystyrene microbeads in water in principle may be calculated. However, the assumption of no solute-solvent interaction is not valid in aqueous solutions. It is hence also necessary to introduce a theoretical formalism to deal with the case of aqueous solutions.

2.4 Ultrasonic velocimetry in aqueous solutions

The theory presented in this section is the theory used in contemporary articles on ultrasonic velocimetry on aqueous solutions. This theory differs from the theory just presented on ideal mixtures since it is developed in the case of infinite solute dilution and since it relates the difference between the ultrasonic velocities of an aqueous solution and a relevant reference to the volume and elastic properties of the dissolved solutes rather than to the intrinsic material parameters of the components of the mixture.

In physical chemistry, the volume of solutes dissolved in aqueous solution is typically expressed via the apparent molar volume, ϕV , or partial molar volume, V° . The apparent molar volume is the change of solution volume per mole of added solute given by

$$\phi V = \frac{V - V_0}{n}, \quad (2.24)$$

where V is the volume of a sample including n moles of solute and V_0 is the volume of a reference sample not including any solute. The partial molar volume is the rate of change of sample volume with respect to the number of moles of solute added and is given by

$$V^\circ = \frac{\partial V}{\partial n}. \quad (2.25)$$

Since the theory presented in this section considers the aqueous solutions in the limit of infinite solute dilution, the apparent molar volume and partial molar volume are the same. For this reason, the volume of a solute dissolved in aqueous solution will be described by its partial molar volume in the majority of this report. The partial molar volume is in the limit of infinite dilution calculated from the density of the aqueous solution by

$$V^\circ = \frac{M}{\rho_0} - \frac{\rho - \rho_0}{\rho_0 C}, \quad (2.26)$$

where M is the molar mass, ρ is the mass density of the sample with molar solute concentration C and ρ_0 is the mass density of a reference not containing any solute.

The elastic properties of a sample is often described by the adiabatic compressibility, K_S , defined by

$$K_S \equiv \beta_S V. \quad (2.27)$$

The elastic properties of a solute is then, in the same manner as for the volume, described by its partial molar derivative

$$K_S^\circ = \frac{\partial K_S}{\partial n}. \quad (2.28)$$

The partial molar volume and partial molar adiabatic compressibility of a solute in infinite dilution can be related to the difference in ultrasonic velocity between a sample containing the solute in infinite dilution and a relevant reference not containing any solute. In order to do this, the first step is to differentiate the Newton–Laplace equation [53]

$$\frac{\Delta U}{U_0} = -\frac{\Delta \beta_S}{2\beta_{S0}} - \frac{\Delta \rho}{2\rho_0}, \quad (2.29)$$

where the $\Delta U = U - U_0$, $\Delta\beta_S = \beta_S - \beta_{S0}$ and $\Delta\rho = \rho - \rho_0$, where U_0 , β_{S0} and ρ_0 are the ultrasonic velocity, adiabatic compressibility coefficient and mass density of the reference only comprising solvent and U , β_S and ρ are the ultrasonic velocity, adiabatic compressibility coefficient and mass density of the sample comprising infinitely diluted solute in solvent. Note that differences in ultrasonic velocity, adiabatic compressibility coefficient and density throughout the entire thesis always represent the value of a given sample subtracted the value of a relevant reference sample. Note furthermore that differences in ultrasonic velocity often are referred to as differential ultrasonic velocity. The second step is to insert the partial molar volume and partial molar adiabatic compressibility in Eq. (2.29) to obtain [61].

$$\frac{\Delta U}{U_0} = \left(-\frac{K_S^\circ}{2\beta_{S0}} + V^\circ - \frac{M}{2\rho_0} \right) C. \quad (2.30)$$

Note that the this equation could equally well be derived in the case of partial specific volumes and partial specific adiabatic compressibilities, i.e. where rate of change of the relevant solution parameters is treated with respect to the added mass of the solute instead of the added number of moles of the solute. Such an approach may e.g. be convenient in the case of proteins since they span a wide range of masses.

Ultrasonic velocities recorded in aqueous solutions is typically interpreted in terms of two contributions, namely intrinsic contributions and hydration [16, 53]. Hence the partial molar volume is written as

$$V^\circ = V_M + V_h, \quad (2.31)$$

where V_M is the contribution from intrinsic effects and V_h is the contribution from hydration effects. The partial molar adiabatic compressibility is written as

$$K_S^\circ = K_M + K_h, \quad (2.32)$$

where K_M is the contribution from intrinsic effects and K_h is the contribution from hydration effects. The intrinsic effects originate, as in the case of the ideal mixtures, from the properties of the solute itself. It primarily depends on the atomic packing of the solute and the number of internal voids and cavities. The hydration effect originates from the interaction between the solute and aqueous solvent causing a rearrangement of the structure of the water surrounding the solute, i.e. the concept of hydration refers to solvation of molecular compounds in an aqueous solvent.

Another molecular effect is also frequently mentioned to have an effect on the measured ultrasonic velocities, namely chemical relaxations. Chemical relaxations happens when transitions occurs between different excited states or between excited states and the ground state of the sample under investigation. These transitions could be related to proton transfer, ionization/deionization, and conformational fluctuations between various isomeric structures. Knowing the absorption, σ , due to a specific relaxation process the relative increment in sound velocity due to that relaxation process can be calculated from [52]

$$\frac{U_\infty - U}{U} = \frac{\sigma\lambda}{2\pi} \frac{1}{\omega\tau}, \quad (2.33)$$

where U_∞ is the speed of sound at infinite frequency, U is the speed of sound measured at angular frequency ω , λ is the wavelength of sound and τ is the characteristic relaxation time that can be found using the rate constant for forward and reverse reactions in the relaxation reaction. Hence, if one had exact information about all relevant relaxation reactions, it would in principle be possible to identify the magnitude of the relaxation compressibility contribution. However, estimating the relaxation contribution for a specific model system is a complicated process and beyond the scope of this thesis. Thus this thesis ignores the relaxation contribution to the ultrasonic velocity even though for proteins investigated by acoustics in the ultrasonic frequency range, the change in ultrasonic velocity due to the relaxation contribution may in some cases correspond to a change of 10 % of the total partial specific adiabatic compressibility [51]. Note that relaxation also is neglected in most contemporary studies applying ultrasonic velocimetry to aqueous solutions.

A number of other molecular effects are also known to affect the ultrasonic velocity when a solute is added. These effects include visco-inertial, thermal, relaxation and ideal contributions. However, the importance of all of these effects are also thought to be very small, and hence they are also ignored in this thesis [46].

The theory just presented treats the case of one solute added to a solvent. However, it may also be necessary to have a formalism to treat the case of multiple components affecting the ultrasonic velocity in an aqueous solution. An equation to treat the case of multicomponent systems in the limit of infinite dilution is given by

$$\frac{\Delta U}{U_0} = \sum_i \left(-\frac{K_{Si}^\circ}{2\beta_{S0}} + V_i^\circ - \frac{M_i}{2\rho_0} \right) C_i. \quad (2.34)$$

where V_i° , K_{Si}° and M_i is partial molar volume, partial molar adiabatic compressibility and the molar mass of the i th component, respectively. The multiple components of the system may either be due to multiple solutes dissolved in the system or multiple molecular groups on the same solute each contributing in an additive manner to the ultrasonic velocity.

A more complete derivation of the theory presented in this section is given in Appendix A.

2.5 Ultrasonic absorption

The ResoScan System is also capable of measuring the ultrasonic absorption. Even though ultrasonic absorption is not the primary subject of this thesis, this last section of the chapter gives a brief introduction to this subject. This section is written on the basis of notes from TF Instruments [68].

An amplitude of an acoustical wave propagating a distance r is given by

$$A = A_0 e^{-\alpha r}, \quad (2.35)$$

where A_0 is the arbitrary initial amplitude of the wave, A is the arbitrary amplitude of the wave after propagating a distance r and α is the attenuation coefficient. A number of different molecular effects are known to contribute to the attenuation coefficient and

the interpretation of recorded ultrasonic absorption is related to the identification of these effects. Hence the attenuation coefficient can be expressed as

$$\alpha = \alpha_{\text{cavity}} + \alpha_{\text{visc}} + \alpha_{\text{therm}} + \alpha_{\text{relax}} + \alpha_{\text{particles}}, \quad (2.36)$$

where α_{cavity} is related to the dimensions of the resonator cavity, i.e. the small size of the resonator cavities of the ultrasonic equipment will entail a loss of ultrasonic energy, α_{visc} is related to the losses of ultrasonic energy due to the shear viscosity, α_{therm} is related to the conduction of heat, α_{relax} is related to the chemical relaxation phenomena mentioned in Section 2.4 and $\alpha_{\text{particles}}$ is due to the reflection and diffraction of the particles in the given sample. Note that the ultrasonic absorption is typically written as αf^{-2} since a number of the above mentioned contributions to the ultrasonic attenuation coefficient is proportional to f^2 [68]. The ultrasonic absorption can be used to e.g. detect aggregation processes occurring in protein solutions due to the altered properties of the particles in the solution [46]. Ultrasonic absorption measurements for varying frequency may also be combined with acoustic scattering theory to obtain estimates of the particle size distribution function of such aggregate solutions [8].

Chapter 3

Experimental setup

To be capable of investigating the applicability of the ResoScan System as a stand-alone equipment for characterizing aqueous solutions, it is certainly important to have a thorough theoretical understanding. However, it is equally important to have a thorough technical and practical literacy concerning the capabilities of the ResoScan System. Thus this chapter presents the ResoScan System by outlining its working principle and technical properties.

3.1 The time-harmonic solution to the wave equation

To fully understand the working principle of the ResoScan System, it is necessary to have a basic understanding on the concept of acoustic resonances. Acoustic resonances are often actuated by the mechanical motion of piezoelectric transducers controlled by an AC voltage source. The mechanical motion of these piezoelectric transducers is ideally described as time-harmonic [3] generating plane sound waves [56]. The equations arising when applying a time-harmonic wave solution to the wave equation are therefore highly useful for investigating the concept of acoustic resonances. The theory presented in this section introduces these equations. This section and Section 3.2 are mainly based on the master theses by Barnkob [3] and Skafte-Pedersen [56].

3.1.1 Inviscid system

Consider a plane pressure wave given by the form

$$p_1 = p_A e^{i(\mathbf{k}_0 \cdot \mathbf{r} - \omega t)}, \quad (3.1)$$

where p_A is the pressure amplitude of the wave, \mathbf{k}_0 is the real wave propagation vector, \mathbf{r} is the position and $\omega = 2\pi f$ is the angular frequency of the wave [3]. Inserting the plane pressure wave into the inviscid pressure wave equation, given in Eq. (2.10), directly yields the dispersion relation

$$\omega = U k_0. \quad (3.2)$$

Assuming that the spatial component of the time-harmonic pressure wave is implicitly given, $p_1 = p_1(\mathbf{r})e^{-i\omega t}$, and applying the dispersion relation, the insertion of p_1 into the inviscid pressure wave equation, given by Eq. (2.10), yields the Helmholtz equation

$$\nabla^2 p_1(\mathbf{r}) = -k_0^2 p_1(\mathbf{r}). \quad (3.3)$$

Choosing the correct boundary conditions dependent on the geometrical and material properties of the investigated system, the Helmholtz equation can be solved as an eigenvalue equation to determine the eigenfrequencies and eigen wave functions of acoustic resonances.

The assumption of time-harmonic waves also indirectly leads to a number of other useful relations. Hence applying a time-harmonic velocity field to Eq. (2.8a) implies that the velocity field is a gradient field and thus irrotational $\nabla \times \mathbf{v} = 0$. Therefore the first-order velocity-field \mathbf{v}_1 is related to a first-order velocity potential ϕ_1 by

$$\mathbf{v}_1 \equiv \nabla \phi_1. \quad (3.4)$$

The pressure and density perturbations can then, using Eqs. (2.8a) and (2.13), be written as

$$p_1 = -\rho_0 \frac{\partial \phi_1}{\partial t}, \quad (3.5)$$

$$\rho_1 = -\frac{\rho_0}{U^2} \frac{\partial \phi_1}{\partial t}. \quad (3.6)$$

The equations introduced in this section can in principle be used to treat acoustic resonances in systems with no energy dissipation. However, in real systems, like aqueous solutions, viscosity may significantly dampen the amplitude of the traveling sound wave, see Section 2.5. Thus the following section introduces the background equations on time-harmonic sound waves in viscous media.

3.1.2 Viscous system

Consider again a time-harmonic pressure wave with implicit spatial dependence $p_1 = p_1(\mathbf{r})e^{-i\omega t}$. Applying this time-harmonic pressure wave to the viscous wave equation, given by Eq. (2.11), leads to the lossy Helmholtz equation

$$\nabla^2 p_1(\mathbf{r}) = -k^2 p_1(\mathbf{r}), \quad (3.7)$$

where k in this case is

$$k = k_0 \frac{1}{\sqrt{1 - i2\gamma}}, \quad (3.8)$$

where γ is the dimensionless viscosity damping coefficient given by

$$\gamma \equiv \frac{(1 + \beta)\eta\omega}{2\rho_0 U^2}. \quad (3.9)$$

Since $\gamma \sim 10^{-5}$, the wave vector, k , can be approximated by

$$k = k_0(1 + i\gamma) + \mathcal{O}(\gamma^2). \quad (3.10)$$

One solution to the lossy Helmholtz equation are traveling damped plane pressure waves given by

$$p_1 = p_A e^{i(\mathbf{k}_0 \cdot \mathbf{r} - \omega t)} e^{-\gamma \mathbf{k}_0 \cdot \mathbf{r}}, \quad (3.11)$$

For time-harmonic waves in the viscous system, it is still possible to define a first-order velocity potential [3] given by Eq. (3.4) leading once again to equations relating the first-order pressure and density fields to the first-order velocity potential

$$p_1 = -\frac{U^2 \rho_0 k^2}{\omega^2} \frac{\partial \phi_1}{\partial t}, \quad (3.12)$$

$$\rho_1 = -\frac{\rho_0 k^2}{\omega^2} \frac{\partial \phi_1}{\partial t}. \quad (3.13)$$

Hence the necessary remedies to consider acoustic resonances in aqueous solutions are now introduced.

3.2 The concept of acoustic resonance

Consider now a one-dimensional model system with two parallel planar harmonically oscillating walls with a viscous compressible medium in-between, e.g. an aqueous solution. A sketch of the model system is seen in Fig. 3.1. The two walls are centered around $x = \pm L$

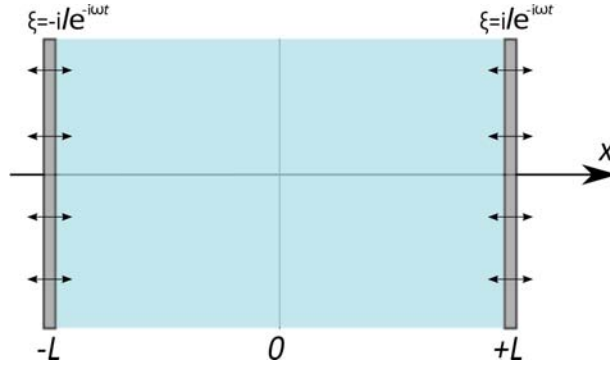


Figure 3.1: Sketch of double-actuated one-dimensional acoustic slab used to elucidate the concept of acoustic resonances. The medium between the two acoustic actuators is assumed to be compressible and viscous.

and oscillates in antiphase with amplitude l so the displacement of each of the walls at time t is given by

$$\xi = \pm i l e^{-i\omega t}, \quad (3.14)$$

respectively. The velocity of the walls must then at time t be given by

$$v_{\text{wall}} = \pm \omega l e^{-i\omega t}. \quad (3.15)$$

The first-order velocity field generated due to the vibrating walls must comprise the superposition of two time-harmonic damped plane waves traveling in opposite direction

$$v_1(x, t) = A_1 e^{i(kx - \omega t)} + A_2 e^{i(-kx - \omega t)}. \quad (3.16)$$

Since the vibrating walls comprise the boundary conditions to the solution of this problem, i.e. the first-order fluid velocity at the walls are equal to the velocity of the walls, the coefficient A_1 and A_2 are found to be

$$A_1 = -A_2 = -\frac{i\omega l}{2 \sin(kL)}. \quad (3.17)$$

Hence the velocity field for the one-dimensional acoustic resonator is given by

$$v_1(x, t) = \omega l \frac{\sin(kx)}{\sin(kL)} e^{-i\omega t}. \quad (3.18)$$

Using the relations Eq. (3.4) and Eq. (3.12), the pressure profile for the one-dimensional acoustic resonator is found to be

$$p_1(x, t) = -i\rho_0 U^2 k l \frac{\cos(kx)}{\sin(kL)} e^{-i\omega t}. \quad (3.19)$$

Note that Eqs. (3.18) and (3.19) imply a phase shift between the pressure and velocity in space and time of $\pi/2$.

Acoustic resonances are found under conditions where the energy density of the system is at its maximum, i.e. for maximal amplitude of $v_1(x, t)$ and $p_1(x, t)$. To determine the resonance condition in the case of the one-dimensional double-actuated model system, Eqs. (3.18) and (3.19) are expanded around $k = k_0$

$$v_1(x, t) = \omega l \frac{\sin(k_0 x) + i\gamma k_0 x \cos(k_0 x)}{\sin(k_0 L) + i\gamma k_0 L \cos(k_0 L)} e^{-i\omega t}, \quad (3.20)$$

$$p_1(x, t) = -i\rho_0 U \omega l \frac{\cos(k_0 x) - i\gamma k_0 x \sin(k_0 x)}{\sin(k_0 L) + i\gamma k_0 L \cos(k_0 L)} e^{-i\omega t}. \quad (3.21)$$

From these expressions, the resonant condition is found

$$k_0 L = N\pi, \quad (3.22)$$

where N is an integer. Since the wavenumber is related to the wavelength by $k_0 = 2\pi/\lambda_0$, the resonant condition can also be expressed by

$$\lambda_0 = \frac{2L}{N}, \quad (3.23)$$

i.e. a resonance emerges in the one-dimensional model resonator when the length of the resonator corresponds to an integer number of half wavelengths of the standing waves found

at resonance. Finally, the resonance frequency is also found by applying the dispersion relation, given by Eq. (3.2) to Eq. (3.22)

$$f_{\text{res}} = \frac{NU}{2L}. \quad (3.24)$$

Hence it is clear that for some wave frequencies the resonance condition will be met and the amplitudes of physical fields associated with the sound wave will increase dramatically whereas for other wave frequencies the amplitudes will be imperceptible.

A characteristic quantity of acoustic resonators is the Q-factor. The Q-factor represents the relative energy loss per oscillation cycle of the system [22]

$$Q = 2\pi \frac{E_{\text{tot}}}{\Delta E}, \quad (3.25)$$

where E_{tot} is the total energy of the resonator and ΔE is the energy lost per oscillation cycle. In the viscous system considered in the above, the Q-factor can be related to the energy dissipation from the viscosity by [3]

$$Q = \frac{1}{2\gamma}. \quad (3.26)$$

The magnitude and sharpness of the resonant peak in frequency space is related to the amount of energy dissipation through the Q-factor [3]

$$Q = \frac{f_N}{\Delta f_{3\text{dB}}}, \quad (3.27)$$

where f_N is the resonance frequency of the N th resonance and $\Delta f_{3\text{dB}}$ is the full width half maximum of the resonance in frequency space. Hence the larger the Q-factor, i.e. the lower the energy dissipation, the larger the magnitude and sharpness of the resonance peak in frequency space [22]. Acoustic resonances are also associated with changes in phase between the input actuation and the output acoustic resonance. Increasing the frequency from a frequency below the resonance frequency to a frequency above the resonance frequency thus shifts this phase by 180° [66]. The sharpness of the phase shift is also related to the Q-factor, i.e. the larger the Q-factor the sharper the phase shift [22].

3.3 The ResoScan System

3.3.1 Design

The ResoScan System contains two resonator cavities. This construction allows for an exact measurement of the differences in ultrasonic velocity and ultrasonic absorption between a given sample and a relevant reference. Fig. 3.2 shows a schematic representation of these two resonator cavities. The resonator cavities can contain a sample volume between $180 \mu\text{L}$ to $250 \mu\text{L}$ and are built in titanium and gold. The ultrasonic transducers used to create the acoustic resonances in the resonator cavities are constructed using lithium

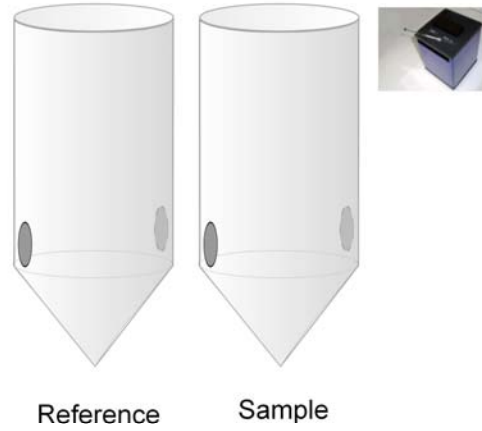


Figure 3.2: Schematic drawing of the geometry of the two resonator cavities of the ResoScan System. The upper parts of the cavities are cylindrical whereas the lower parts are conical. Each cavity can contain a volume of between 180 and 250 μL . The two darker circular patches located opposite each other on the lower part of the cylindrical shape represent the ultrasonic transducers. The ultrasonic path length is approximately 7 mm. Inset: Real image of the ResoScan System taken from the homepage of the producer [76].

niobate which is a piezoelectric material. By placing a gold electrode on each side of the lithium niobate crystal, it is then possible to convert the electrical energy of an AC voltage source into mechanical energy causing a mechanical motion of the transducer elements entailing a sound wave in the resonator cavities, and at the correct frequencies an ultrasonic resonance. Hence one of the ultrasonic transducers actuates an ultrasonic resonance whereas the other transducer detects the resonance. The ultrasonic path length is approximately 7 mm [67, 76]. Since the ultrasonic velocity is extremely sensitive to even small variations in temperature, about $3 \text{ m s}^{-1} \text{ K}^{-1}$ in water, the ResoScan System also contains a Peltier temperature controller. This controller is capable of heating and cooling the specimens in the resonator cavities in a temperature range between 5 to 85°C with a stability of $\pm 0.003^\circ\text{C}$ [67].

3.3.2 Working principle

The technology underlying the ResoScan System allows for accurate determination of ultrasonic resonances. Hence the ResoScan System is capable of recording the wave amplitude and phase as a function of frequency to precisely determine the resonance frequencies of the acoustic resonances in the resonator cavities. Differences in resonance frequencies between two acoustic resonances can then be used to calculate the ultrasonic velocity. For example, in the ideal one-dimensional double-actuated case depicted in Section 3.2, the differences in resonance frequencies between the acoustic resonances were associated to the ultrasonic velocity through a simple relation obtained by rewriting Eq. (3.24)

$$U = 2\Delta fL. \quad (3.28)$$

In the non-ideal resonator cavities of the ResoScan System, it is necessary to take into account the coupling between sample resonances and transducer resonances to correctly interpret the differences between the resonance frequencies in terms of ultrasonic velocities. Thus the differences between the resonance frequencies for resonances of order N_1 and N_2 , respectively, is given by [66]

$$f_{N_1} - f_{N_2} = \frac{U}{2D} \left[N_1 + \frac{2}{\pi} \tan^{-1} \left(\frac{U\rho}{U_T\rho_T \tan\left(\pi\frac{f_{N_1}}{f_T}\right)} \right) \right], \quad (3.29)$$

where ρ is the density of the sample in the resonator cavity, U_T is the ultrasonic velocity in the transducer material, ρ_T is the density of the transducer material and f_T is the resonance frequency of the transducer.

The ResoScan System only records all the resonance frequencies during an initialization procedure and fit the results to Eq. (3.29). After this initialization, only a single resonance peak is tracked since changes in the resonance frequency of this peak is sufficient to quantitatively identify changes in ultrasonic velocity. The resonance peak tracked during experiments with the ResoScan System is chosen automatically. All experiments conducted in this thesis tracks a resonance peak of approximately 7.82 MHz.

To measure the ultrasonic absorption, the ResoScan System records the change in phase as a function of frequency at the tracked resonance peak. As mentioned previously, this change can be directly related to the Q-factor and hence to the absorption of the ultrasonic wave.

3.3.3 Accuracy

The data sheet concerning the technical specifications of the ResoScan System states that the uncertainty of the measured absolute and differential ultrasonic velocities is given by $\pm 25 \text{ cm s}^{-1}$ and $\pm 15 \text{ cm s}^{-1}$, respectively [67]. The experimental work conducted during this thesis however indicates that the ResoScan System is capable of recording the differential ultrasonic velocities more accurately than the accuracy specified by the data sheet. To assess the accuracy of the ResoScan System consider the results of 6 experiments conducted with HEPES buffer solution in resonator cavity 1 and Lipolase HEPES buffer solution in resonator cavity 2 with constant Lipolase concentration of $63.4 \mu\text{M}$, where the Lipolase HEPES buffer solution samples all are taken from the same stock sample. The 6 data points on the differential ultrasonic velocity, ΔU , is given by $\{0.4996; 0.5797; 0.5302; 0.5683; 0.4527; 0.5464\}$ (m s^{-1}). The standard deviation of the differential ultrasonic velocity, $\delta\Delta U$, can then be calculated using [31]

$$\delta\Delta U = \sqrt{\frac{\sum_{i=1}^{N_p} (\Delta U_i - \Delta U_{\text{mean}})^2}{N_p - 1}}, \quad (3.30)$$

where ΔU_i is the value of the i th data point and ΔU_{mean} is the mean of the N_p recorded data points. Thus $\delta\Delta U$ is calculated to be $\pm 4.7 \text{ cm s}^{-1}$. This standard deviation is ap-

plied throughout this thesis as the experimental uncertainty of the recorded differential ultrasonic velocities since no data allowing for further analysis on the accuracy of the recorded differential ultrasonic velocities was measured during the thesis work. Note however that empirical observations do in fact indicate that the uncertainty of samples with a lower chemical complexity, like aqueous salt solutions, may be smaller than in the case of aqueous protein solutions.

No information about the uncertainty of the ultrasonic absorption is given in the data sheet. However, the standard deviation of the differential ultrasonic absorption, $\delta\Delta\alpha f^{-2}$, can be evaluated using the 6 data points recorded with HEPES buffer solution in resonator cavity 1 and Lipolase HEPES buffer solutions in resonator cavity 2. Since the 6 data points on the differential ultrasonic absorption is given by $\{-1.12 \times 10^{-15}; 5.96 \times 10^{-16}; 2.77 \times 10^{-17}; 6.88 \times 10^{-16}; -8.16 \times 10^{-16}; -2.23 \times 10^{-16}\}$ ($\text{s}^2 \text{m}^{-1}$), the standard deviation of the differential ultrasonic absorption is found to be $\pm 7 \times 10^{-16} \text{ s}^2 \text{m}^{-1}$. This standard deviation is taken to represent the experimental uncertainty on the differential ultrasonic absorption recorded in this thesis.

3.3.4 Typical experimental procedure

The following section outlines the typical experimental procedure for carrying out experiments on the ResoScan System. There may of course be additional experimental details associated with the concrete individual experiments than outlined in this section. These details will be given in later sections concerned with these experiments.

Cleaning of the ResoScan System

The operational procedure of a typical experiment performed with the ResoScan System is commenced with a clean-up of the resonator cavities. The first step of the normal cleaning procedure is to remove the existing samples in the resonator cavities by vacuuming with the cleaning equipment concomitant with the ResoScan System. The second step is to thoroughly wash the resonator cavities with pure Milli-Q water while constantly vacuuming the cavities. The third step is to wash the cavities with ResoScan Wash detergent rinsing mixture to remove any remainders of samples used in previous experiments by filling each cavity 2-3 times with the rinsing mixture and removing the rinsing mixture again by vacuuming with the cleaning equipment. The fourth step is again to wash the resonator cavities thoroughly with Milli-Q water while constantly vacuuming. The fifth step of the cleaning procedure is to remove any remainders of the detergent rinsing mixture by filling each resonator cavity with 70 % aqueous ethanol solution 2-3 times and removing it again by vacuuming with the cleaning equipment. The sixth and last step is again to wash thoroughly with water while constantly vacuuming the cavities. This cleaning procedure will in most cases clean the resonator cavities sufficiently to allow for new experiments to be performed with the ResoScan System. However, in some cases, e.g. in cases where heating of samples have entailed a number of complex chemical reactions in the investigated samples, this procedure is not adequate. Hence it may be necessary to employ other cleaning procedures. The details on these more advanced cleaning procedures are

however not presented in this report since they are rated as confidential by Novozymes.

Injecting samples into the resonator cavities

After proper cleaning of the resonator cavities, the ResoScan System is ready to be initialized. However, before proceeding to the initialization procedure of the ResoScan System, it is necessary to dwell for a moment on the process of injecting samples into the resonator cavities. Whereas filling the resonator cavities with the liquids used in cleaning process is done directly from wash bottles and disposable pipettes, the process of sample injection is done from pipettes containing an accurately measured out sample volume between 180 μL to 250 μL , and typically of 200 μL . While emptying the samples from the pipettes it is necessary to lower the pipette down into the small resonator cavities to avoid that samples adhere to the upper parts of the resonator cavity surfaces and that air bubbles are formed. This however causes the process of sample injecting to require an extremely steady hand since touching the surface of the lower parts of the resonator cavities with the hard material of the pipette tip may risk severely damaging the ultrasonic transducers entailing unfortunate losses in terms of expensive financial expenses for reparation as well as wasted project time.

When samples are injected into the resonator cavities, they are typically injected twice to ensure that remnants of any previous samples are diluted. Hence samples are first injected, then removed by vacuuming and finally injected again into the resonator cavities. The temperature difference between the injected samples and the resonator cavities is not allowed to be more than 5°C as a higher difference could risk damaging the equipment. The temperature of the resonator cavities is typically 25°C.

Initializing an experiment

The initialization procedure is carried out subsequent to the cleaning procedure. Hence a chemically inert aqueous liquid called ResoScan Standard is injected into each of the two resonator cavities and the automatic initialization procedure is run, cf. Section 3.3.2. After identification of a usable resonance peak, the ResoScan System starts logging data on the absolute and differential values of the ultrasonic velocities and absorption. Data is logged by the ResoScan System once every 11 s. Ideally, the velocity difference between the two resonator cavities recorded with ResoScan Standard in both cavities should be 0 m s^{-1} . However, a velocity difference smaller than $\pm 5 \text{ cm s}^{-1}$ is taken to be acceptable representing a fundamental uncertainty of the ResoScan System. A velocity difference larger than $\pm 5 \text{ cm s}^{-1}$ is interpreted as a sign of contamination on one of the resonator cavities entailing the necessity of further and more thorough cleaning. If the differential velocity difference is smaller than $\pm 5 \text{ cm s}^{-1}$ after the initialization procedure, the ResoScan System is ready to be used to conduct the actual experiments.

Conducting the experiments

The injection of samples to conduct experiments is typically done in a step-wise manner subsequent to the initialization procedure. Hence after the ResoScan Standard is removed

from both resonator cavities by vacuuming, a relevant reference sample is injected into both resonator cavities and a number of data points are recorded to ensure that this step did not compromise the differential properties between the two resonator cavities, i.e. the velocity difference should still be smaller than $\pm 5 \text{ cm s}^{-1}$. After this step, the reference sample is removed from resonator cavity 2 by vacuuming and instead a sample of interest is injected, while the reference sample in resonator cavity 1 is retained. Thus the ResoScan System is prepared to conduct experiments.

The time spent to record a useful data point depends on the samples under investigation. Even though data points are logged by the ResoScan System once every 11 seconds, it is rare that useful data points are found within the first 5 minutes after having injected the relevant samples due to the necessity for equilibration of various experimental parameters, including the temperature. The data points presented in this thesis are normally the final data point logged for a given sample-reference experiment.

Temperature scans

The ResoScan System is capable of varying the cavity temperature while recording the ultrasonic properties of the samples in the cavities. The experimental work of this thesis relies heavily on this feature to characterize aqueous solutions. The scan rate and scan range of these temperature-varying experiments is manually designed in scripts in software concomitant to the ResoScan System. The temperature scans conducted in this thesis are conducted using two such scripts. In the first of these scripts the temperature is scanned once between 5 to 85°C by a scan rate of 300 mK min⁻¹. In the second script, the temperature is scanned twice between 5 to 85°C by a scan rate of 500 mK min⁻¹ allowing for an examination on the reversibility of any reactions induced by heating the aqueous solutions under investigation. Note that results from the temperature scans presented in this thesis comprise all data points logged by the ResoScan System during the temperature scans, i.e. since the temperature is continuously scanned, it is not possible to wait for the samples in the resonator cavities to equilibrate with respect to temperature before logging a data point at a given temperature. In both types of temperature scans, samples are injected into the resonator cavities at a temperature of 25°C before the experiment is commenced and temperature is stepped down to 5°C.

Chapter 4

Test experiments

To draw any conclusion from the case studies in Chapters 5, 6 and 7, it is first necessary to check whether the ResoScan System is capable of reproducing results on model systems where the expected outcome is well-known. Therefore, the following section outlines and analyzes the results of test experiments conducted on two well-documented model systems, namely pure water and polystyrene microbead suspensions.

4.1 Test experiments on Milli-Q water

4.1.1 Introduction to water

Sound knowledge about the properties of liquid water is extremely important for a long number of scientific and technological purposes. The purposes of this thesis are no exception as the interaction between water and dissolved solutes is one of the main determinants of the three-dimensional conformational structure of the dissolved solutes. Thus besides serving as an excellent model system for conducting test experiments on the ResoScan System, water also comprise a highly relevant starting point of the experimental investigations of aqueous solutions. Hence this section is commenced with a short introduction to water and its chemical and ultrasonic properties.

4.1.2 Relevant chemical background theory

Water is known to be a liquid with peculiar properties that resemble the properties of no other liquid. For example, whereas the density of other liquids decreases monotonously with temperature due to thermal expansion, the density of water at atmospheric pressure is found to exhibit a maximum at 4°C. It is generally accepted that the reasons of these peculiar properties are to be found in the unique chemical properties of water [42].

A water molecule is a small molecule consisting of one oxygen atom covalently bonded to two hydrogen atoms, see Fig. 4.1. The oxygen atom is more electronegative than the hydrogen atoms causing negative charge from the hydrogen atoms to be drawn to the oxygen atom. Hence the water molecule is electrically polar. This polar nature of water entails intermolecular bonding between the oxygen atoms and the hydrogen atoms in the

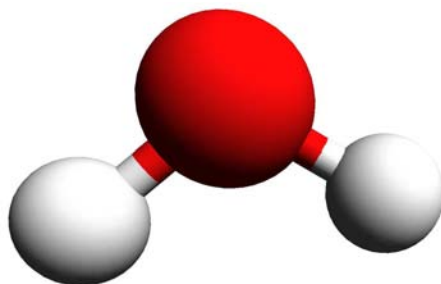


Figure 4.1: Ball-and-stick model of water molecule. The white balls represent hydrogen atoms whereas the red ball represent an oxygen atom. Since the oxygen atom is more electronegative than the hydrogen atoms, a net negative charge is found on the oxygen atoms and a net positive charge is found on the hydrogen atoms allowing the water molecule to form hydrogen bonds.

water molecules through the highly directional hydrogen bonds. The formation of these hydrogen bonds is known to be cooperative in the sense that the formation of one hydrogen bond to a water molecule causes the molecule to be apt to further hydrogen bonding [25].

When water is found in its solid form, i.e. as ice, the water molecules are found in a tetrahedral arrangement with 4 such hydrogen bonds per molecule. The packing fraction of this tetrahedral structure is known to be low causing the low density of ice [25]. When the temperature is increased and ice melts to liquid water, a significant amount of the hydrogen bonding structure is still preserved. For example, computer calculations on liquid water at room temperature imply that each water molecule is involved in 2.8 to 3.4 hydrogen bonds [42].

The maximal density at 4°C for liquid water can be explained by two trends, i.e. the disruption of the low density ice structure and thermal expansion [77]. However, no generally accepted description on the structure of liquid water exists to explain all of its peculiar properties [42]. Some models thus propose that the hydrogen bonds are conserved but distorted, whereas other models propose that some of the hydrogen bonds are actually broken [25].

4.1.3 Ultrasonic introduction

It is widely known that also the temperature dependence of the ultrasonic velocity in water exhibits a peculiar behavior compared to the temperature dependence of the ultrasonic velocity in other types of liquids. Thus the ultrasonic velocity in normal liquids decreases monotonously with increasing temperature while the ultrasonic velocity in water is maximal at 74°C. Furthermore, minimal adiabatic compressibility of water is found at 64°C [70].

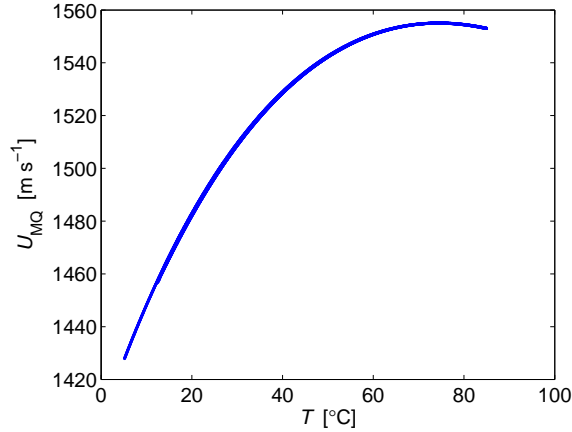


Figure 4.2: Absolute ultrasonic velocities recorded in Milli-Q water, U_{MQ} , as a function of temperature, T , utilizing the script using a scan rate of 300 mK min^{-1} . The curve has the expected shape with a single maximum at 74.4°C . Results obtained utilizing the script using a scan rate of 500 mK min^{-1} appear to be exactly the same when represented in this type of plot and are hence omitted from the figure.

4.1.4 Experimental procedure

The control experiments were conducted using Milli-Q water. Milli-Q water is water purified by ion exchange techniques to attain a very high purity. Two experiments were conducted. In both of these experiments, both resonator cavities were filled with $200 \mu\text{L}$ Milli-Q water and the temperature is scanned between 5 and 85°C using the two scripts described in Section 3.3.4, i.e. with scan rates of 300 mK min^{-1} and 500 mK min^{-1} , respectively.

4.1.5 Results and discussion

The absolute ultrasonic velocity in Milli-Q water recorded as a function of temperature is shown in Fig. 4.2 for the experiment utilizing the script with a scan rate of 300 mK min^{-1} . The shape of the curve on Fig. 4.2 represents the characteristic temperature-dependence of the ultrasonic velocity of water on temperature. The maximum of the ultrasonic velocity is found at 74.4°C relatively close to the expected value [70]. The absolute ultrasonic velocity recorded in the experiment utilizing the script with a scan rate of 500 mK min^{-1} appear to give similar results when represented in the same type as shown in Fig. 4.2 and are thus omitted in this figure.

The subtle phenomena examined in the case studies on aqueous solutions in Chapters 5, 6 and 7 require extremely accurate measurements of the ultrasonic velocity. It is therefore necessary to perform a more thorough assessment of the accuracy of the ResoScan System than possible from Fig. 4.2. The recorded ultrasonic velocities are therefore compared to two different sources from the literature. Firstly it is compared to the values from the 1995 formulation of the International Association of Properties of Water and Steam (IAPWS-95)

[71]. The ultrasonic velocities for water are, using the IAPWS-95 formulation, determined with an uncertainty of $\pm 0.005\%$ within the temperature and pressure regimes considered in this thesis rendering the IAPWS-95 formulation as a perfect source for testing the accuracy of the data recorded with the ResoScan System. Since the formalism used in the IAPWS-95 formulation is fairly complicated, this thesis does not directly calculate the ultrasonic velocities using the formalism, but fits a polynomial of degree 4 to 46 data points, for temperatures between 0 to 100°C , calculated in the article presenting the formalism [71]. The polynomial is fitted to the data points using a least squares fitting algorithm included in MATLAB. The fit is found to be $U_{\text{wa}} = \sum_{i=0}^4 U_i T^i$ where $U_0 = 1402.3 \text{ m s}^{-1}$, $U_1 = 5.0094 \text{ m s}^{-1} \text{ }^\circ\text{C}^{-1}$, $U_2 = -0.0559 \text{ m s}^{-1} \text{ }^\circ\text{C}^{-2}$, $U_3 = 2.7029 \times 10^{-4} \text{ m s}^{-1} \text{ }^\circ\text{C}^{-3}$ and $U_4 = -7.2327 \times 10^{-7} \text{ m s}^{-1} \text{ }^\circ\text{C}^{-4}$. Secondly, data is compared to a recent experimental study, conducted by Benedetto *et al.* [5], using an ultrasonic double-reflector pulse-echo method to accurately determine the speed of sound in water. A comparison of the data recorded by the ResoScan System on Milli-Q water to the polynomial fitted to the IAPWS-95 formulation and the experimental study of Benedetto is shown in Fig. 4.3 for (a) the script utilizing a scan rate of 300 mK min^{-1} and (b) the script utilizing a scan rate of 500 mK min^{-1} .

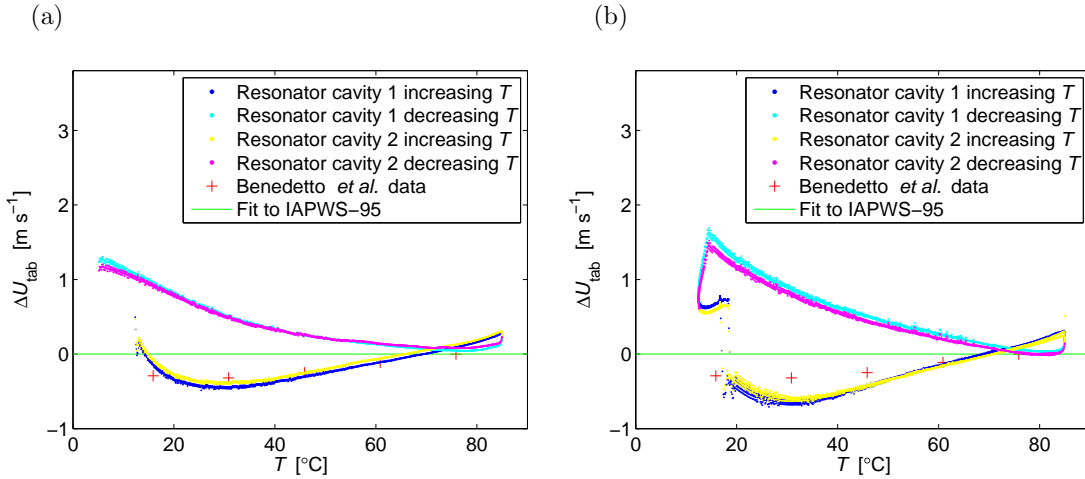


Figure 4.3: Comparison of absolute ultrasonic velocities recorded using the ResoScan System for (a) experiments utilizing the script using a scan rate of 300 mK min^{-1} and (b) experiments utilizing the script using a scan rate of 500 mK min^{-1} to ultrasonic velocities calculated using the IAPWS-95 formulation [71] and a recent experimental study by Benedetto *et al.* [5] for varying temperature, T . ΔU_{tab} is the difference between the ultrasonic velocities in water either measured using the ResoScan System or by Benedetto *et al.*, U_{MQ} , and the ultrasonic velocities determined by fitting a polynomial of degree 4 to the IAPWS-95 formulation, U_{IAPWS} . Hence ΔU_{tab} is given by $U_{\text{MQ}} - U_{\text{IAPWS}}$. Results imply that there may be temperature gradients between the sample and the actual temperature controller as well as other unfortunate systematic errors.

The comparison of the ultrasonic velocities recorded by the ResoScan System to the

IAPWS-95 formulation as well as the experimental data by Benedetto *et al.* in Fig. 4.3 reveals that absolute ultrasonic velocities recorded by the ResoScan System during temperature scans significantly deviate from data from the literature. These deviations are larger in the case of the experiment utilizing the script with a scan rate of 500 mK min^{-1} than for the experiment utilizing the script with a scan rate of 300 mK min^{-1} . The deviations imply that there may be temperature gradients between the temperature of the samples in the cavities and the temperature actually measured by the ResoScan System. Thus the absolute velocities recorded for a given temperature using the ResoScan System are lower for increasing temperature than for decreasing temperature when the temperature is below 74°C and higher when the temperature is above 74°C implying a constant lag between the temperature measured by the ResoScan System and the actual sample temperature. However, other effects than temperature gradients may also play a role in explaining some of the deviations revealed in Fig. 4.3, e.g. unfortunate design of the electric circuitry of the ResoScan System may also play a role. It should also be mentioned that there is a significant discrepancy between actual data recorded by ResoScan System after the temperature scans utilizing a scan rate of 300 mK min^{-1} and the expected value of the data but since this discrepancy is not seen during the temperature scans it is not ascribed any importance in the interpretation of the recorded data. Moreover, it should be mentioned that the temperature scans utilizing a scan rate of 500 mK min^{-1} in fact only scan the temperature between 11 to 85°C .

Most of the experimental work of this thesis is concerned with differential data, i.e. the difference in ultrasonic properties between a sample in one resonator cavity and a relevant reference in the other resonator cavity. The question is then if the systematic errors revealed by Fig. 4.3, whatever their underlying reason, also impinges on the differential ultrasonic velocities. Fig. 4.4 shows the differences in ultrasonic velocities between the two resonator cavities recorded using (a) the script with a temperature scan rate of 300 mK min^{-1} and (b) a temperature scan rate of 500 mK min^{-1} . Both experiments show that also the differential velocity is affected by errors, i.e. the difference in ultrasonic velocity between the two resonator cavities, ΔU , should ideally be 0 m s^{-1} as the two cavities contain exactly the same samples. Even though these errors are relatively small, they may significantly affect the interpretation of the subtle effects considered in the later case studies. However, comparison of course of events of the curves on Fig. 4.4 to differential velocities curves recorded in other temperature scans during the thesis work imply that the errors seen in Fig. 4.4 are a general and consistent feature of all curves recorded using the two types of temperature scans. This in turn implies that it may be possible to construct a systematic procedure that can be used to correct all the differential ultrasonic velocity curves recorded using temperature scans.

4.1.6 Calibration of the ResoScan System

The correction procedure is designed by considering the temporal course of events of the differential ultrasonic velocities of the temperature scans conducted with Milli-Q water in both resonator cavities. In the case of the experiment utilizing the script with a scan rate of 300 mK min^{-1} , a single polynomial is used to fit the recorded differential ultrasonic

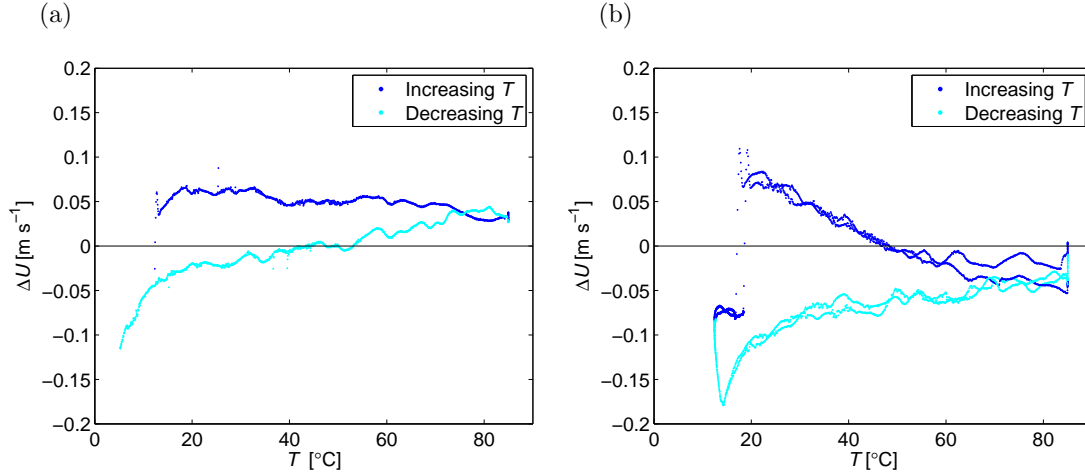


Figure 4.4: Differential ultrasonic velocities recorded with Milli-Q water in both resonator cavities, $\Delta U = U_2 - U_1$, for (a) experiments utilizing the script using a scan rate of 300 mK min^{-1} and (b) experiments utilizing the script using a scan rate of 500 mK min^{-1} as a function of temperature, T . Erroneous deviations in the differential ultrasonic velocities appear to be associated with both types of temperature scans.

velocities over the entire time period of the temperature scan. In the case of the experiment utilizing the scan rate of 500 mK min^{-1} , the correction procedure involves fitting three polynomials to the differential ultrasonic velocities in three distinct time periods of the temperature scan. The polynomials are then assumed to represent the magnitude of the errors observed when using the two types of temperature scans to investigate other types of aqueous samples, i.e. it is possible to remove errors from the differential ultrasonic velocities recorded during experiments based on the two types of temperature scans by subtracting the polynomials from the recorded differential ultrasonic velocities. Further details on the calibration procedures are given in Appendix B.

All differential velocity curves recorded as a function of temperature in this thesis are corrected by this calibration procedure. To remove noisy effects, all differential ultrasonic velocity curves recorded during the temperature scans are also smoothed subsequently to the calibration procedure by recalculating a given data point to represent the average value of that data point and the 5 data points recorded just before and just after the given data point. Correcting the curves from Fig. 4.4 by first calibration and then smoothing yields the curves on Fig. 4.5. Note that the curves on Fig. 4.5 are not located exactly in 0 m s^{-1} as they ideally should. This is because the differential ultrasonic velocities recorded with Milli-Q water in both resonator cavities at 25°C just before the temperature scans was not exactly 0 m s^{-1} either, i.e. the difference in ultrasonic velocity at 25°C recorded just before the experiment utilizing the script with a scan rate of 300 mK min^{-1} was 1.7 cm s^{-1} while the difference recorded just before the experiment utilizing the script with a scan rate of 500 mK min^{-1} was -1.5 cm s^{-1} . These non-zero differential velocities recorded at 25°C are assumed to be specific to the individual experiments and arise due to e.g. contamination

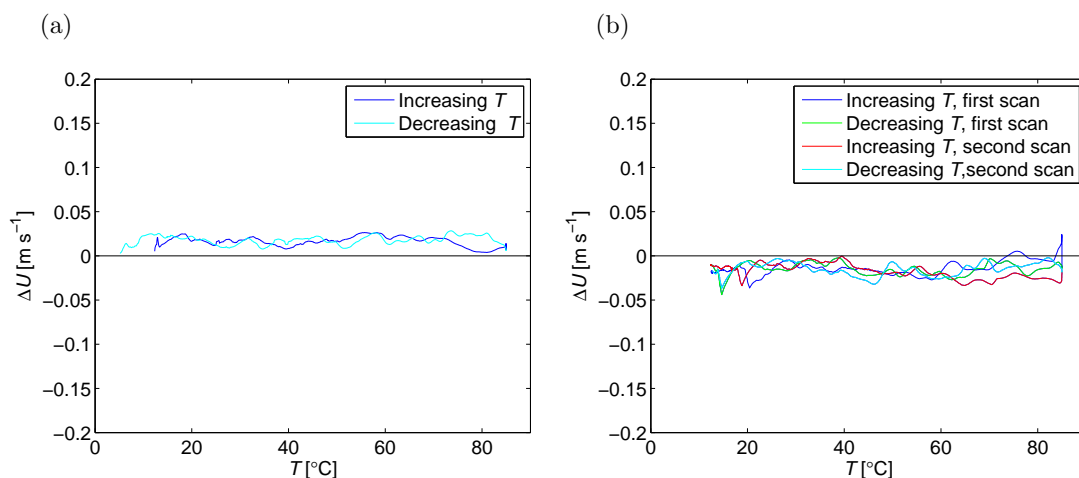


Figure 4.5: Corrected and smoothed differential ultrasonic velocities, ΔU , recorded for varying temperature, T , with Milli-Q water in both resonator cavities for as a function of temperature scan (a) utilizing the script using a scan rate of 300 mK min^{-1} and (b) utilizing the script using a scan rate of 500 mK min^{-1} . The resulting non-zero values of the differential ultrasonic velocities are assumed to represent the correct differential ultrasonic velocities for the specific experiments when the same type of sample is injected into both resonator cavities.

of the resonator cavities. In other words, the differential ultrasonic velocities recorded at 25°C just before the individual experiments are assumed to represent the correct zero-point for the differential ultrasonic velocities for these individual experiments.

To fully confirm the validity of the correction scheme presented in the above, it is of course necessary to test it on other model systems than the data that it was actually designed to correct. Such tests are not directly performed in this thesis. However, the fact that application of the correction scheme to the differential ultrasonic velocities corrects a number of curves from an apparently irreversible to a complete reversible course of events is taken as evidence for the validity of the correction scheme.

4.2 Compressibility of polystyrene

The ResoScan System can also be tested by calculating the adiabatic compressibility coefficient of polystyrene, which is a hydrocarbon-based compound, and compare the results of the calculations to the literature.

4.2.1 Experimental procedure

Polystyrene microbeads were provided in an unknown buffer in a 10 % w/v suspension. A number of samples of varying polystyrene microbead concentration, between 0.001 to 0.1 %, were then produced by performing a serial dilution using a 0.01 % Tween20 buffer, which is a polysorbate surfactant buffer used to reduce the aggregation of the microbeads

and adsorption of the microbeads to the surfaces of the resonator cavities [4]. Experiments were conducted at 25°C with Tween20 buffer in resonator cavity 1 and polystyrene microbead samples of varying microbead concentration in resonator cavity 2. The first data point was obtained with the most dilute polystyrene microbead sample in resonator cavity 2. Subsequent data points were then obtained by injecting microbead samples into resonator cavity 2 in order of increasing microbead concentration, i.e. the old sample in resonator cavity 2 was removed and a new more concentrated sample was instead injected while the same Tween20 buffer sample remained in resonator cavity 1. Resonator cavity 2 was not cleaned between the injections of the individual samples since any small remnants of the more diluted polystyrene microbead samples were not expected to introduce any significant errors to the recorded data when samples of higher microbead concentrations were injected into the resonator cavities. Note that data points ideally should be recorded multiple times and in a completely randomized order to maximize the probability that results are indeed statistically significant and reproducible. However, even though this approach is preferable it is also extremely time consuming due to the extensive amount of cleaning required and is thus not within the scope of this thesis.

To attain knowledge about the effect of the unknown buffer in which the polystyrene microbeads were originally supplied, an experiment was also conducted at 25°C using Tween20 buffer in resonator cavity 1 and a sample approximately comprising a 50/50 mixture of Tween20 buffer and unknown buffer in resonator cavity 2.

A potential problem associated with performing experiments on the polystyrene microbead suspensions is associated to sedimentation. For each polystyrene microbead sample that was injection in the resonator cavity 2, care had to be taken that the polystyrene microbeads were properly mixed with the Tween20 buffer and not precipitated.

4.2.2 Results and discussion

Relative increments in ultrasonic velocity, $\Delta U/U_{Tw}$, where U_{Tw} is the ultrasonic velocity in the Tween20 buffer, are plotted in Fig. 4.6 as a function of microbead volume fraction, x . The volume fractions are readily obtained by dividing the weight per volume percentage by 100 times the density of polystyrene. Uncertainties are assumed to be $\pm 4.7 \text{ cm s}^{-1}$, cf. Section 3.3.3. Differential ultrasonic velocities were also recorded for x equal to 9.5×10^{-3} but high attenuation spoiled the results of the measurement. This high attenuation is probably due to acoustic scattering or diffraction due to the polystyrene particles.

It is clear from Fig. 4.6 that the recorded relative increments in ultrasonic velocities approaches the fundamental uncertainty limit of the ResoScan System, i.e. it may very well be that the recorded differential ultrasonic velocities only represent noise. However, the following still attempts to use the data on this figure to calculate the compressibility of polystyrene.

To determine the adiabatic compressibility coefficient of polystyrene, the theory on ideal mixtures, given in Section 2.3, is applied. However, the applicability of this theory is in principle troubled by the fact that the unknown buffer concomitant with the provided 10 % w/v polystyrene particle samples not is included in resonator cavity 1 whereas it still comprise a small part of the samples in resonator cavity 2, i.e. the reference sample

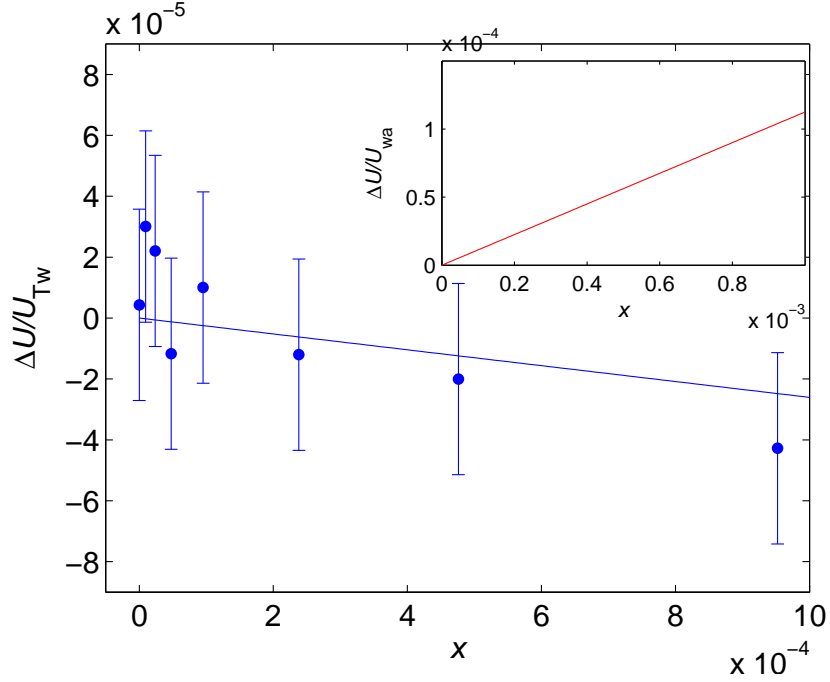


Figure 4.6: Relative increment in ultrasonic velocity $\Delta U/U_{Tw}$ for varying volume fraction x of polystyrene. The blue data points are data points obtained using the ResoScan System. Uncertainties are taken to be $\pm 4.7 \text{ cm s}^{-1}$. The blue line is fitted to the data points using the theory on ideal two-component mixtures implying that the adiabatic compressibility coefficient of polystyrene is $4.63 \times 10^{-10} \text{ Pa}^{-1}$ which unfortunately is far from the correct value of $3.30 \times 10^{-10} \text{ Pa}^{-1}$. The inset is the theoretically expected curve for polystyrene microbeads in water calculated using the theory on ideal two-component mixtures.

in resonator cavity 1 and the background buffer mixture in the polystyrene microbead samples in resonator cavity 2 are not directly comparable. Fortunately the differential measurement for Tween20 buffer in resonator cavity 1 and the 50/50 mixture of Tween20 buffer and unknown buffer in resonator cavity 2 yields a velocity difference of 1.1 cm s^{-1} , i.e. this difference is so small that it is significantly smaller than the uncertainty of the ResoScan System. Hence it is in the following assumed that the ultrasonic properties of the unknown buffer and the Tween20 buffer are comparable. Furthermore, comparison to experiments conducted with Milli-Q water show that the absolute ultrasonic velocity in water and Tween20 buffer is virtually the same implying that the density and adiabatic compressibility coefficient of Tween20 buffer is approximately the same as the density and adiabatic compressibility of water. Eq. (2.23) can then be used to calculate the adiabatic compressibility coefficient of polystyrene by writing

$$\frac{\Delta U}{U_{Tw}} = \left([1 + (\tilde{\rho} - 1)x] [1 + (\tilde{\beta}_s - 1)x] \right)^{-1/2} - 1, \quad (4.1)$$

where $\tilde{\rho} = \rho_{\text{ps}}/\rho_{\text{wa}}$ and $\tilde{\beta}_S = \beta_{S_{\text{ps}}}/\beta_{S_{\text{wa}}}$. Fitting this expression to the data in Fig. 4.6 using that $\rho_{\text{ps}} = 1050 \text{ kg m}^{-3}$ and $\rho_{\text{wa}} = 998 \text{ kg m}^{-3}$ yields $\tilde{\beta}_S = 1.0343$. Since the adiabatic compressibility of water, $\beta_{S_{\text{wa}}}$, at 25°C is given by $4.48 \times 10^{-10} \text{ Pa}^{-1}$, it is then found that the adiabatic compressibility coefficient of polystyrene is equal to $4.63 \times 10^{-10} \text{ Pa}^{-1}$ which is far from adiabatic compressibility coefficient of $3.30 \times 10^{-10} \text{ Pa}^{-1}$ known for polystyrene at 20°C [7]. For comparison to the recorded results, the inset in Fig. 4.6 shows the calculated relative increment in ultrasonic velocity for polystyrene beads in water at 20°C using the correct values of the adiabatic compressibility coefficient of polystyrene.

Reasons for the bad agreement between theory and experiment may be related to the fact that experiments are performed in the vicinity of the limit of accuracy of the ResoScan System or that the theoretical model is incomplete. Other reasons may be related to aggregation of particles and adhesion of particles to the surfaces of the resonator cavities. However, the Tween20 is expected to prevent this scenario. Another possible reason is sedimentation but calculations not shown here indicate that this effect should not play a role due to the short time duration of the experiments. Finally, micellar formation of the buffer molecules may also potentially inflict on the results of the experiments even though this does not seem like a likely explanation for the bad results either.

4.3 Summary

A basic introduction has now been given to both the theoretical framework for the interpretation of ultrasonic velocities as well as the capabilities of the ResoScan System. Furthermore, the ResoScan System was tested using Milli-Q water and polystyrene microbeads. The experiments on Milli-Q water revealed that ultrasonic velocities recorded during temperature scans were affected by systematic errors and thus a correction procedure was developed. The experiments on the polystyrene microbeads were unfortunately not usable to assess the accuracy of the ResoScan System. Nevertheless, the experiments conducted on the polystyrene microbeads were educational as they revealed that the process of performing experiments on systems with a relatively high chemical complexity is not trivial and that several sources of errors may lead to unsuccessful experiments. This emphasizes the need for a high thoroughness when conducting the experiments in the case studies considered in the following three chapters.

Chapter 5

Case study: Low-weight molecules

The simplest of the three classes of aqueous solutions considered in the three case studies is the solutions containing low-weight molecules. Thus the first of the case studies is concerned with this class of solutions, with special emphasis put on aqueous solutions containing two different types of salts, namely NaCl and CaCl₂.

5.1 Relevant chemical introduction

When NaCl and CaCl₂ on crystallized form is added to water, the crystal dissociates causing the dissolution of Na⁺, Ca²⁺ and Cl⁻ ions indicating that the free energy of water-ion interaction is lower than the free energy of ion-ion interaction [49].

The interaction between the dissolved ions and the water solvent will entail an altered structure of the water solvent due to two reasons. Firstly, the water in the solution will be directly excluded from a cavity arising due to the intrinsic volume of the ions as well as their thermal fluctuations. Secondly, the structure of the water will be altered due to the chemical interaction between the water and the ions [17]. This interaction can be described as ion-dipole interactions since the water molecule is electrically polar. Thus the net negative charge on the oxygen atoms will be attracted to the cations whereas the net positive charge on the hydrogen atoms will be attracted to anions causing the water molecules to be directly organized in hydration shells around the ions [49]. A schematic drawing of this situation is seen in Fig. 5.1 in the case of Na⁺ and Cl⁻ assuming a coordination number of 5 for Na⁺ and 7 for Cl⁻ [42].

The strength of the interaction between water molecules and the ionic compounds depends on the charge density of the ions. The higher the charge density, the stronger the interaction. The properties of the water in the vicinity of the ions depend on the strength of this interaction. Hence ions with a high charge density will cause an immobilization and electrostriction of their surrounding water and will thus entail a higher degree of order in the water in the vicinity of the ions. However, if the charge density of the ions is sufficiently low, as in the case of K⁺, the ion-water interactions may actually be weaker than the water-water interactions. Hence water in the vicinity of such ions may actually be more mobile than water found in the bulk. Note that an anion of the same numerical

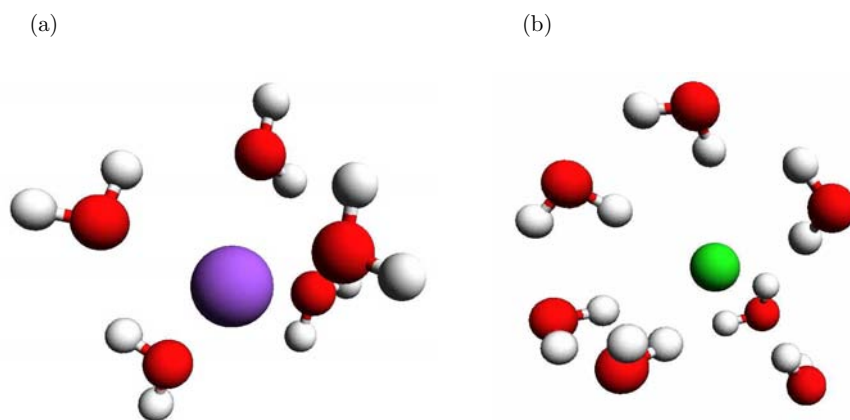


Figure 5.1: Ball-and-stick diagram of the hydration of (a) Na^+ and (b) Cl^- . The red balls represent oxygen atoms, the white balls represent hydrogen atoms, the purple ball represents a sodium ion and the green ball represent a chlorine ion. A coordination number of 5 is assumed for Na^+ and 7 for Cl^- . The cationic Na^+ interacts with the net negative charge on the water oxygen atoms whereas the anionic Cl^- interacts with the net positive charge on the water hydrogen atoms.

charge density as a given cation will interact more strongly with the water. This is because of the strong electronegativity of the oxygen atoms inducing a higher affinity for interaction between the water hydrogen atom and the anion. Furthermore, the intra-shell hydrogen bonding in the first hydration shell also plays a role in the stronger anionic hydration [20].

In the case of increasing temperature, the ion-water interaction also depends on the charge density of the hydrated ion. Increasing the temperature, and thereby decreasing the strength of the bulk water-water interactions, will thus cause the hydration shell surrounding ions with high charge density to contract and the water molecules in this hydration shell to bind more strongly to the ion. In the case of ions with low charge density the situation is opposite as the water in the hydration shells will expand and bind more weakly to the ions [77].

5.2 Ultrasonic introduction

When simple salt such as NaCl and CaCl_2 , and low-weight molecules in general, are added to water to create an aqueous solution, the ultrasonic properties of the emerging solution are altered compared to a pure water sample. For example, the ultrasonic velocity increases when NaCl and CaCl_2 is added to water. As discussed in Section 2.4, the differential ultrasonic velocity between an aqueous solution and a water reference can be interpreted in terms of intrinsic and hydration effects. However, since the intrinsic compressibility of solutes is related to the compressibility of the atomic van der Waals volumes and the intramolecular covalent bonds, it is widely acknowledged that the intrinsic contribution

from low-weight molecules to the compressibility can be neglected [16, 36, 47].

5.3 Experimental procedure

The experiments conducted in this case study applied five different types of samples. Firstly, pure Milli-Q. Secondly, aqueous NaCl solutions created by adding proper amounts of NaCl on crystallized form to Milli-Q water. Thirdly, a HEPES buffer that is used in all experiments conducted in the case studies in Chapters 6 and 7 on surfactants and proteins and thus designed for this purpose. The HEPES buffer was prepared from Milli-Q water and contained 10 mM HEPES buffering agent to ensure a pH of approximately 7.0, 1 mM sodium azide to prevent microbial growth, 0.05 mM EDTA chelator to bind polyvalent ions and thus prevent contamination from e.g. specific binding of divalent calcium ions, and finally 10 mM NaCl to screen electrostatic repulsions, i.e. the Debye screening from the monovalent ions diminishes the electrostatic repulsions from charged residues in the solution which from previous experience in the laboratories on Novozymes is known to give better and more predictable behavior of the sample under investigation. pH of the HEPES buffer was adjusted to 7.0 by NaOH and HCl. Fourthly, NaCl HEPES buffer solutions created by adding proper amounts of NaCl on crystallized form to the HEPES buffer. Fifthly, CaCl₂ HEPES buffer solutions created by adding proper amounts of CaCl₂ on crystallized form to the HEPES buffer.

Experiments were conducted using five different combinations of the aforementioned five types of samples. Firstly, experiments were conducted with Milli-Q water in resonator cavity 1 and aqueous NaCl solutions in resonator cavity 2 for both varying NaCl concentration and varying temperature. The experiment with varying NaCl concentration was conducted at 25°C using a number of aqueous NaCl samples of varying NaCl concentration up to 100 mM prepared by serial dilution from a stock aqueous 100 mM NaCl solution. The aqueous NaCl samples were injected into resonator cavity 2 using an approach similar to the approach for the experiments on the polystyrene microbead suspensions described in Section 4.2.1. The temperature scan was conducted using an aqueous 40 mM NaCl solution utilizing the script with a scan rate of 300 mK min⁻¹. Secondly, a temperature scan was conducted with HEPES buffer in resonator cavity 1 and 60 mM NaCl HEPES buffer solution in resonator cavity 2 utilizing the script a scan rate of 500 mK min⁻¹. Thirdly, a temperature scan was conducted with Milli-Q water resonator cavity 1 and HEPES buffer in resonator cavity 2 utilizing the script with a scan rate of 300 mK min⁻¹. Fourthly, experiments were conducted for aqueous NaCl solution in resonator cavity 1 and NaCl HEPES buffer solution with the same NaCl concentration in resonator cavity 2 for both varying NaCl concentration between 0 to 100 mM and temperature. Samples used in the concentration scans were prepared by performing a serial dilution from a stock aqueous 100 mM NaCl solution and a 100 mM NaCl HEPES buffer solution and conducted by injecting samples into the resonator cavities in order of increasing NaCl concentration again using an approach similar to the approach for the experiments on the polystyrene microbeads described in Section 4.2.1. The temperature scan was conducted with aqueous 40 mM NaCl solution in resonator cavity 1 and 40 mM NaCl HEPES buffer solution in

resonator 2 by running the script with scan rate of 500 mK min^{-1} . Fifthly, a temperature scan was conducted on HEPES buffer in resonator cavity 1 and 60 mM CaCl_2 HEPES buffer solution in resonator cavity 2 by running the script with 500 mK min^{-1} .

5.4 Results

Differential ultrasonic velocities recorded for Milli-Q water in resonator cavity 1 and aqueous NaCl solutions in resonator cavity 2 at 25°C for varying NaCl concentration are shown in Fig. 5.2 (a). Uncertainties are assumed to be 4.7 cm s^{-1} cf. Section 3.3.3. The dif-

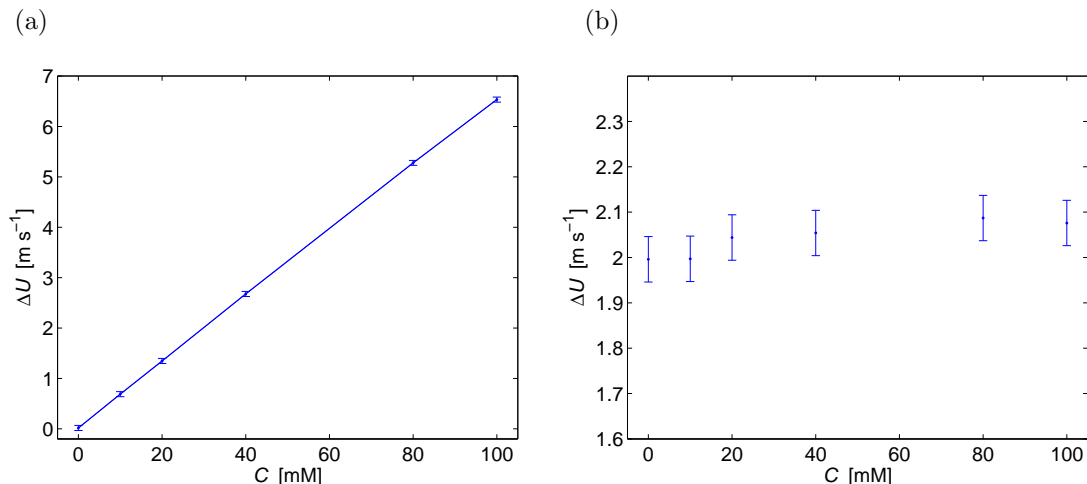


Figure 5.2: Differential ultrasonic velocity, ΔU , for varying NaCl concentration, C , recorded at 25°C with (a) Milli-Q water in resonator cavity 1 and aqueous NaCl solution in resonator cavity 2 and (b) aqueous NaCl solution in resonator cavity 1 and NaCl HEPES buffer solution of the same NaCl concentration in resonator cavity 2. The results imply that the assumption of infinite dilution is valid and that the effect of intermolecular interaction is negligible.

Differential ultrasonic velocity in Fig. 5.2 (a) agrees well with the literature [28]. The linear concentration-dependence indicates that the equations based on the assumption of infinite dilution derived in Section 2.4 are sufficient to account for the recorded differential ultrasonic velocities. Furthermore, the linear dependence also indicates that the effect of the long-range coulombic interactions between the ionic components to the differential ultrasonic velocity are negligible [28]. Differential ultrasonic velocities recorded for aqueous NaCl solution in resonator cavity 1 and NaCl HEPES buffer solution of the same NaCl concentrations in resonator cavity 2 for varying NaCl concentrations are shown in Fig. 5.2 (b). The recorded differential ultrasonic velocities are given by an approximately constant level implying that the assumptions of infinite dilution and no solute-solute interaction also are valid in the case of the NaCl HEPES buffer solutions.

The differential ultrasonic velocities recorded in the temperature scans are shown in Fig. 5.3. All curves are corrected by the correction procedure presented in Section 4.1.6 and

subsequently smoothed. The differential ultrasonic velocities recorded with Milli-Q water in resonator cavity 1 and aqueous 40 mM NaCl solution in resonator cavity 2 are multiplied by $3/2$ to make them directly comparable to differential ultrasonic velocities recorded with HEPES buffer in resonator cavity 1 and 60 mM HEPES buffer solution in resonator cavity 2. All curves exhibit a characteristic decreasing trend. The interpretation of this trend is

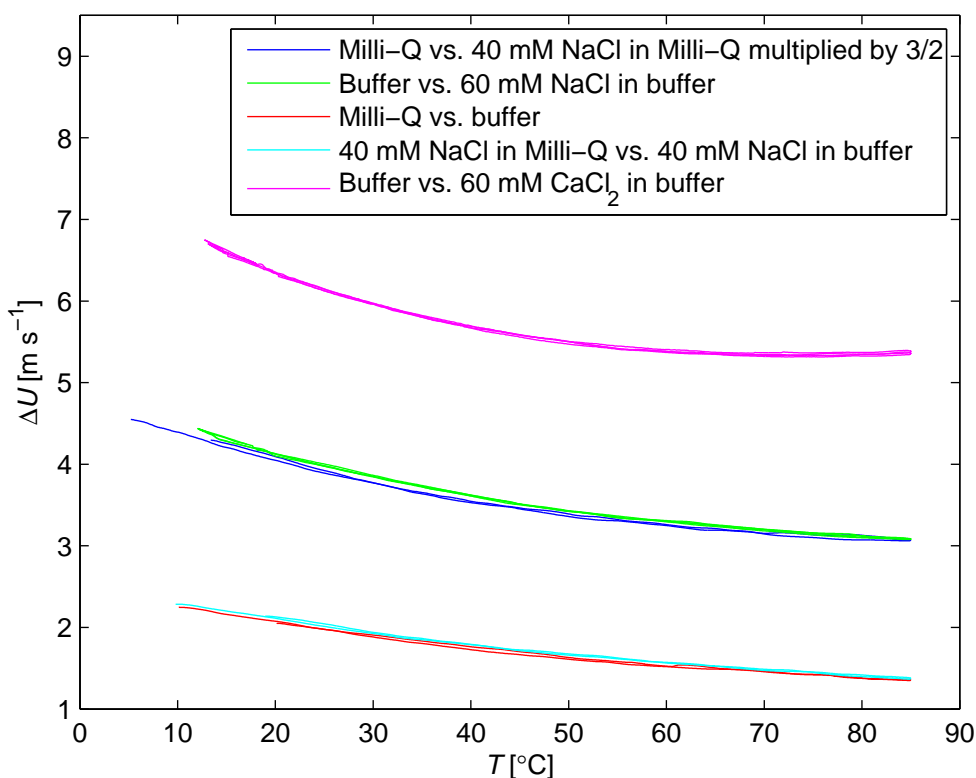


Figure 5.3: Differential ultrasonic velocities, ΔU , recorded using a number of aqueous solutions containing NaCl, CaCl_2 and low-weight buffer molecules for varying temperature, T . ΔU represents the differential ultrasonic velocity given by $U_2 - U_1$ where U_1 is the absolute ultrasonic velocity in resonator cavity 1 and U_2 is the absolute ultrasonic velocity in resonator cavity 2. The legends in the figure show the sample in resonator cavity 1 vs. the sample in resonator cavity 2. The buffer is the HEPES buffer introduced in Section 5.3. Differential ultrasonic velocities recorded for aqueous 40 mM NaCl solution are multiplied by $3/2$ to directly compare to the differential velocities recorded for 60 mM NaCl HEPES buffer solution. All curves exhibit a characteristic decreasing trend. Some of the curves on the figure are coinciding implying that an additive assumption is true over the entire temperature range.

discussed in Sections 5.5.2 and 5.5.3. The curve obtained for aqueous 40 mM NaCl solution in resonator cavity 1 and 40 mM NaCl HEPES buffer solution in resonator cavity 2 and

the curve obtained for Milli-Q water in resonator cavity 1 and HEPES buffer in resonator cavity 2 are only separated by a small difference of approximately 10 cm s^{-1} over the entire temperature range, while the curve obtained with Milli-Q water in resonator cavity 1 and aqueous 40 mM NaCl solution in resonator cavity 2 and the curve obtained with HEPES buffer in resonator cavity 1 and 60 mM NaCl HEPES buffer solution in resonator cavity 2 is coincident over the entire temperature range when first curve is multiplied by $3/2$. The implications of these observation are discussed in Section 5.5.1.

The ultrasonic absorption did not react upon addition of salt and thus no absorption results are presented in this chapter.

5.5 Discussion

5.5.1 The additive assumption

The linear trends seen for aqueous NaCl solutions at 25°C in Fig. 5.2 are also well-known for a number of other low-weight molecules dissolved in aqueous solutions such as a number of different salts [28] and monomeric surfactants [27] when the temperature is in the vicinity of room temperature. As mentioned in the previous section, these linear trends indicate that the assumption of infinite dilution is valid and that the solutes in the solution do not interact. This in turn also implies that the contributions from the individual solutes of a solution to the differential ultrasonic velocity are additive, cf. Eq. (2.34). For example, differential ultrasonic velocity due to a given salt dissociating in aqueous solution can be related to the contribution from the individual ions comprising the salt.

Interestingly, the fact that some of the curves on Fig. 5.3 are coincident over the entire temperature range implies that the assumption of additivity of the individual components of the solution also holds true for the entire temperature range and not just in the vicinity of room temperature. This leads to interesting possibilities for the interpretation of the differential ultrasonic velocities recorded for salt in aqueous to be discussed in Section 5.5.3.

The linear curves recorded in this section also implies that the partial molar volume and partial molar adiabatic compressibility is constant in the concentration and temperature regimes considered, see Eq. (2.30). However, it is known from the literature that the partial molar volume of a given solute in fact is dependent on the concentration of that solute [43, 45]. During the work of this thesis, no articles in the literature were found to treat this emerging paradox and the duration of the project time did not allow for a thorough analysis on the problem.

5.5.2 Density or compressibility

It is by now well-known to the reader that the ultrasonic velocity of a given medium depends on the density and adiabatic compressibility coefficient of that medium. This raises the question whether the differential ultrasonic velocities recorded in this chapter can be related to density or compressibility changes of the aqueous solutions. To answer this question, knowledge on the densities of the investigated aqueous solutions is needed. As mentioned in Chapter 1, densimetric equipment is not available for this thesis. However,

densimetric data is readily accessible in the literature for aqueous solutions based on 306 inorganic compounds, including NaCl and CaCl₂ through a wide concentration and temperature ranges [45]. Hence the density of an aqueous salt solution, ρ_{salt} , with molar salt concentration C at temperature T can be calculated from

$$\rho_{\text{salt}}(C, T) = \rho_{\text{wa}}(T) + AC + BCT + KCT^2 + DC^{3/2} + EC^{3/2}T + FC^{3/2}T^2, \quad (5.1)$$

where ρ_{wa} is the density of water given by

$$\begin{aligned} \rho_{\text{wa}}(T) = & 999.65 \text{ (kg m}^{-3}\text{)} + 2.0438 \text{ (kg }^\circ\text{C}^{-1} \text{ m}^{-3}\text{)} \times 10^{-1}T - \\ & 6.174 \text{ (kg }^\circ\text{C}^{-3/2} \text{ m}^{-3}\text{)} \times 10^{-2}T^{3/2}, \end{aligned} \quad (5.2)$$

and the constants A , B , K , D , E and F are dependent on the type of salt dissolved. For NaCl the constants are given by

$$A_{\text{NaCl}} = 0.4485 \times 10^2 \text{ kg M}^{-1} \text{ m}^{-3}, \quad (5.3a)$$

$$B_{\text{NaCl}} = -0.9634 \times 10^{-1} \text{ kg M}^{-1} \text{ }^\circ\text{C}^{-1} \text{ m}^{-3}, \quad (5.3b)$$

$$K_{\text{NaCl}} = 0.6136 \times 10^{-3} \text{ kg M}^{-1} \text{ }^\circ\text{C}^{-2} \text{ m}^{-3}, \quad (5.3c)$$

$$D_{\text{NaCl}} = -2.712 \text{ kg M}^{-3/2} \text{ m}^{-3}, \quad (5.3d)$$

$$E_{\text{NaCl}} = 1.009 \times 10^{-2} \text{ kg M}^{-3/2} \text{ }^\circ\text{C}^{-1} \text{ m}^{-3}, \quad (5.3e)$$

$$F_{\text{NaCl}} = 0 \text{ kg M}^{-3/2} \text{ }^\circ\text{C}^{-2} \text{ m}^{-3}. \quad (5.3f)$$

Densities calculated for water and aqueous NaCl solutions using the above equations compare well with other values in the literature [39, 40].

The importance of changes in density for the NaCl solution over the entire temperature range can thus be calculated using Eq. (2.29). Hence defining the relative molar increment in ultrasonic velocity, $[U]$, to be

$$[U] = \frac{U - U_0}{U_0 C}, \quad (5.4)$$

the contribution to the relative molar increment from density, $[U]_\rho$, is found by calculating the fraction

$$[U]_\rho = -\frac{\rho - \rho_0}{2C\rho_0}, \quad (5.5)$$

Results of calculations for aqueous NaCl solutions are shown in Fig. 5.4 (a). The compressibility contribution to the relative increment in ultrasonic velocity, $[U]_{\beta_S}$, in the figure is calculated by taking $[U] - [U]_\rho$.

For aqueous CaCl₂ solutions, the densities are calculated using [45]

$$A_{\text{CaCl}_2} = 1.012 \times 10^2 \text{ kg M}^{-1} \text{ m}^{-3}, \quad (5.6a)$$

$$B_{\text{CaCl}_2} = -6.156 \times 10^{-1} \text{ kg M}^{-1} \text{ }^\circ\text{C}^{-1} \text{ m}^{-3}, \quad (5.6b)$$

$$K_{\text{CaCl}_2} = 1.028 \times 10^{-3} \text{ kg M}^{-1} \text{ }^\circ\text{C}^{-2} \text{ m}^{-3}, \quad (5.6c)$$

$$D_{\text{CaCl}_2} = -9.749 \text{ kg M}^{-3/2} \text{ m}^{-3}, \quad (5.6d)$$

$$E_{\text{CaCl}_2} = 96.94 \times 10^{-2} \text{ kg M}^{-3/2} \text{ }^\circ\text{C}^{-1} \text{ m}^{-3}, \quad (5.6e)$$

$$F_{\text{CaCl}_2} = -3.165 \times 10^{-4} \text{ kg M}^{-3/2} \text{ }^\circ\text{C}^{-2} \text{ m}^{-3}, \quad (5.6f)$$

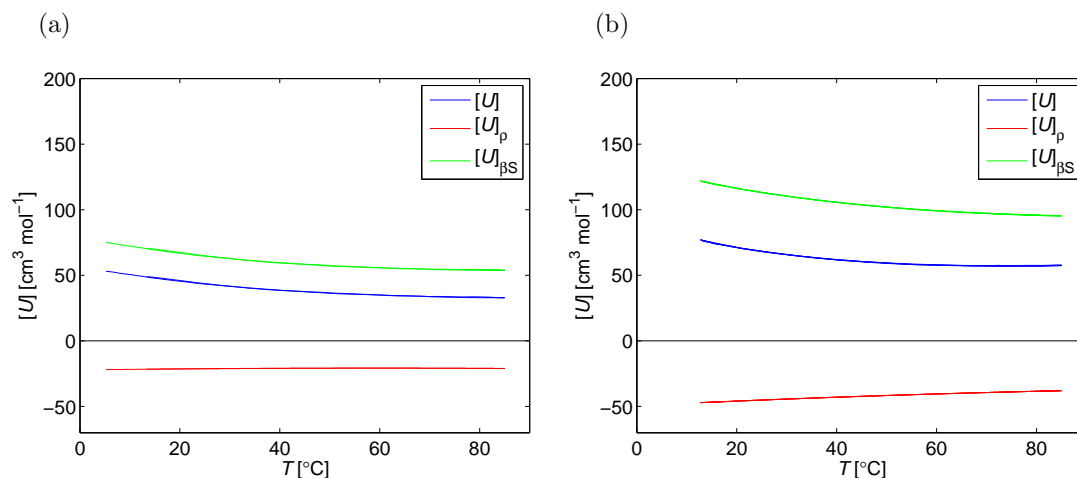


Figure 5.4: Calculated values of the relative importance of density contributions, $[U]_\rho$, and compressibility contributions, $[U]_{\beta_S}$, to the relative molar increments in ultrasonic velocity, $[U]$ as a function of temperature, T , for (a) aqueous NaCl solutions and (b) aqueous CaCl_2 solutions. $[U]_\rho$ is calculated using density information from the literature [45] whereas $[U]_{\beta_S}$ is calculated by taking $[U] - [U]_\rho$. Figures show that both density and compressibility are in general important to account for $[U]$. Calculations for the NaCl solutions however imply that temperature-dependent variations in $[U]$ are primarily due to variations in solution compressibility. Calculations for CaCl_2 solutions show that temperature-dependent variations in $[U]$ are both due to density and compressibility effects, but the strength of this conclusion is questioned by the accuracy of the calculated density contributions.

where the constant B_{CaCl_2} is corrected from what appears to be a misprint in the article. Densities calculated for aqueous CaCl_2 compare reasonable well, although not completely perfect, with values found in the literature [40]. Calculations on the importance of density and compressibility changes in aqueous CaCl_2 solutions are then performed using the same procedure as the calculations on the aqueous NaCl solutions and results are shown in Fig. 5.4 (b).

Results in Fig. 5.4 show that changes in ultrasonic velocities that occur when NaCl and CaCl_2 are added to water are related to both changes in solution density and compressibility. Thus the densities of the solutions increase when salt is added entailing a negative contribution to the differential ultrasonic velocities whereas the compressibilities of the solutions decrease, due to the structuring of the water in the hydration shells surrounding the ions, entailing a positive contribution to the differential ultrasonic velocities. However, the results also show that in the case of aqueous NaCl solutions, the characteristic decreasing trends of the differential ultrasonic velocities, seen in Fig. 5.3, are primarily related to changes in compressibility, i.e. the density contribution to the relative molar increment in ultrasonic velocity, seen in Fig. 5.4 (a), only account for approximately 5 % of the temperature-dependent variations in the relative molar increment in ultrasonic

velocity for the aqueous NaCl solutions. In the case of the aqueous CaCl₂ solutions it is found that the density contribution to the temperature-dependent variations in the relative molar increment, seen in Fig. 5.4 (b), in ultrasonic velocity is approximately 50 %. It is however strongly suspected that this high percentage is found due to a too low quality of the fit to the densities of aqueous CaCl₂ solutions.

5.5.3 Hydration

It is clear that the hydration of low-weight molecules is an important contribution to the differential ultrasonic velocities recorded in this case study. The question is then if ultrasonic velocimetry as a stand-alone technique can be used to obtain hydration information of low-weight molecules. To answer this question, the topic of ionic hydration, discussed in Section 5.1, is reexamined in this section. Hence consider the results obtained by Uedaira and Suzuki who examined the effect of adding 0.5 mol kg⁻¹ alkali-metal chlorides to water on the ultrasonic velocity [70]. Assuming the validity of the additive assumption from Section 5.5.1 in this concentration regime, it is possible to relate differences in ultrasonic velocities recorded for the various types of alkali-metal chlorides solely to the properties of the alkali-metal ions since the contribution from the Cl⁻ ions are the same for all samples. It was found that the alkali metal with the highest charge densities and thus the strongest hydration also in general increased the ultrasonic velocity the most. In the case of the weakly hydrated Cs⁺ ion, the ultrasonic velocity was actually found to decrease. The only exception to this rule is Na⁺ and Li⁺ since Na⁺ increases the ultrasonic velocity more than Li⁺. However, other effects related to the size and thus the hydration number of the ion may explain this discrepancy.

Another way to use the ultrasonic velocity to examine the hydration strength is to consider the temperature scans measured using the ResoScan System for NaCl and CaCl₂. It is found that the temperature curve for CaCl₂ seems to flatten slightly more when the temperature is increased than the temperature curve for NaCl in Fig. 5.3. This may be indicative of stronger hydration of the Ca²⁺ or Cl⁻ ions than the Na⁺ ion since the strongly hydrated ions bind the surrounding water more strongly when the temperature is high than the weakly hydrated ions [77]. Even though this is only a rough hypothesis that can not be confirmed before the contributions from the individual ions via systematic experiments and the additive assumption are surveyed, it is clear that the ultrasonic velocity as a stand-alone technique applied on aqueous solutions containing low-weight molecules may potentially give rise to interesting hypotheses on the hydration of these molecules.

In the case of the 306 inorganic substances where density data is given directly in the literature [45], it is actually not necessary to have access to densimetric equipment to volumetrically characterize the properties of the dissolved substances, as exemplified in Section 5.5.2. Hence a more complete theory for these substances can be developed only conducting ultrasonic velocimetry experiments to obtain compressibility information which in turn can be used to formulate mathematical models on ionic hydration like the models formulated by Onori *et al.* [47, 48].

5.6 Summary

After the introduction of basic chemical theory on ionic hydration, results recorded for low-weight molecules dissolved in aqueous solutions were presented. These results implied that the additive assumption, well-known from several sources in the literature, is applicable to the entire temperature range between 5 and 85°C. This observation is of fundamental importance when interpreting data obtained using ultrasonic velocimetry. Furthermore, a literature source for calculating the densities of 306 inorganic compounds [45] was presented thus obviating the necessity of densimetric equipment to characterize these compounds allowing for the use of ultrasonic velocimetry as a stand-alone technique. Using this literature source, calculations were conducted to assess the relative importance of density and compressibility to differential ultrasonic velocities recorded for aqueous salt solutions and it was found that both density and compressibility contributions are important. However, it was also found that in the case of aqueous NaCl solutions, the density contribution was relatively constant across the entire temperature range. Calculations for aqueous CaCl₂ found that the temperature-dependence of both the density contribution and the compressibility contribution are important to describe the temperature-dependent properties of differential ultrasonic velocities, but results were affected by insufficient accuracy of the density calculations rendering any conclusions drawn upon the results highly questionable. Finally, the possibility of using ultrasonic velocities alone to obtain information on the hydration of ionic compounds in aqueous solution was discussed.

Chapter 6

Case study: Surfactants

The second case study is concerned with aqueous solutions containing surfactants. The properties of surfactants make them usable in a long number of applications, including detergent applications. Hence their amphiphilic nature make them capable of associating to various kinds of dirt and thereby removing the dirt [10]. The chemical complexity of the aqueous surfactant solutions is higher than the complexity of the solutions containing simple salts and low-weight molecules considered in the previous case study. Therefore it is necessary to consider the hypotheses and conclusions developed in the previous case study and evaluate their extent of validity in the case of aqueous surfactant solutions.

6.1 Relevant chemical introduction

In general, surfactants consist of two types of segments with hydrophilic and hydrophobic properties. The hydrophilic segment is polar or charged in nature whereas the hydrophobic segment is nonpolar in nature. The hydrophobic segment typically comprises a hydrocarbon chain [25]. The following case study considers two different surfactants, namely octyl glucoside (OG) and sodium dodecyl sulfate (SDS). OG contains a polar glucose head group bound to an alkyl chain containing 8 carbon atoms, see Fig. 6.1 (a), whereas SDS contains an anionic sulfate head group associated with an alkyl chain containing 12 carbon atoms, see Fig. 6.1 (b). One of the characteristic features of surfactants is their propensity to associate into dynamic aggregate structures with a hydrophobic core and a hydrophilic exterior. These aggregate structure emerge when the surfactant concentration is above a critical concentration called the critical micelle concentration (cmc) [25]. An important contribution to the driving forces underlying the formation of these aggregate structures, is the tendency of hydrophobic molecules to cluster in water. To understand the molecular origins of the hydrophobic effect, imagine a small nonpolar molecular compound located in a water sample. Due to the nonpolar properties of the molecular compound, the water molecules will not directly bind to the compounds as in the case of ionic hydration. Rather, the adjacent water molecules will spatially reorganize to sustain the same extent of hydrogen bond network as in bulk water. This spatial structuring of the water will however have an entropic cost favoring the direct association of nonpolar compounds in water

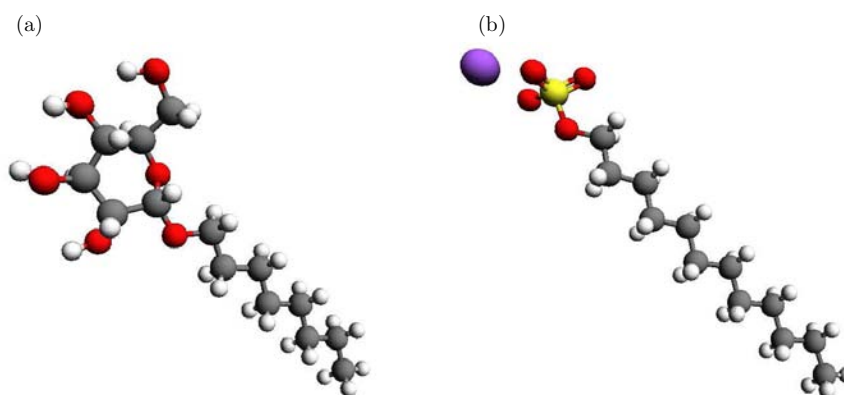


Figure 6.1: Ball-and-stick diagram of (a) octyl glucoside (OG) comprising a polar glucose head group and a hydrocarbon chain with 8 carbon atoms and (b) sodium dodecyl sulfate (SDS) comprising an anionic sulfate head group and a hydrocarbon chain with 12 carbon atoms. The grey balls represent carbon atoms, the white balls represent hydrogen atoms, the red balls represent oxygen atoms, the yellow ball represents a sulfur atom and the purple ball represents a sodium ion.

and thus the formation of the aforementioned dynamic surfactant aggregate structures. A number of other contributions to the free energy of aggregate formation should also be taken into account. These include the free energy of mixing that is dominant at low surfactant concentration causing the surfactants to remain in their monomer form. Furthermore, the aggregate formation is opposed by the free energy contribution arising from the formation of interfaces and the spatial configurational constraint of the surfactants when they are organized in the aggregate structures [18].

The type of aggregate structure and size depends on the geometrical properties of the considered surfactant molecules. Typically surfactants aggregate into spherical or prolate ellipsoid micelle structures. Adding electrolytes to solutions containing ionic surfactants will decrease the cmc and increase the size of the micelle due to the electrical screening from the electrolyte whereas adding electrolytes to nonionic solutions not will affect the cmc and micellar size. In contrast, varying the temperature has a relatively small effect on the aggregation number and micellar size of ionic surfactants, whereas heating of solutions containing nonionic surfactants may affect the cmc. Moreover, heating of nonionic surfactants solutions may result in turbidity of the solution at a characteristic temperature due to occurrence of two phases in the solution. This characteristic temperature is called the cloud point [25].

OG forms micelles in water at a cmc of approximately 25 mM [35] at 25°C. For varying temperature between 0 to 30°C the cmc for OG varies between 39 to 21 mM [1]. The aggregation numbers of OG micelles is approximately 25 across a temperature range from 25 to 45°C [12]. MD simulations imply that the polar glucose head group is fully hydrated in the micelle state whereas the hydrophobic interior is relatively inaccessible to

the aqueous solvent [35]. SDS forms micelles in water at a critical micelle of approximately 9 mM [23, 32] across a wide temperature range [25]. The aggregation number of SDS in water is 60 [32].

6.2 Ultrasonic introduction

Even though the chemical complexity of aqueous solutions containing surfactants is higher than the aqueous solutions containing salt, it can still be assumed that contribution from the compressibility to the differential ultrasonic velocity between an aqueous reference sample and an aqueous surfactant solution below the cmc is due to hydration [36]. However, above the cmc, the intrinsic micelle compressibility also plays a role and can not be neglected in the theoretical description of the ultrasonic velocity [27, 36].

In the case study on low-weight molecular solutions, it was found that the contributions from the individual molecular components of the solutions to the differential ultrasonic velocity were additive. This raises the question whether the contributions from the individual molecular groups on the surfactants molecules also can be viewed as additive, i.e. does the contribution from a given molecular group in a molecule depend on the properties of the adjacent molecules groups. In fact, it is well-known that volumes of individual molecular groups on a given molecule can be treated in an additive manner, but that the compressibilities can not due to subtle effects related to intramolecular interaction [16]. To further elucidate this subject, a mathematical model is formulated.

6.2.1 Mathematical model

The mathematical model is inspired by the model found in a paper written by Galán *et al.* [27] and takes its point of origin in the multicomponent formulation in Eq. (2.34), i.e. it is formulated in the limit of infinite dilution. Furthermore, it is assumed that the contributions from the individual molecular groups on the surfactant molecules are additive. Moreover, it is assumed that the surfactant solution can be viewed as a phase separation model where the cmc represents a saturation point of the monomeric surfactants, i.e. when the surfactant concentration is above the cmc, the monomeric surfactant concentration is constant and the micelles are treated as a distinct phase [25]. Hence the dynamical properties of the micelles are neglected in this formulation. Finally, it is assumed that the ultrasonic properties of the molecular groups in the surfactant solution are not affected by the low-weight molecules in the buffer dissolving the surfactants.

Below the cmc the differential ultrasonic velocity between an aqueous surfactant solution and a relevant aqueous water reference system must then according to multicomponent formulation be given by

$$\Delta U = \left(-\frac{K_{\text{mon}}^{\circ}}{2\beta_{S0}} + V_{\text{mon}}^{\circ} - \frac{M_{\text{sur}}}{2\rho_0} \right) C_{\text{sur}} U_0, \quad (6.1)$$

where V_{mon}° and K_{mon}° is the partial molar volume and partial molar adiabatic compressibility of the surfactants in their monomeric state, respectively, M_{sur} is the molar mass of the surfactants and C_{sur} is the concentration of the surfactants. When the surfactant

concentration is above the cmc this equation must be extended to include the contribution from the micelles emerging in the solution. Thus the change in ultrasonic velocity must now be given by

$$\Delta U = \left(-\frac{K_{\text{mon}}^{\circ}}{2\beta_{S0}} + V_{\text{mon}}^{\circ} - \frac{M_{\text{sur}}}{2\rho_0} \right) C_{\text{cmc}} U_0 + \left(-\frac{K_{\text{mic}}^{\circ}}{2\beta_{S0}} + V_{\text{mic}}^{\circ} - \frac{M_{\text{sur}}}{2\rho_0} \right) (C_{\text{sur}} - C_{\text{cmc}}) U_0, \quad (6.2)$$

where V_{mic}° and K_{mic}° is the partial molar volume and partial molar adiabatic compressibility of the surfactants in their micelle state, respectively, and C_{cmc} is the cmc.

For OG solutions below the cmc, the monomeric contributions are split into contributions from 7 -CH₂- groups and methyl glucoside, see Fig. 6.1 (a). Thus Eq. (6.1) can be rewritten into

$$\Delta U = \left(-\left[\frac{7K_{\text{CH}_2}^{\circ} + K_{\text{MG}}^{\circ}}{2\beta_{S0}} \right] + 7V_{\text{CH}_2}^{\circ} + V_{\text{MG}}^{\circ} - \left[\frac{7M_{\text{CH}_2} + M_{\text{MG}}}{2\rho_0} \right] \right) C_{\text{sur}} U_0, \quad (6.3)$$

where $V_{\text{CH}_2}^{\circ}$, $K_{\text{CH}_2}^{\circ}$ and M_{CH_2} is the partial molar volume, partial molar adiabatic compressibility and molar mass of a single -CH₂- group in the alkyl chain of a monomeric surfactant, respectively, and V_{MG}° , K_{MG}° and M_{MG} is the partial molar volume, partial molar adiabatic compressibility and molar mass of methyl glucoside, respectively. Above the cmc, the micelle contributions are split into contributions from the -CH₂- groups in the hydrocarbon cores and the polar glucose head groups, where it is assumed that the contributions from the glucose head groups in micelles are the same as the contributions from the glucose head groups in monomeric OG. Hence it is assumed that the hydration of the glucose head groups in their micelle state is the same as the hydration of glucosde head groups in the monomer state [35] and Eq. (6.2) is rewritten to

$$\Delta U = \left(-\left[\frac{7K_{\text{CH}_2}^{\circ} + K_{\text{MG}}^{\circ}}{2\beta_{S0}} \right] + 7V_{\text{CH}_2}^{\circ} + V_{\text{MG}}^{\circ} - \left[\frac{7M_{\text{CH}_2} + M_{\text{MG}}}{2\rho_0} \right] \right) C_{\text{cmc}} U_0 + \left(-\left[\frac{7K_{\text{core}}^{\circ} + K_{\text{MG}}^{\circ}}{2\beta_{S0}} \right] + 7V_{\text{core}}^{\circ} + V_{\text{MG}}^{\circ} - \left[\frac{7M_{\text{CH}_2} + M_{\text{MG}}}{2\rho_0} \right] \right) (C_{\text{sur}} - C_{\text{cmc}}) U_0, \quad (6.4)$$

where V_{core}° and K_{core}° is the partial molar volume and partial molar adiabatic compressibility of a single -CH₂- group in the core of the micelles, respectively.

Using an approach similar to the above approach for OG, the change in ultrasonic velocity occurring when SDS, below the cmc, is added to an aqueous solution is given by

$$\Delta U = \left(-\left[\frac{11K_{\text{CH}_2}^{\circ} + K_{\text{SMS}}^{\circ}}{2\beta_{S0}} \right] + 11V_{\text{CH}_2}^{\circ} + V_{\text{SMS}}^{\circ} - \left[\frac{11M_{\text{CH}_2} + M_{\text{SMS}}}{2\rho_0} \right] \right) C_{\text{sur}} U_0, \quad (6.5)$$

where V_{SMS}° , K_{SMS}° and M_{SMS} is the partial molar volume, partial molar adiabatic compressibility and molar mass of a sodium methyl sulfate, respectively. Above the cmc, the

differential ultrasonic velocity can be calculated by

$$\Delta U = \left(- \left[\frac{11K_{\text{CH}_2}^{\circ} + K_{\text{SMS}}^{\circ}}{2\beta_{S0}} \right] + 11V_{\text{CH}_2}^{\circ} + V_{\text{SMS}}^{\circ} - \left[\frac{11M_{\text{CH}_2} + M_{\text{SMS}}}{2\rho_0} \right] \right) C_{\text{cmc}}U_0 + \quad (6.6)$$

$$\left(- \left[\frac{11K_{\text{core}}^{\circ} + K_{\text{SMS}}^{\circ}}{2\beta_{S0}} \right] + 11V_{\text{core}}^{\circ} + V_{\text{SMS}}^{\circ} - \left[\frac{11M_{\text{CH}_2} + M_{\text{SMS}}}{2\rho_0} \right] \right) (C_{\text{sur}} - C_{\text{cmc}})U_0.$$

Proper choices of the parameters comprising the above equations are of course important to use the equations to predict the differential ultrasonic velocities of OG and SDS, respectively. The remainder of this section is thus concerned with choosing these parameters by surveying the relevant literature as well as considering data recorded by the ResoScan System. This investigation will show that it is possible to identify values for all parameters at 25°C allowing for direct comparison of the model to some of the experiments to be presented later in this chapter. However, as seen in the case on aqueous solutions containing low-weight molecules, the temperature-dependence of the differential ultrasonic velocity may also contain important information. Hence the extent of availability of temperature-dependent data on the parameters is also assessed.

Consider first the parameters associated with the reference sample, i.e. U_0 , β_{S0} and ρ_0 . In the experiments to be presented later in this chapter, this reference is the HEPES buffer solution introduced in Section 5.3. The absolute ultrasonic velocity of the reference HEPES buffer, U_0 , at 25°C is recorded using the ResoScan System and found to be 1498.5 m s⁻¹. The density and adiabatic compressibility coefficient of the HEPES buffer is unknown but since the difference in the ultrasonic velocity between the HEPES buffer and Milli-Q water is only approximately 2 m s⁻¹ throughout the entire temperature range, it is assumed that $\rho_0 = \rho_{\text{wa}}$ and $\beta_0 = \beta_{\text{wa}}$. The density of water, here denoted ρ_0 , at 25°C is 0.99704 g cm⁻³ [45]. Using this value for the density, the adiabatic compressibility coefficient of water is calculated via the Newton–Laplace equation using the ultrasonic velocity at 25°C in Milli-Q water recorded with the ResoScan System. The adiabatic compressibility coefficient of water, here denoted β_{S0} at 25°C is thus found to be 4.48×10^{-5} bar⁻¹. It should also be noted that data associated with the reference sample is accessible within a wide temperature range. Hence the ultrasonic velocities recorded using the ResoScan System is available between 5 and 85°C while data on the density and adiabatic compressibility for water is available in the literature for an even wider temperature range.

The next step is to determine the partial molar volume and partial molar adiabatic compressibility of the individual molecular groups contributing to the total change in ultrasonic velocity. Firstly, -CH₂- is considered. In the literature, the volumetric and elastic properties of -CH₂- are typically identified by systematic experiments on e.g. alkyl chains of varying chain length. Hence the partial molar volume and partial molar adiabatic compressibility of -CH₂- have been estimated using several different molecular compounds. Thus the partial molar volume of -CH₂-, $V_{\text{CH}_2}^{\circ}$, is approximately equal to 15.8 cm³ mol⁻¹ and relatively insensitive to the properties of the molecular groups found adjacent to the -CH₂- group in a given molecule [14, 36, 44]. The partial molar adiabatic compressibility of -CH₂- is much more sensitive to the nature of the adjacent molecular groups on the molecular compounds considered. For -CH₂- groups located in an alkyl chain sufficiently far from any polar or charged residues for the -CH₂- group to interact with these residues, the

Parameter	Value at 25°C	Temperature range	refs.
U_0	1498.5 m s ⁻¹	11 – 85°C	This work
ρ_0	0.99704 g cm ⁻³	0 – 100°C	[45]
β_{S0}	4.48×10^{-5} bar ⁻¹	11 – 85°C	This work and [45]
$V_{\text{CH}_2}^\circ$	15.8 cm ³ mol ⁻¹	5 – 55°C	[14, 36, 44]
V_{core}°	16.3 cm ³ mol ⁻¹	N/A	[36]
V_{MG}°	135.5 cm ³ mol ⁻¹	5 – 25°C	[33]
V_{SMS}°	50.6 cm ³ mol ⁻¹	N/A	[34]
K_{CH_2}	-1.9×10^{-4} cm ³ bar ⁻¹ mol ⁻¹	5 – 55°C	[14, 36, 44]
K_{core}	9.7×10^{-4} cm ³ mol ⁻¹ bar ⁻¹	N/A	[36]
K_{MG}	-9.8×10^{-4} cm ³ bar ⁻¹ mol ⁻¹	5 – 25°C	[33]
K_{SMS}	-45.0×10^{-4} cm ³ bar ⁻¹ mol ⁻¹	N/A	[34]

Table 6.1: Values at 25°C of the parameters used in Eqs. (6.3), (6.4), (6.5) and (6.6) to calculate the differential ultrasonic velocity. The availability of these parameters for varying temperature is also summarized.

partial molar adiabatic compressibility, K_{CH_2} , is found at 25°C to be approximately equal to -1.9×10^{-4} cm³ bar⁻¹ mol⁻¹ even though some disagreement exists in the literature of the exact value of this parameter [14, 36]. Data on the partial molar volume and partial molar adiabatic compressibility coefficient of -CH₂- is available at temperatures between 5 to 55°C [14]. The partial molar volume and partial molar adiabatic compressibility of -CH₂- is altered when -CH₂- is found in the interior of micelles. At 25°C, the partial molar volume of -CH₂-, V_{core}° , is equal to 16.3 cm³ mol⁻¹ while the partial molar adiabatic compressibility, K_{core} , is approximately equal to 9.7×10^{-4} cm³ mol⁻¹ bar⁻¹ [36]. No data on the temperature-dependence of the partial molar volume and partial molar adiabatic compressibility of -CH₂- in the micelle core were found surveying the literature.

The partial molar volume of β -methyl glucoside, V_{MG}° , and partial molar adiabatic compressibility of β -methyl glucoside, K_{MG} , in aqueous solution is at 25°C equal to 135.5 cm³ mol⁻¹ and -9.8×10^{-4} cm³ bar⁻¹ mol⁻¹, respectively [33]. Data on the partial molar volume and partial molar adiabatic compressibility of β -methyl glucoside is also available at 5°C.

The changes in ultrasonic velocity and density upon addition of sodium methyl sulfate to water have been investigated at 25°C, albeit for high concentrations in the range between 1 to 5 M [34]. Since the differential ultrasonic velocity and density are approximately linearly dependent on the concentration of sodium methyl sulfate throughout the entire concentration range, it is assumed that the data can be used to calculate the partial molar volume, V_{SMS}° , and partial molar adiabatic compressibility, K_{SMS} , of sodium methyl sulfate. At 1 M, the density of the aqueous sodium methyl sulfate solution is 1.0807 g cm⁻³. The partial molar volume of sodium methyl sulfate can then be calculated

by

$$V_{\text{SMS}}^{\circ} = \frac{M_{\text{SMS}}}{\rho_0} - \frac{\rho - \rho_0}{\rho_0 C_{\text{SMS}}}, \quad (6.7)$$

where $M_{\text{SMS}} = 134.09 \text{ g mol}^{-1}$ is the molar mass of sodium methyl sulfate. Using that the reference density is equal to the density of pure water at 25°C the partial molar volume of sodium methyl sulfate is found to be $50.6 \text{ cm}^3 \text{ mol}^{-1}$. The ultrasonic velocity in the 1 M sodium methyl sulfate solution is equal to 1546.8 m s^{-1} . Hence using Eq. (2.30) and the fact that the ultrasonic velocity in water at 25°C is equal to 1496.5 m s^{-1} , it is found that K_{SMS} is equal to $-45.0 \times 10^{-4} \text{ cm}^3 \text{ mol}^{-1} \text{ bar}^{-1}$. No temperature-dependent data on sodium methyl sulfate was found surveying the literature.

The parameters determined in the above are summarized in Table 6.1. It is clear that the availability of temperature-dependent data in the literature is not sufficient to apply the model to predict the temperature dependence of the differential ultrasonic velocities. However, it is still possible to use the model to calculate differential ultrasonic velocities at 25°C to compare with the differential ultrasonic velocities experimentally recorded for surfactant solutions at 25°C .

The molar masses used in the mathematical model are summarized in Table 6.2.

Group	M
-CH ₂ -	14.03 g mol^{-1}
Methyl glucoside	$194.18 \text{ g mol}^{-1}$
Sodium methyl sulfate	$134.09 \text{ g mol}^{-1}$

Table 6.2: Molecular masses, M , of the groups used in Eqs. (6.3), (6.4), (6.5) and (6.6) to calculate the differential ultrasonic velocity.

6.3 Experimental procedure

From the stock HEPES buffer solution, two stock surfactant solutions containing OG and SDS, respectively, were prepared by weighing out a suitable amount of surfactant powder. Hence 20 mL of 100 mM OG stock solution was prepared from OG powder of minimally 98 % purity while 20 mL of 25 mM SDS stock solution was prepared from SDS powder of approximately 95 % purity. pH of both stock surfactant solutions was adjusted to 7.0 by NaOH and HCl. The concentration of the SDS stock solution was chosen to be four times smaller than the concentration of the OG stock solution, since the cmc of SDS is expected to be approximately four times smaller than the cmc of OG. A number of surfactant solution samples of varying surfactant concentration were then created for both types of surfactants by performing a serial dilution from the stock surfactant solutions.

Experiments were conducted examining the effects of varying surfactant concentration and sample temperature. The experiments varying the surfactant concentration were conducted at 25°C with HEPES buffer in resonator cavity 1 and OG HEPES buffer solution or SDS HEPES buffer solution in resonator cavity 2 by injecting surfactant samples into resonator cavity 2 in order of increasing surfactant concentration, i.e. using an approach

similar to the approach for the polystyrene microbead suspensions. Two data points were recorded for each surfactant concentration. Two experiments on the effect of varying temperature were conducted with HEPES buffer in resonator cavity 1 and 12 mM OG and 100 mM OG, respectively, in resonator cavity 2 using the script with scan rate 300 mK min^{-1} .

6.4 Results

Results obtained for the concentration scans are presented in Fig. 6.2. Consider first the

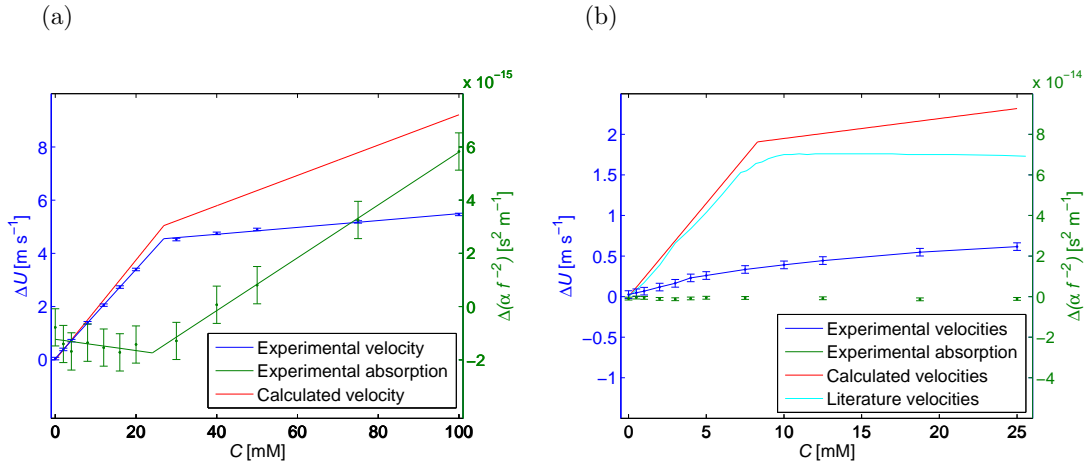


Figure 6.2: The left vertical axes on the figures represent the differential ultrasonic velocities whereas the right vertical axes represent the differential ultrasonic absorption. (a) is concerned with the setup with HEPES buffer in resonator cavity 1 and OG HEPES buffer solution of varying OG concentration in resonator cavity 2 at 25°C . The blue and dark green lines show the differential ultrasonic velocities, ΔU , and differential ultrasonic absorption, $\Delta(\alpha f^{-2})$, respectively, recorded for varying OG concentration, C . Results clearly show the existence of the cmc. The red line presents the results of the theoretical calculations showing relatively good agreement below the cmc and poor agreement above the cmc to the recorded differential ultrasonic velocities. (b) is concerned with the setup with HEPES buffer in resonator cavity 1 and SDS HEPES buffer solution of varying SDS concentration in resonator cavity 2 at 25°C . The blue line shows the experimentally recorded differential ultrasonic velocities whereas the dark green data points show the experimentally recorded differential ultrasonic absorption. Hence data recorded for SDS do not imply the existence of a cmc. However the experimentally recorded differential ultrasonic velocities do not compare well with results from the literature represented by the cyan line. Calculations from the theoretical model, shown by the red line, agree relatively well with the literature values below the cmc whereas poor agreement is seen above the cmc. Uncertainties are assumed to be $\pm 4.7 \text{ cm s}^{-1}$ and $\pm 7 \times 10^{-16} \text{ s}^2 \text{ m}^{-1}$ for the differential ultrasonic velocity and absorption, respectively.

results in Fig. 6.2 (a) recorded at 25°C for HEPES buffer in resonator cavity 1 and OG HEPES buffer solution in resonator cavity 2 for varying OG concentration. The inflections in the differential ultrasonic velocity and differential ultrasonic absorption implies that the cmc, C_{cmc} , is equal to 26.9 mM and 24.1 mM, respectively. Fortunately, the two values for C_{cmc} of OG determined from the ultrasonic velocity and ultrasonic absorption agree well to values for C_{cmc} of OG found literature [12]. A linear line is fitted to the differential ultrasonic velocities below the cmc. This line is given by: $\Delta U = 0.1673 \text{ (m s}^{-1} \text{ mM}^{-1}) \cdot C + 0.0517 \text{ m s}^{-1}$. The differential ultrasonic velocities recorded above the cmc are also fitted by a linear line given by: $\Delta U = 0.0129 \text{ (m s}^{-1} \text{ mM}^{-1}) \cdot C + 4.2030 \text{ m s}^{-1}$. The red curve on Fig. 6.2 (a) is calculated using Eqs. (6.3) and (6.4) and the parameters from Tables 6.1 and 6.2 and assuming that C_{cmc} is equal to 26.9 mM. Relatively good agreement between calculations and experiments is found below the cmc where the small difference is close to the limit of uncertainties due to uncertainties of the applied parameters. However, above the cmc, poor agreement is found between experiments and calculations.

Fig. 6.2 (b) shows results obtained at 25°C for HEPES buffer in resonator cavity 1 and SDS HEPES buffer solution in resonator cavity 2 for varying SDS concentration. The differential ultrasonic velocities exhibit an increasing trend as a function of temperature but data do not imply that the cmc is within the considered concentration range. The differential ultrasonic absorption is not sensitive to SDS concentration, except for a single outlier at 10 mM SDS concentration (not shown in the figure). The differential ultrasonic velocities recorded with the ResoScan System compare poorly to data from the literature recorded with SDS in water [32] as well as to the results of calculations using Eqs. (6.5) and (6.6) and the parameters from Tables 6.1 and 6.2 and a cmc of 8.3 mM [32]. This poor agreement implies that the experiment conducted on SDS HEPES buffer solutions using the ResoScan System is not successful and that some source of error, e.g. related to adsorption of the surfactants to the resonator cavity surfaces, significantly impinge on the experiments. Relatively good agreement between the theoretical calculations and the literature data is seen below the cmc whereas a significant discrepancy again is seen above the cmc.

Finally, consider Fig. 6.3 which shows the differential ultrasonic velocities recorded during the two temperature scans conducted with HEPES buffer in resonator cavity 1 and 12 mM and 100 mM OG HEPES buffer solution, respectively, in resonator cavity 2, i.e. the temperature scans are conducted for samples with and without micelles. The differential ultrasonic velocities recorded for the 100 mM OG HEPES buffer solution is multiplied by 0.12 to make the two curves on the figure directly comparable. Differential ultrasonic velocities exhibit a decreasing trend for both specimens, but for the 100 mM OG HEPES buffer solution, the differential ultrasonic velocities are actually observed to become negative above 57°C implying that the adiabatic compressibility coefficient of the micelles is higher than the adiabatic compressibility coefficient of bulk water.

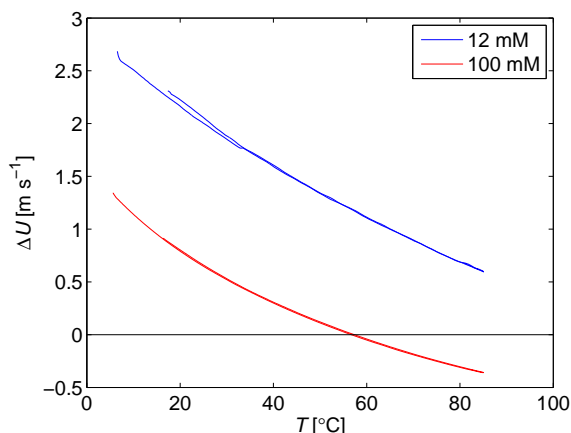


Figure 6.3: Differential ultrasonic velocities, ΔU , recorded for HEPES buffer in resonator cavity 1 and 12 mM and 100 mM OG HEPES buffer solution in resonator cavity 2 for varying temperature, T . The curve recorded for 100 mM OG solution is multiplied by 0.12 to make the two curves directly comparable. Both curves exhibit the characteristic decreasing trend but the curve for the 100 mM OG solution becomes negative for temperatures above 57°C implying that the adiabatic compressibility coefficient of the micelles is higher than the adiabatic compressibility coefficient of bulk water.

6.5 Discussion

6.5.1 The additive assumption

The linear trends seen in Fig. 6.2 for (a) the differential ultrasonic velocities on aqueous OG solutions recorded using the ResoScan System and (b) the differential ultrasonic velocities for aqueous SDS solutions found in the literature, imply that the additive assumption introduced for the low-weight molecules considered in the previous chapter, also is valid for the aqueous surfactant solutions. Furthermore, the relatively good agreement of the mathematical model to the experimentally recorded results for OG and to the literature results for SDS below the cmc also imply that the contributions from the individual molecular groups on the surfactant molecules in this regime, at least to some extent, can be treated as additive. The reason for the good results obtained for the mathematical model below the cmc is probably related to the linear nature of the surfactant molecules. For examples, it is known from data on n -alkanols and α, ω -alkane diols that the range of the effect of the polar groups in these molecules on the partial molar adiabatic compressibility of the adjacent $-\text{CH}_2-$ groups only is limited to the two nearest $-\text{CH}_2-$ groups [44]. This implies that the effect of the glucose head group in OG on the compressibility of the adjacent $-\text{CH}_2-$ groups also is limited to the nearest $-\text{CH}_2-$ groups explaining the relatively good results for the calculations conducted on the OG solutions.

Above the cmc, a reasonable large discrepancy is seen in Fig. 6.2 between the calculated curves and (a) the differential ultrasonic velocities on aqueous OG solutions recorded

using the ResoScan System and (b) the differential ultrasonic velocities for aqueous SDS solutions found in the literature. Three reasons may explain this discrepancy. Firstly, the hydration properties of the hydrophilic head groups may be altered when the surfactants aggregate into micelles. However, as mentioned previously, the hydration for the glucose head groups is similar in the monomer and micelle state implying that this is not the reason for the observed discrepancy, at least in the case of the OG systems. Secondly, since the contributions for the $-\text{CH}_2-$ groups in the micelle interior used in the calculations are determined from experiments on surfactants varying the alkyl chain length between 10 to 16 [36], the contributions from $-\text{CH}_2-$ in the inner part of the micelle interior may be different from the contributions from $-\text{CH}_2-$ in the outer part of the micelle interior. However, results from the literature indicate that the partial molar adiabatic compressibility of $-\text{CH}_2-$ in the outer part of the micelle core actually decreases [36]. Thus if the differential properties of $-\text{CH}_2-$ in the inner and outer parts were taken into account, the discrepancy for the recorded and calculated curves above the cmc in Fig. 6.2 would actually increase. Thirdly, the assumption of constant monomer surfactant concentration above the cmc may be invalid [25].

Finally, note that ultrasonic velocimetry may also potentially be used to examine the dependence of the interior part of the hydrophobic micelle core on temperature using the additive approach in the mathematical model introduced in the above. Hence systematically varying the alkyl chain length for a given surfactant at concentration above the cmc, it is possible to determine the temperature-dependent contribution to the differential ultrasonic velocities from the $-\text{CH}_2-$ groups in the interior of the micelles. A comparison of these contributions to the temperature-dependence on the ultrasonic velocity in other hydrocarbon structures may help reveal important information of similarities and differences between these structures.

6.5.2 Density or compressibility

Density data is not as readily available for aqueous surfactant solutions as for the aqueous salt solutions considered in the previous chapter. Hence it is not easy to track down temperature-dependent density data for aqueous surfactant solutions that can be used to consider the density contribution to the relative molar increment in the ultrasonic velocity over the entire temperature range examined in the experiments performed in this thesis. For OG in aqueous solution, partial molar volumes, V° , for 15 and 25°C were found in the literature [38]. V° can be used to calculate the density contribution to the relative molar increment in ultrasonic velocity, $[U]_\rho$, by combining Eqs. (2.26) and (2.29)

$$[U]_\rho = -\frac{\rho - \rho_0}{2C\rho_0} = \frac{1}{2} \left(V^\circ - \frac{M}{\rho_0} \right). \quad (6.8)$$

Using that the differential ultrasonic velocity for 12 mM OG at 15°C is 2.33 m s^{-1} , see Fig. 6.3, and that the absolute ultrasonic velocity in the HEPES buffer solution at 15°C is equal to 1468.9 m s^{-1} , the relative molar increment of the ultrasonic velocity, $[U]$, for OG at 15°C is calculated to be $132.2 \text{ cm}^3 \text{ mol}^{-1}$. The density contribution to the relative molar increment in ultrasonic velocity at 15°C can be calculated using that the partial

molar volume of OG in aqueous solution, V_{OG}° , at 15°C is equal to 243.35 cm³ mol⁻¹ [38], that the density of water at 15°C is equal to 0.99913 g cm⁻³ [45] and that the molar mass of OG is equal to 292.4 g mol⁻¹. Thus the density contribution, $[U]_{\rho}$, is at 15°C calculated to be -24.7 cm³ mol⁻¹. The relative molar increment in the ultrasonic velocity for OG at 25°C can be calculated using that the absolute ultrasonic velocity in the HEPES buffer solution at 25°C is 1498.5 m s⁻¹ and that the slope of the linear curve fitted to the experimentally recorded differential ultrasonic velocities below the cmc on Fig. 6.2 (a) is 0.1673 m s⁻¹ mM⁻¹. Thus the relative molar increment in ultrasonic velocity at 25°C is calculated to be 111.6 cm³ mol⁻¹. Using that the partial molar volume of OG at 25°C is 245.79 cm³ mol⁻¹ [38] and that density of water at 25°C is 0.99704 g cm⁻³, the density contribution to the relative molar increment in the ultrasonic velocity at 25°C is found to be -23.8 cm³ mol⁻¹. Thus the density contribution to the differential ultrasonic velocity of aqueous OG solutions is found to be significant. Furthermore, it is found that the density contributions calculated at 15°C and 25°C are similar implying that changes in differential ultrasonic velocity occurring as a function of temperature are dominated by changes in solution compressibility.

It is also possible to assess the density contribution to the relative molar increment in ultrasonic velocity at 25°C for OG in micelles assuming that the concentration of monomeric surfactants is constant above the cmc. Hence the slope of the linear line fitted to the differential ultrasonic velocities recorded above the cmc in Fig. 6.2 (a), given by 0.0129 m s⁻¹ mM⁻¹, is used to determine that the relative molar increment in ultrasonic velocity of OG in micelles is equal to 8.6 cm³ mol⁻¹. The density contribution to this relative molar increment at 25°C is calculated, using that the partial molar volume of OG above the cmc is approximately 255 cm³ mol⁻¹ [38], to be -19.1 cm³ mol⁻¹. Hence the density contribution is also significant above the cmc. Note that this density contribution is actually rather close to the density contribution for monomeric OG implying that difference in relative molar increments in ultrasonic velocity for monomer and micelle OG is related to differences in compressibility. Calculations on the density contribution to the relative molar increment in ultrasonic velocity were not conducted for SDS due to the disagreement between the experimentally recorded results and the literature results.

6.6 Summary

Basic chemical theory on surfactants and the hydrophobic effect was introduced and a mathematical framework for interpretation of differential ultrasonic velocities in aqueous surfactant solutions was presented. Experimental results showed that ultrasonic velocimetry can be used to detect the cmc, even though results for SDS did not agree with the literature, and that micelles are actually more compressible than water. Using the mathematical model to account for the differential ultrasonic velocities below the cmc implied that the long range effect of the hydrophilic head groups on the -CH₂- groups in the alkyl chains was not a dominant effect. Poor agreement was found between the mathematical model and experimental results above the cmc, which may be due to the fact that the assumption of constant surfactant concentration above the cmc is not valid. Calculations

on the importance of density and compressibility showed that both effects were important to the relative molar increment in ultrasonic velocity, but that variations in the relative molar increment in ultrasonic velocity occurring when the temperature is varied between 15 and 25°C is due to variations in the compressibility contribution. Differences between the relative molar increment in ultrasonic velocity for monomer and micelle OG is also related to differences in the compressibility contribution.

Chapter 7

Case study: Proteins

The third and final case study is concerned with aqueous solutions containing proteins. The chemical complexity of aqueous protein solutions is higher than the chemical complexity of the aqueous low-weight molecule solutions and the aqueous surfactant solutions. Therefore it is once again necessary to examine the validity and the extent of applicability of the conclusions drawn in Chapters 5 and 6. The experimental work on protein solutions is conducted using Lipolase and is *inter alia* concerned with the effect of adding NaCl and CaCl₂ to HEPES buffer solutions containing Lipolase.

7.1 Relevant chemical introduction

Proteins are a class biological macromolecules taking part in a wealth of biological functions. For example, proteins are involved in catalysis of biochemical metabolic reactions, in cellular transport of other types of biomolecules, in signal transmission and in cellular structural support. All proteins have in common that they are built of amino acids, see Fig. 7.1 (a) [6]. This is used within the field of gene technology to create proteins with tailor-made properties by systematic exchange of the amino acids of a given protein [11].

Catalytic proteins, called enzymes, are very important to detergent applications as they are used to degrade various types of dirt and stain material. For example, enzymes called proteases are used to degrade proteins whereas enzymes called amylases are used to degrade starch. The third major class of enzymes used in detergent applications are lipases. Lipases are a class of enzymes catalyzing the degradation of lipids. The enzyme considered in the experimental work of this case study, namely Lipolase, is a lipase developed by Novo in 1988 widely used in detergent products, see Fig. 7.1 (b). Lipolase is developed through gene technology and is a wild type from yeast *Thermomyces lanuginosus* [11].

The functional properties of proteins are intimately related to their three-dimensional structure. This structure is determined from the interaction between the amino acids comprising a given protein as well as the interaction between the amino acids and solvent surrounding the protein. Most proteins are by nature designed to function in aqueous solvents. A general feature of these proteins is thus that their interior mainly comprises non-polar residues whereas their surface comprise both charged, polar, and nonpolar residues

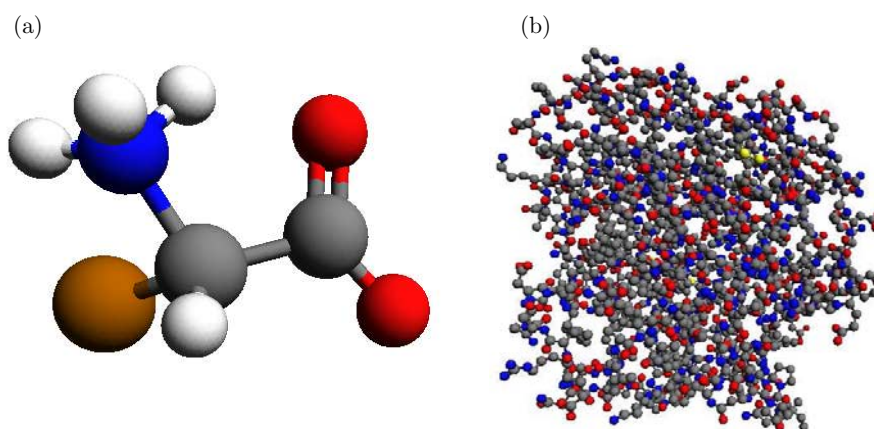


Figure 7.1: Ball-and-stick diagram of (a) amino acid and (b) monomer moiety of thermomyces (*Humicola*) lanuginosa lipase [78], which is structurally equivalent to Lipolase. Red balls represent oxygen atoms, white balls represent hydrogen atoms, grey balls represent carbon atoms, blue balls represent nitrogen atoms and the yellow ball in the amino acid is a general representation of the side chain of the amino acid which varies dependent on the type of amino acid considered.

[6].

The three-dimensional protein structure, and hence protein functionality, is disrupted by protein denaturation induced by altered physical and chemical conditions in aqueous protein solutions. This disruption of the three-dimensional structure of the protein may lead to exposure of the hydrophobic residues in the protein interior to the aqueous solvent. This may in turn favor intermolecular interaction between denatured proteins leading to irreversible aggregation and precipitation [25]. Many variables related to aqueous protein solutions may induce protein denaturation and aggregation. For example, temperature variations may affect protein stability destabilizing the native protein structure [19, 25, 41]. Variations in pH may also affect protein stability. Hence extreme pH may result in protein denaturation and subsequent aggregation due to a high surface charge entailing intramolecular electrostatic repulsion. However, a pH close to the protein isoelectric point may also result in aggregation as a lower surface charge limits electrostatic repulsion between proteins favoring intermolecular aggregation interactions [19].

The addition of salt to aqueous protein solutions may also affect the conformational stability of the proteins. Thus increasing the ionic strength may lead to a neutralization of the surface charge of the protein due to electrostatic screening [25]. However, simple electrostatic screening is not enough to completely account for the effect of ions on protein stability. For example, the charge density of the ions, and thus the strength of the hydration of these ions, may affect the solubility of proteins. This is normally described through the Hofmeister series ordering the ions dependent on their effect on protein solubility, i.e. ions with a high charge density, called kosmotropes, are known to increase the solubility of proteins whereas ions with a low charge density, called chaotropes, are known to decrease

the protein solubility [20]. No explanation of the mechanisms underlying the Hofmeister series is yet generally accepted [42]. Finally, multivalent ions may also bind directly to unpaired charged residues on the protein surface also affecting the protein stability [19].

Due to the multiple effects of salt on the stability of proteins, it is hard to generally predict the effect of adding NaCl and CaCl₂ to aqueous protein solutions to protein denaturation and stability. NaCl is thus known to decrease the aggregation rates for recombinant factor VIII SQ and recombinant keratinocyte growth factor and increase the aggregation rate for rhGCSF [19]. CaCl₂ is known to play a role on thermal aggregation of whey protein mixtures and purified β -lactoglobulin solutions hypothesized to be due to site-specific binding of the Ca²⁺ ions to the protein surface. Hence NaCl will not entail aggregation to the same extent as CaCl₂ in whey protein mixtures or β -lactoglobulin solutions when the two types of salts are considered at similar ionic strength [55].

7.2 Ultrasonic introduction

The differential ultrasonic velocity between an aqueous protein solution and an aqueous reference sample is related to both intrinsic as well as hydration contributions. Hence the intrinsic compressibility contribution arises due to imperfect internal protein atomic packing resulting in internal voids and cavities [15]. In order to further elucidate the ultrasonic properties of proteins, a mathematical model is presented.

7.2.1 Mathematical model

The model to be presented in the following was first presented in an article by Chalikian *et al.* [15]. Assuming infinite dilution, the authors proposed that the differential ultrasonic velocity could be properly accounted for by intrinsic contributions as well as distinct hydration contributions from charged, polar and nonpolar areas of the surface. Hence the partial specific protein volume, v° , was proposed to be given by given by

$$v^\circ = C_M v_M + \frac{C_n S_n + C_c S_c + C_p S_p}{M}, \quad (7.1)$$

where v_M is the specific intrinsic protein volume, C_M is a temperature-dependent expansion factor, S_c , S_p and S_n are the charged, polar and nonpolar solvent accessible surface areas of the protein, respectively, and C_c , C_p and C_n are temperature-dependent parameters accounting for the contributions from the charged, polar and nonpolar solvent accessible surface areas of the protein, respectively, to v° .

Using a similar approach, the partial specific adiabatic compressibility is expressed as

$$k_s^\circ = \beta_M v_M + \frac{B_c S_c + B_p S_p + B_n S_n}{M}, \quad (7.2)$$

where β_M is the intrinsic adiabatic compressibility coefficient and B_c , B_p and B_n are the compressibility contribution per solvent accessible surface area from charged, polar and nonpolar surface areas, respectively. The intrinsic adiabatic compressibility coefficient is

Parameter	Unit	Fit
C_M		$3 \times 10^{-4}T + 1.02380$
C_{cp}	$\text{cm}^3 \text{mol}^{-1} \text{\AA}^{-2}$	-0.47
C_n	$\text{cm}^3 \text{mol}^{-1} \text{\AA}^{-2}$	0.62
B_M	$10^{-6} \text{cm}^3 \text{mol}^{-1} \text{bar}^{-1} \text{\AA}^{-3}$	$1.06 \times 10^{-2}T + 10.73$
B_c	$10^{-6} \text{cm}^3 \text{mol}^{-1} \text{bar}^{-1} \text{\AA}^{-2}$	-15
B_p	$10^{-6} \text{cm}^3 \text{mol}^{-1} \text{bar}^{-1} \text{\AA}^{-2}$	$-6.0 \times 10^{-3}T^2 + 0.67T - 75.66$
B_n	$10^{-6} \text{cm}^3 \text{mol}^{-1} \text{bar}^{-1} \text{\AA}^{-2}$	$-7.8 \times 10^{-3}T^2 + 0.80T - 24.50$

Table 7.1: Polynomial fits to the temperature-dependence of the parameters C_M , C_{cp} , C_n , B_M , B_c , B_p and B_n used in the theoretical model on the effect of protein on the differential ultrasonic velocity. Polynomial fits are valid for temperatures between 18 to 55°C. Since some of the parameters are rather independent of temperature, they are just represented as constants in the table.

calculated by

$$\beta_M = \frac{B_M V_M^2}{M V_W v_M}, \quad (7.3)$$

where B_M is a temperature-dependent parameter, V_M is the intrinsic volume of the protein and V_W is the van der Waals volumes of the atoms of the proteins. Note that this formula is corrected from what appears to be a misprint in the article by Chalikian *et al.* Furthermore, it should be noted that V_M in Eq. (7.3) represent a real volume as opposed to the general convention in this thesis where V_M represent a molar volume.

The change in ultrasonic velocity occurring upon addition of proteins to an aqueous solvent is found by inserting Eqs. (7.1) and (7.2) into Eq. (2.30)

$$\frac{\Delta U}{U_0} = \left(-\frac{\beta_M v_M^0}{2\beta_{S0}} - \frac{B_c S_c + B_p S_p + B_n S_n}{2\beta_{S0} M} + C_M v_M \right) CM + \left(\frac{C_n S_n + C_c S_c + C_p S_p}{M} - \frac{1}{2\rho_0} \right) CM. \quad (7.4)$$

Chalikian *et al.* considered X-ray data from 12 different globular proteins to determine the intrinsic volumes as well as the solvent accessible surface areas of the charged, polar and nonpolar surface areas of the considered proteins. Measured changes in ultrasonic velocities and partial specific volumes recorded for each of these proteins at 18, 25, 35, 45 and 55°C were then used to perform a linear regression to determine the values of C_M , C_c , C_p , C_n , B_M , B_c , B_p and B_n at each temperature [15]. Note that C_p and C_c during the course of the linear regression were rewritten by the authors to one constant, namely C_{cp} . Polynomials fitted using MATLAB to values of the parameters determined in the study by Chalikian *et al.* are shown in Table 7.1. Since some of the parameters were virtually independent of temperature, they are just represented as constants throughout the temperature range between 18 to 55°C.

7.3 Experimental procedure

Lipolase was supplied dissolved in another buffer than the HEPES buffer used in the previous chapters. To isolate Lipolase from its original buffer and instead dissolve it in the HEPES buffer, column chromatography was applied. The columns used in column chromatography contain a porous medium entailing a differential flow rate for the macromolecular proteins and the buffer molecules. Hence the columns allow for a separation of Lipolase from its original buffer and hence for the solvation of Lipolase in the HEPES buffer. Two stock aqueous Lipolase HEPES buffer solutions were prepared using column chromatography. To determine the Lipolase concentration of the created stock Lipolase HEPES buffer solutions, photometric measurements were applied. Since the absorbance of light with a wavelength of 280 nm is directly proportional to the protein concentration in the sample, the Lipolase concentration of the two created Lipolase HEPES buffer solutions were hence determined to be 59.4 μM and 63.4 μM , respectively.

Experiments, for both varying Lipolase concentration and for varying temperature, were conducted with HEPES buffer in resonator cavity 1 and Lipolase HEPES buffer solutions in resonator cavity 2. Experiments on varying Lipolase concentration were conducted at 25°C for Lipolase concentrations between 0 to 20 μM and between 39.5 to 59.4 μM . Experiments conducted on Lipolase concentration between 0 to 20 μM were performed using a number of samples prepared from serial dilution of the stock 59.4 μM Lipolase HEPES buffer solution. These samples were then injected into resonator cavity 2 in order of increasing Lipolase concentration using an approach similar to the approach used for the polystyrene microbead suspensions. Experiments conducted for higher Lipolase concentrations between 39.5 to 59.4 μM were conducted using an approach designed to limit the consumption of Lipolase since Lipolase only was available in limited amounts. Hence the first data point in this experiment was obtained with 180 μL HEPES buffer in resonator cavity 1 and 180 μL of the stock 59.4 μM Lipolase HEPES buffer solution in resonator cavity 2. Subsequently, 10 μL HEPES buffer was injected into both resonator cavities and a new data point was obtained after the samples in the resonator cavities had equilibrated. This procedure was repeated until the maximally allowed sample volume of 250 μL was attained in both resonator cavities corresponding to a Lipolase concentration of 39.5 μM in the Lipolase HEPES buffer solution in resonator cavity 2. Experiments on varying temperature was performed by running the script with a scan rate of 500 mK min^{-1} with HEPES buffer in resonator cavity 1 and a sample taken from the stock 63.4 μM Lipolase HEPES buffer solution in resonator cavity 2.

Experiments were also conducted to examine the effect of adding NaCl and CaCl₂ to the Lipolase HEPES buffer solutions. These experiments were conducted at 25°C with salt HEPES buffer solution in resonator cavity 1 and the same type of salt at the same concentration in Lipolase HEPES buffer solution in resonator cavity 2. Two experimental procedures were applied to conduct these experiments. Both of these procedures were designed to minimize the consumption of Lipolase. In both procedures, the first data point was obtained with 180 μL HEPES buffer in resonator cavity 1 and 180 μL of the stock 63.4 μM Lipolase HEPES buffer solution in resonator cavity 2, i.e. no salt was present in the samples when the first data point was recorded. To introduce salt into the

two resonator cavities, salt HEPES buffer solution was injected into both resonator cavities from a micropipette. In the first procedure, these salt HEPES buffer solutions were injected from a micropipette adjusted to contain $10\ \mu\text{L}$ and filled with salt HEPES buffer solutions by releasing the operating button from the second stop, i.e. the pipette tip was filled with an additional volume of salt HEPES buffer solution to the preadjusted $10\ \mu\text{L}$. The pipette tip was then immersed into a sample in one of the resonator cavities and the salt HEPES buffer solution in the pipette was mixed with the sample in the resonator cavity by approximately 10 times in turns pressing the operating button to the first stop and releasing the operating button. The operating button was finally pressed to the first stop and the pipette removed from the resonator cavity, i.e. the volume of the samples in the resonator cavities increased by $10\ \mu\text{L}$ each time a salt HEPES buffer solution was injected into the cavities during the first procedure. Thus the experiment was proceeded until the sample volume of the resonator cavities attained the maximally allowed $250\ \mu\text{L}$. The large advantage associated with the first procedure is the avoidance of formation of air bubbles. However, the first procedure was very time consuming due long equilibration times of the samples in the resonator cavities due to the time required for the injected salt HEPES buffer solutions to properly diffuse around in the resonator cavities. The aim of the second experimental procedure was to rectify this problem. Hence, in the second procedure, salt HEPES buffer solution was injected into the resonator cavities from accurately volume of $10\ \mu\text{L}$ from a micropipette and subsequently mixed by immersing the pipette tip, adjusted to contain $50\ \mu\text{L}$, into the resonator cavities and approximately 10 to 20 times in turns pressing the operating button to the first stop and releasing the operating button. The second procedure thus corrected the problem with the poor mixing but in return it entailed an unfortunate tendency of forming air bubbles in the resonator cavities which may entail erroneous results during experiments. Hence none of the experimental procedures was flawless but they represented the best solution under the circumstances where the ideal possibility of using samples mixed in test tubes outside of the resonator cavities was not accessible. Two temperature scans were also conducted. The first temperature scan was conducted on $60\ \text{mM NaCl}$ HEPES buffer solution in resonator cavity 1 and $60\ \text{mM NaCl}$ $42.1\ \mu\text{M}$ Lipolase HEPES buffer solution in resonator cavity 2. The second temperature scan was conducted on $49.23\ \text{mM CaCl}_2$ HEPES buffer solution in resonator cavity 1 and $49.23\ \text{mM CaCl}_2$ $42.6\ \mu\text{M}$ Lipolase HEPES buffer solution. Both temperature scans were conducted running the script with a scan rate of $500\ \text{mK min}^{-1}$.

7.4 Results

Results for experiments for Lipolase concentration scans conducted with HEPES buffer solution in resonator cavity 1 and Lipolase HEPES buffer solution in resonator cavity 2 at 25°C are shown in Fig. 7.2. Uncertainties of the differential ultrasonic velocity and differential ultrasonic absorption are assumed to be $\pm 4.7\ \text{cm s}^{-1}$ and $\pm 7 \times 10^{-16}\ \text{s}^2\ \text{m}^{-1}$, respectively, in accordance with Section 3.3.3. The differential ultrasonic velocity on (a) appear to be linearly dependent on Lipolase concentration indicating the validity of the assumption of infinite dilution. For small Lipolase concentrations below $4\ \mu\text{M} \approx 0.1\ \text{mg mL}^{-1}$

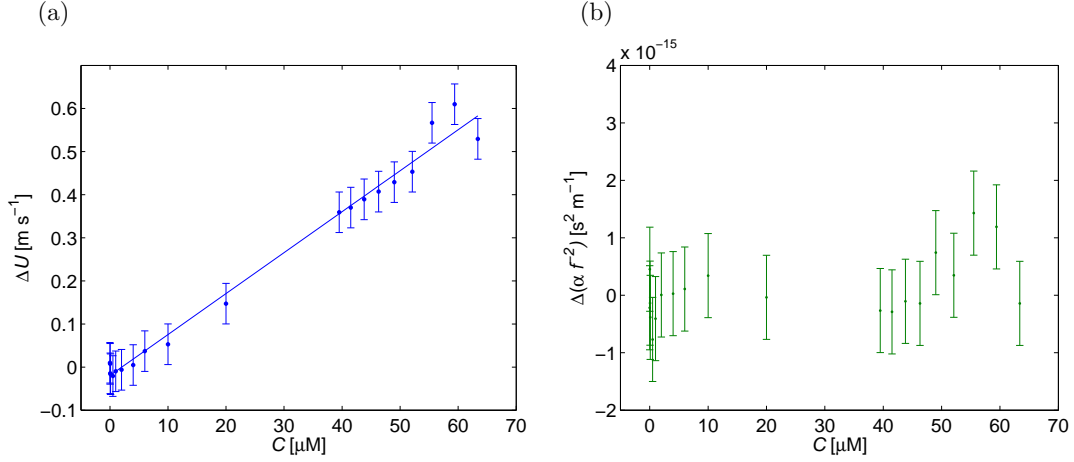


Figure 7.2: Results for experiments measuring the differential ultrasonic properties with HEPES buffer solution in resonator cavity 1 and Lipolase HEPES buffer solution in resonator cavity 2 at 25°C as a function of Lipolase concentration. The data points on (a) show the differential ultrasonic velocity. These differential ultrasonic velocities appear to be linearly dependent on the Lipolase concentration. Error bars are assumed to be $\pm 4.7 \text{ cm s}^{-1}$. The data points on (b) show the differential ultrasonic absorption. Error bars are assumed to be $\pm 7 \times 10^{-16} \text{ s}^2 \text{ m}^{-1}$. Only noise is found for the differential ultrasonic velocities and no real signal is emergent.

the recorded differential ultrasonic velocities just represent noise in accordance with the fundamental concentration limit of the ResoScan System discussed in Section 1.1. The recorded differential ultrasonic absorption on (b) is dominated by noise and no real signal is identifiable.

Since the experimental procedures on injecting salt into the resonator cavities caused a dilution of the Lipolase sample, the experimentally differential ultrasonic velocities recorded during these experiments are normalized to a Lipolase concentration of $63.4 \mu\text{M}$ by multiplying by $(63.4 \mu\text{M})/C$, where C in this case is the concentration of Lipolase. Normalized differential ultrasonic velocities, ΔU_{norm} , recorded for salt HEPES buffer solution in resonator cavity 1 and Lipolase salt HEPES buffer solution in resonator cavity 2 for both NaCl and CaCl_2 are presented in Fig. 7.3. Uncertainties on this figure are calculated using that $\Delta U_{\text{norm}} = (\Delta U_{\text{Lipo}} + \Delta U_{\text{salt}}) \cdot 63.4 \mu\text{M}/C$, where ΔU_{Lipo} is the contribution from Lipolase and ΔU_{salt} is the contribution from differences in salt concentration between the two resonator cavities. A test experiment conducted by injecting similar amounts of NaCl solution in resonator cavities using micropipettes adjusted to $10 \mu\text{L}$ indicates that the uncertainty in ΔU_{NaCl} , denoted $\delta \Delta U_{\text{NaCl}}$, was given by $\pm 6.2 \text{ cm s}^{-1}$. Neglecting the uncertainty of the Lipolase concentration, C , the uncertainties in the normalized differential ultrasonic velocity, $\delta \Delta U_{\text{norm}}$, are calculated using the law of error propagation [65]

$$\delta \Delta U_{\text{norm}} = \sqrt{\left(\frac{63.4 \mu\text{M}}{C} \delta \Delta U_{\text{Lipo}}\right)^2 + \left(\frac{63.4 \mu\text{M}}{C} \delta \Delta U_{\text{NaCl}}\right)^2}, \quad (7.5)$$

where $\delta\Delta U_{\text{Lipo}}$ is the uncertainties in the differential ultrasonic velocity for Lipolase given by $\pm 4.7 \text{ cm s}^{-1}$. Both normalized differential ultrasonic velocities presented in Fig. 7.3 for

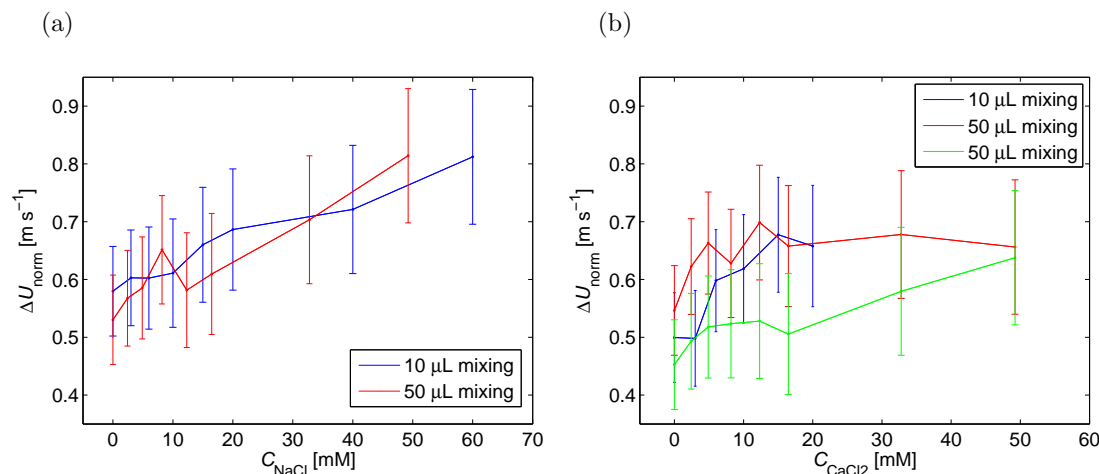


Figure 7.3: Normalized differential ultrasonic velocities recorded at 25°C for experiments injecting (a) NaCl HEPES buffer solutions and (b) CaCl_2 HEPES buffer solution into both resonator cavities so that resonator cavity 1 contains a salt HEPES buffer solution and resonator cavity 2 contains a Lipolase salt HEPES buffer solution at the same salt concentration, i.e. C represent the common salt concentration of both resonator cavities so that the only difference between the two resonator cavities are related to the existence of Lipolase in resonator cavity 2. In general, curves appear to exhibit an increasing trend although further experiments are needed in order to confirm that this trend is indeed significant.

(a) addition of NaCl to the samples in the resonator cavities and (b) addition of CaCl_2 to the samples in resonator cavities appear exhibit increasing trends although further experiments are needed to fully confirm the statistical significance of this trend. Based on the curves in Fig. 7.3, it is not possible to conclude that there are any differences on the effect of NaCl and CaCl_2 on Lipolase at 25°C in the considered salt concentration intervals. A discussion of the biochemical interpretation of this increasing trend is given in Section 7.5.5. Note that the ultrasonic absorption is not sensitive to the addition of salt to the samples in the resonator cavities.

Differential ultrasonic velocities normalized to a Lipolase concentration of $63.4 \mu\text{M}$ for temperature scans are presented in Fig. 7.4 for (a) HEPES buffer solution in resonator cavity 1 and $63.4 \mu\text{M}$ Lipolase HEPES buffer solution in resonator cavity 2, (b) 60 mM NaCl HEPES buffer solution in resonator cavity 1 and 60 mM NaCl $42.1 \mu\text{M}$ Lipolase HEPES buffer solution in resonator cavity 2 and (c) 49.23 mM CaCl_2 HEPES buffer solution in resonator cavity 1 and 49.23 mM CaCl_2 $42.6 \mu\text{M}$ Lipolase HEPES buffer solution in resonator cavity 2. All curves are corrected by the correction procedure presented in Section 4.1.6 and subsequently smoothed. It is known that Lipolase denatures when heated to approximately 70°C . The differential ultrasonic velocities in Fig. 7.4 (a) and (b)

do however not indicate the occurrence of any denaturation and furthermore the differential ultrasonic velocities imply that any reactions occurring upon heating of Lipolase in HEPES buffer or heating of Lipolase in 60 mM NaCl HEPES buffer solution are reversible. However, in the case of Lipolase in 49.23 mM CaCl_2 buffer solution, results imply that a completely irreversible reaction occurs during the first temperature scan, since a dramatic decrease in ultrasonic velocity is seen at 72°C . In fact, the sample with Lipolase and CaCl_2 had changed its visible appearance after the temperature scan to become opaque implying aggregation induced by CaCl_2 and heating. These results are further discussed in Section 7.5.5. Small variations in ultrasonic absorption were also seen during the course of the experiments. Hence the differential ultrasonic absorption exhibited a minimum at approximately 72°C for the experiments on CaCl_2 Lipolase solutions indicating that absorption data also might reveal interesting information on protein denaturation. However, further interpretation of these results are unfortunately beyond the scope of this thesis.

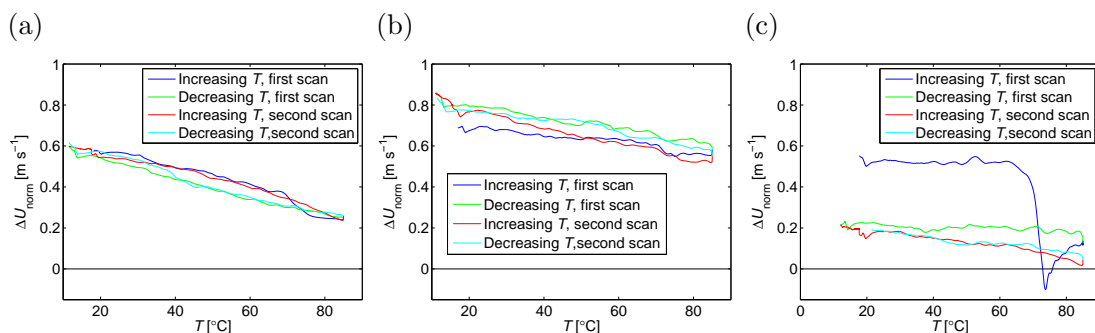


Figure 7.4: Differential ultrasonic velocities normalized to a Lipolase concentration of $63.4 \mu\text{M}$ for temperature scans of (a) HEPES buffer solution in resonator cavity 1 and $63.4 \mu\text{M}$ Lipolase HEPES buffer solution in resonator cavity 2, (b) 60 mM NaCl HEPES buffer solution in resonator cavity 1 and 60 mM NaCl $42.1 \mu\text{M}$ Lipolase HEPES buffer solution in resonator cavity 2 and (c) 49.23 mM CaCl_2 HEPES buffer solution in resonator cavity 1 and 49.23 mM CaCl_2 $42.6 \mu\text{M}$ Lipolase HEPES buffer solution in resonator cavity 2. The curves indicate that Lipolase in HEPES buffer as well as Lipolase in NaCl HEPES buffer exhibit a reversible course of events when heated where irreversible aggregation occurs for Lipolase in CaCl_2 HEPES buffer.

To further investigate the results of the temperature scans in Fig. 7.4, the first derivatives of the recorded differential ultrasonic velocities are plotted in Fig. 7.5. The procedure of plotting the first derivatives is well-known for a number of other physical experimental techniques, including calorimetric methods. However, in this case the first derivatives in Fig. 7.5 do not seem to provide any new interesting information than what is already seen in Fig. 7.4.

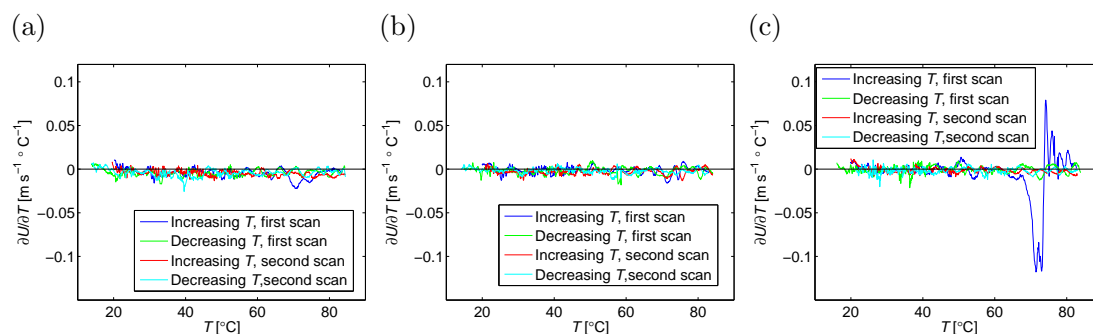


Figure 7.5: First derivatives of differential ultrasonic velocities recorded during the temperature scans conducted for (a) HEPES buffer solution in resonator cavity 1 and 63.4 μM Lipolase HEPES buffer solution in resonator cavity 2, (b) 60 mM NaCl HEPES buffer solution in resonator cavity 1 and 60 mM NaCl 42.1 μM Lipolase HEPES buffer solution in resonator cavity 2 and (c) 49.23 mM CaCl_2 HEPES buffer solution in resonator cavity 1 and 49.23 mM CaCl_2 42.6 μM Lipolase HEPES buffer solution in resonator cavity 2.

7.5 Discussion

7.5.1 The additive assumption

The linear trends of the differential ultrasonic velocity in Fig. 7.2 indicate that the additive assumption is also applicable to native globular proteins. In fact it is known that partial specific volume and partial specific adiabatic compressibility is independent of concentration in intervals between 0 to 5 mg mL^{-1} for globular proteins [15]. Since the molar mass of Lipolase is approximately 30 kg mol^{-1} , the maximal applied Lipolase concentration of 63.4 μM is equal to 1.9 mg mL^{-1} well within this interval.

The mathematical model presented in Section 7.2.1 is based on the assumption that the contributions from the different types of solvent accessible surface areas of proteins are additive. It is however important to note that the contributions per surface area for proteins do not compare well with contributions identified for low-weight molecules [15]. This discrepancy is related to intramolecular interaction between the residues on the protein surface.

Interestingly, the addition of NaCl and CaCl_2 to Lipolase solutions seem to entail the breakdown of the additive assumption. Hence, Fig. 7.3 shows that the contribution per Lipolase molecule to the differential ultrasonic velocity apparently increases when NaCl or CaCl_2 is added. In Fig. 7.4 it is also clear that the contributions per Lipolase molecules is significantly affected by the presence of both NaCl and CaCl_2 when samples are heated. These results imply that some interaction between the salt molecules and Lipolase must take place. This interaction is discussed further in Section 7.5.5.

T [$^{\circ}\text{C}$]	18	25	35	45	55
v° [$\text{cm}^3 \text{g}^{-1}$]	0.742	0.745	0.748	0.750	0.753
$[u]$ [$\text{cm}^3 \text{g}^{-1}$]	0.180	0.164	0.147	0.142	0.138

Table 7.2: 5 data points taken from an article by Chalikian *et al.* [15] on the partial specific volume, v° , and relative specific increment in ultrasonic velocity, $[u]$, of myoglobin in water at temperature, T , of 18, 25, 35, 45 and 55 $^{\circ}\text{C}$. These data points are used to assess the importance of density changes to the relative molar increment in ultrasonic velocity, $[U]$, for aqueous protein solutions.

7.5.2 Density or compressibility

The calculations performed in the previous chapters implied that the relative molar increment in ultrasonic velocity, $[U]$, for aqueous salt solutions as well as for aqueous surfactant solutions can not be understood when solely considering density or compressibility. The question is then if this is any different for aqueous protein solutions. This question is elucidated using 5 data points for the relative specific increment in ultrasonic velocity, $[u]$, and 5 data points for the partial specific volume, v° , for aqueous native state myoglobin solutions for temperatures between 18 to 55 $^{\circ}\text{C}$. These data points are taken from the article by Chalikian *et al.* [15] and summarized in Table 7.2. The data points for the relative specific increment in ultrasonic velocity, $[u]$, is fitted by a polynomial of degree 2 given by: $3.6332 \times 10^{-5} (\text{cm}^3 \text{g}^{-1} \text{ } ^{\circ}\text{C}^{-2}) \cdot T^2 - 3.7553 \times 10^{-3} (\text{cm}^3 \text{g}^{-1} \text{ } ^{\circ}\text{C}^{-1}) \cdot T + 0.2354 (\text{cm}^3 \text{g}^{-1})$ and data points for the partial specific volume, v° , is fitted by a linear curve given by: $2.8539 \times 10^{-4} (\text{cm}^3 \text{g}^{-1} \text{ } ^{\circ}\text{C}^{-1}) \cdot T + 0.7374 (\text{cm}^3 \text{g}^{-1})$. The relative specific increment in ultrasonic velocity, $[u]$, and partial specific volume, v° , are used to calculate the relative molar increment in ultrasonic velocity, $[U]$, and partial molar volume, V° , respectively, by multiplying by the molar mass, M , of myoglobin which is equal to 17.8 kg mol^{-1} [15]. Using Eq. (6.8) and the fit to the density of water from Eq. (5.2), the density contribution to the relative molar increment in ultrasonic velocity, $[U]_{\rho}$, is then found. $[U]$, $[U]_{\rho}$ and $[U]_{\beta_S}$ are shown in Fig. 7.6, where $[U]_{\beta_S}$ is calculated from $[U] - [U]_{\rho}$.

Just as it was seen for aqueous solutions containing simple salts and surfactants, both density and compressibility are important contributors to the relative molar increment in ultrasonic velocity for aqueous myoglobin solutions. Furthermore, it is also again found that the variations in density contribution associated to temperature variations between 18 and 55 $^{\circ}\text{C}$ only corresponds to $\sim 3\%$ of the total magnitude of the variations in $[U]$. In other words, it is again found that variations in differential ultrasonic velocity associated with variations in temperature are primarily related to variations in compressibility. Note finally that changes in differential ultrasonic velocity associated with protein denaturation and aggregation are also known to be primarily associated with changes in sample compressibility [62].

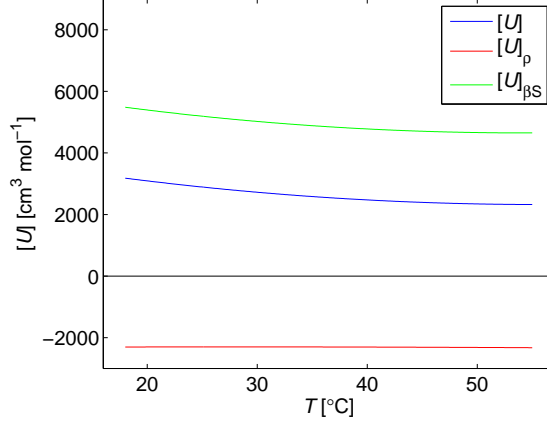


Figure 7.6: Density contribution, $[U]_{\rho}$, and compressibility contribution, $[U]_{\beta S}$, to the relative molar increment in ultrasonic velocity, $[U]$, for aqueous native state myoglobin solutions calculated for temperatures, T , between 18 and 55°C using data from an article by Chalikian *et al.* [15]. $[U]_{\beta S}$ is indirectly determined by taking $[U] - [U]_{\rho}$. It is found that both density and compressibility contributes to $[U]$ and that changes in $[U]$ occurring during a temperature scan are primarily associated to changes in compressibility.

7.5.3 Intrinsic contributions or hydration

Both intrinsic and hydration contributions affect differential ultrasonic velocity recorded in aqueous protein solution. However, the question is then of one if these effects are more important than the other. The intrinsic contribution to the relative molar increment in ultrasonic velocity, $[U]_M$, is given by

$$[U]_M = -\frac{K_M}{2\beta_{S0}} + V_M - \frac{M}{2\rho_0}, \quad (7.6)$$

whereas the hydration contribution to the relative molar increment in ultrasonic velocity, $[U]_h$, is found to be

$$[U]_h = -\frac{K_h}{2\beta_{S0}} + V_h. \quad (7.7)$$

Applying the mathematical model, given in Section 7.2.1, to Eqs. (7.6) and (7.7), it is possible to evaluate the relative importance of hydration and intrinsic contributions to the relative molar increment in ultrasonic velocity for proteins. Thus $[U]_M$ is written as

$$[U]_M = \left(-\frac{\beta_M v_M}{2\beta_{S0}} + C_M v_M - \frac{1}{2\rho_0} \right) M, \quad (7.8)$$

whereas $[U]_h$ is written as

$$[U]_h = -\frac{B_c S_c + B_p S_p + B_n S_n}{2\beta_{S0}} + C_n S_n + C_c S_c + C_p S_p. \quad (7.9)$$

Using the parameters for myoglobin, given in Sections 7.5.2 and 7.5.4, yields the results on Fig. 7.7. It is seen on the figure that the magnitude of the hydration contribution is much higher than the magnitude of the intrinsic contribution. However, it is also seen that both changes in intrinsic and hydration contributions as a function of temperature are important to understand the decreasing trend of the differential ultrasonic velocity in aqueous protein solutions.

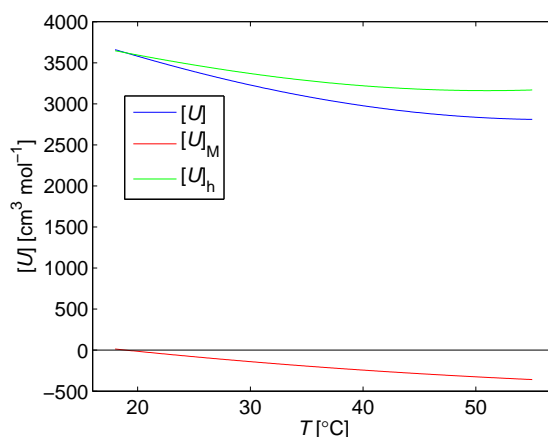


Figure 7.7: Hydration contributions, $[U]_h$, and intrinsic contributions, $[U]_M$, to the relative molar increment in ultrasonic velocity, $[U]$, calculated for aqueous myoglobin solutions using the mathematical model in Section 7.2.1. Results imply that the magnitude of the hydration contribution is much higher than the magnitude of the intrinsic contribution, but that both contributions are important to account for changes in ultrasonic velocity occurring when temperature is increased.

7.5.4 The protein surface

The model presented in Section 7.2.1 implies that it is in principle possible to characterize the surface of native proteins using ultrasonic velocimetry as a stand-alone technique since the contributions to the differential ultrasonic velocity from charged, polar and nonpolar protein surfaces in water all have different temperature-dependent characteristics [15]. Thus using the relative specific increments in ultrasonic velocity at two different temperatures, Eq. (7.4) can be evaluated for these two temperatures leading to two equations that in principle can be used to determine two unknowns, i.e. if v_M and S_c are known for a given protein, then S_p and S_n can in principle be determined solely considering the ultrasonic velocity. Furthermore, altering the solvent environment in a manner that does not perturb the native protein state, e.g. by adding small amounts of cosolvent or changing the solvent isotope, may potentially alter the characteristic contributions to the differential ultrasonic velocity from the different surface types, S_c , S_p and S_n , principally allowing for an increase in the number of equations and thus for a determination of all three surface types.

To examine the feasibility of ultrasonic velocimetry as a stand-alone technique for characterizing the native protein surface, consider again myoglobin. Myoglobin have a specific intrinsic volume, v_M , of $0.685 \text{ cm}^3 \text{ g}^{-1}$, a charged solvent accessible surface area, S_c , of 1242 \AA^2 , a polar solvent accessible surface area, S_p , of 1702 \AA^2 and a nonpolar solvent accessible surface area, S_n , of 4772 \AA^2 [15]. Assume now that only v_M and S_c are known while S_p and S_n are unknown. Using the relative specific increments in ultrasonic velocity at 18 and 55°C given in Table 7.2 and the fitted polynomials in Table 7.1, the mathematical model given by Eq. (7.4) is evaluated for 18 and 55°C leading to two equations containing two unknown, namely S_p and S_n . Hence these two equations can in principle used to determine S_p and S_n . Fig. 7.8 show the solutions emerging when solving each of the equations for $[u] + 0.03 \text{ (cm}^3 \text{ g}^{-1})$ and $[u] - 0.03 \text{ (cm}^3 \text{ g}^{-1})$, respectively. From this figure,

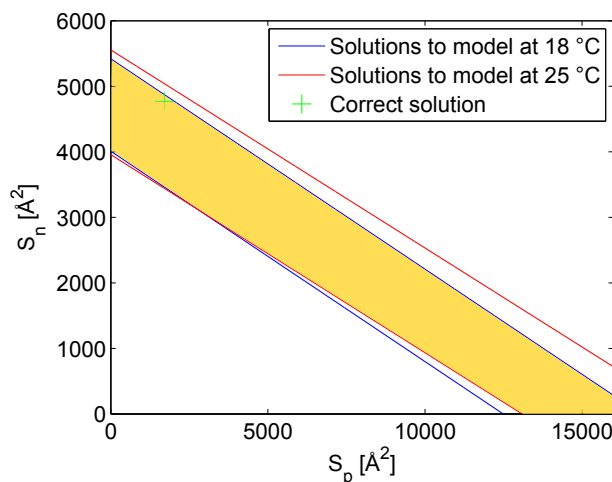


Figure 7.8: Solvent accessible surface areas with polar, S_p , and nonpolar, S_n , properties calculated for myoglobin by solving Eq. (7.4) at 18 and 55°C for $[u] + 0.03 \text{ (cm}^3 \text{ g}^{-1})$ and $[u] - 0.03 \text{ (cm}^3 \text{ g}^{-1})$, respectively. The set of solutions to the two equations is given by the colored area. The large set of solutions complicates the interpretation of the relative specific increment in ultrasonic velocity.

it is clear that a large set of S_p and S_n are solutions to the two equations. Thus although the set of solutions of S_p and S_n shown on Fig. 7.8 also contain the correct solution, a number of wrong solutions are included in the set complicating the interpretation of the differential ultrasonic velocity. Unfortunately, this implies that the theoretical model introduced in Section 7.2.1 is not sufficient to allow for the use of the ultrasonic velocity to characterize the properties of native protein surfaces.

7.5.5 The effect of adding salt to protein solutions

In general, interpretation of differential ultrasonic velocities associated with altered protein structure is challenged by the fact that it is hard to distinguish the intrinsic and hydration contributions. The interpretation of the experimental results recorded in this chapter is no

exception to this challenge. Hence hydration as well as intrinsic contributions may explain the increasing trends of the Lipolase contribution to the differential ultrasonic velocity occurring upon addition of NaCl and CaCl₂ at 25°C, see Fig. 7.3. Altered hydration contributions may arise due to the presence of ions in a diffuse layer surrounding the proteins [25]. Altered intrinsic packing that explains the increasing trend of the differential ultrasonic velocities can be related to a more compact protein structure with a smaller compressibility. Such structure may arise due to electrostatic screening of protein surface charges by the ions surrounding the protein [19, 25] or due to osmotic effects. To validate or dismiss the above hypotheses, it is however necessary to conduct further experiments using other types of experimental techniques, e.g. dynamic light scattering to check whether the Lipolase structure indeed appears to shrink in size upon addition of salt.

The differential ultrasonic velocities presented in Fig. 7.4 (a) for Lipolase HEPES buffer solution as a function of temperature exhibit the characteristic decreasing trend that also is seen in the temperature scans in Chapters 5 and 6. Thermally induced unfolding of Lipolase is expected at approximately 70°C but the curve do not imply that this unfolding takes place for Lipolase in HEPES buffer solution, e.g. due to the 10 mM NaCl found in the HEPES buffer entailing electrostatic screening of the protein surface charges thus enhancing protein stability. The differential ultrasonic velocities for 60 mM NaCl Lipolase HEPES buffer presented in Fig. 7.4 (b) do not show any kind of denaturation behavior either. However when 49.23 mM CaCl₂ is added to Lipolase HEPES buffer and the sample is heated, a dramatic and completely irreversible decrease in ultrasonic velocity is seen at 72°C indicating that an irreversible aggregation process has taken place [46]. The differential properties between NaCl and CaCl₂ on this aggregation process may be related to differences in ionic strengths of the two types salt [25] or to the site-specific binding of Ca²⁺ previously discussed [55].

7.6 Summary

The chapter was commenced by a chemical introduction to proteins in aqueous solution. After this introduction, a mathematical model was presented based on the formulation by Chalikian *et al.* [15]. Next, the experimental procedure of the experiments was discussed and the results were presented. These results implied that NaCl and CaCl₂ may alter the contributions to the differential ultrasonic velocity from Lipolase in solution by either altering the Lipolase hydration or by entailing a more compact intrinsic atomic packing of Lipolase. Data on aqueous myoglobin solutions from the literature implied that both density and compressibility were important contributors to differential ultrasonic velocities in protein solutions, but that the decreasing trend in differential ultrasonic velocity related to increasing temperature is primarily related to changes in compressibility. The mathematical model was used to assess the importance of intrinsic contributions and hydration contributions to the differential ultrasonic velocity. It was found that the magnitude of the hydration contribution is much higher than the magnitude of the intrinsic contribution, but that the decreasing trend in differential ultrasonic velocity observed for increasing temperature was related to variations in both the intrinsic and hydration contributions.

Finally, it was shown that the mathematical model could not be readily combined with ultrasonic velocimetry data to characterize the surface of proteins.

Chapter 8

Comparison across model systems

The case studies considered in the three previous chapters gave rise to information on the use of ultrasonic velocimetry as a stand-alone technique for characterizing various types of aqueous solutions. However, it is expected that it is also possible to obtain interesting information by comparing the recorded ultrasonic velocities across the individual model systems. Hence this chapter is concerned with the identification of proper methods to perform such a comparison as well as a discussion of the outcome of this comparison.

8.1 Calculations

The calculations on the importance of density and compressibility to the differential ultrasonic velocity were performed by dividing the relative increment in ultrasonic velocity, $\Delta U/U_0$, by the molar solute concentration, C , to obtain the relative molar increment in ultrasonic velocity, $[U]$. However, to compare the results across the case studies, C is not a suitable normalization parameter of the relative increment in ultrasonic velocity because of the large variations in size of the considered solutes. Thus parameters that scale with the size of the solutes are needed. Examples of such parameters are the specific concentration, $c = CM$ that can be used to calculate the relative specific increment in ultrasonic velocity, $[u]$:

$$[u] = \frac{\Delta U}{U_0 c} = \frac{[U]}{M}, \quad (8.1)$$

and the atomic concentration, $C_{\text{at}} = CN_{\text{at}}$, where N_{at} is the number of atoms per solute, that can be used to calculate the relative atomic increment in ultrasonic velocity, $[U]_{\text{at}}$:

$$[U]_{\text{at}} = \frac{\Delta U}{U_0 C N_{\text{at}}} = \frac{[U]}{N_{\text{at}}}. \quad (8.2)$$

Another possible normalization parameter is associated to the surface area of the solutes. Two types of surface areas are often found in the literature, namely the solvent accessible surface area and the solvent excluded surface area. Both of these surface areas are calculated by rolling a spherical probe, with radius of 1.4 Å equal to the effective radius of a water molecule, over the surface of a given molecular compound, see Fig. 8.1. The atoms in

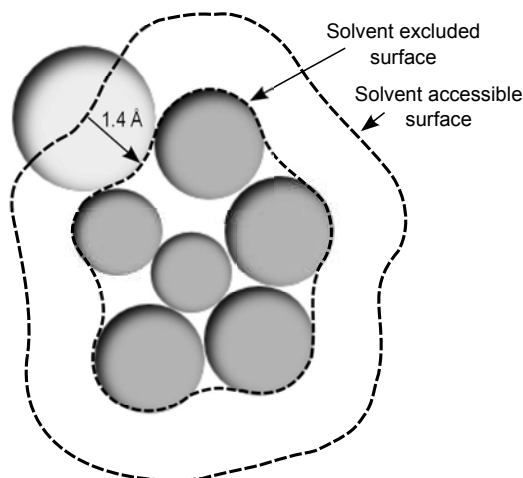


Figure 8.1: Both the solvent accessible surface area and the solvent excluded surface area of a given molecular compounds are calculated by rolling a spherical probe over the surface of the molecular compound. The atoms of the molecular compounds are represented as hard spheres with radius equal to the van der Waals radius. The radius of the probe is 1.4 Å and thus equal to the effective radius of a water molecule. The solvent accessible surface area is equal to the area tracked by the center of the probe whereas the solvent excluded surface area is equal to the contact area between the probe and the molecular compound. The figure is inspired by a figure in an article by Chalikian *et al.* [15].

the molecular compounds are represented as hard spheres with radius equal to the van der Waals radius. The solvent accessible surface area, S_{sas} , is then calculated by tracking the center of the probe as it rolls over the molecular compounds whereas the solvent excluded surface area, S_{ses} , is calculated by tracking the contact area between the probe and the molecular compound. The relative increment in ultrasonic velocity is normalized for S_{sas} to give the relative increment in ultrasonic velocity normalized to the solvent accessible surface area, $[U]_{\text{sas}}$:

$$[U]_{\text{sas}} = \frac{\Delta U}{U_0 C S_{\text{sas}}} = \frac{[U]}{S_{\text{sas}}}, \quad (8.3)$$

and for S_{ses} to give relative increment in ultrasonic velocity normalized to the solvent excluded surface area, $[U]_{\text{ses}}$:

$$[U]_{\text{ses}} = \frac{\Delta U}{U_0 C S_{\text{ses}}} = \frac{[U]}{S_{\text{ses}}}. \quad (8.4)$$

$[u]$, $[U]_{\text{at}}$, $[U]_{\text{sas}}$ and $[U]_{\text{ses}}$ are calculated for NaCl, CaCl₂, -CH₂-, monomeric and micellar OG and Lipolase. Increments in ultrasonic velocity for -CH₂-, used in the calculations, are determined using data for the partial molar volumes of -CH₂-, $V_{\text{CH}_2}^\circ$, and partial molar adiabatic compressibilities of -CH₂-, $K_{\text{CH}_2}^\circ$, between 5 and 55°C [14]. As mentioned in Chapter 6, $V_{\text{CH}_2}^\circ$ is given by 15.8 cm³ mol⁻¹. Furthermore $V_{\text{CH}_2}^\circ$ is also relatively constant over the entire temperature range. The data for $K_{\text{CH}_2}^\circ$ is fitted to a polynomial of degree

2: $-2.5835 \times 10^{-7} (\text{cm}^3 \text{mol}^{-1} \text{bar}^{-1} \text{ }^\circ\text{C}^{-2}) \cdot T^2 + 0.3652 \times 10^{-4} (\text{cm}^3 \text{mol}^{-1} \text{bar}^{-1} \text{ }^\circ\text{C}^{-1}) \cdot T - 9.3915 \times 10^{-4} (\text{cm}^3 \text{mol}^{-1} \text{bar}^{-1})$. For OG micelles, normalized relative increments in ultrasonic velocity are only calculated at 25°C due to the lack of knowledge about the cmc at other temperatures. Calculations are performed assuming a constant cmc. Data for Lipolase that can be used to calculate $[u]$, $[U]_{\text{atom}}$, $[U]_{\text{sas}}$ and $[U]_{\text{ses}}$ is obtained using structural data from the Protein Data Bank on *Thermomyces (Humicola) lanuginosa* lipase [78], which is a dimer protein where the monomeric moieties are structurally equivalent to Lipolase.

Surface calculations are performed using an online algorithm capable of calculating both A_{sas} and A_{ses} when provided with molecular structural information in pdb file format [50, 75]. The structural data from the Protein Data Bank on *Thermomyces (Humicola) lanuginosa* lipase is provided directly in pdb file format. However, to apply this structural data to calculate the surface areas of Lipolase, it is necessary to manually remove one of the monomeric compounds from the pdb file. Structural data in pdb file format for OG is obtained using Avogadro which is a open source program capable of optimizing the molecular geometries using force field algorithms [73]. Hence the molecular structure of OG is built and optimized in Avogadro and the resulting structure is saved in pdb file format. Surface calculations for OG micelles are conducted assuming that the solvent exposed surface of the micelles is given by the surface areas of the glucose head groups [35] and assuming that the aggregation numbers of OG micelles is 25 [12], i.e. the surface areas for methyl glucoside structures defined in Avogadro are calculated and multiplied by 25 to obtain an estimate for the surface area of the micelle. Surface areas for NaCl and CaCl₂ are calculated assuming that the ions are completely dissociated in aqueous solution, i.e. the total surface areas of the salts are calculated by adding the surface areas of the individual ions comprising the salt. These single-atom structural pdb files are also obtained using Avogadro [73]. Parameters used to calculate $[u]$, $[U]_{\text{at}}$, $[U]_{\text{sas}}$ and $[U]_{\text{ses}}$ are summarized in Table 8.1.

Compound	M [g mol ⁻¹]	N_{at}	S_{ses} [Å ²]	S_{sas} [Å ²]
NaCl	58.4	2	86.582	266.027
CaCl ₂	111.0	3	150.795	435.801
-CH ₂ -	14.0	3	18.805	30.745
Monomer OG	292.4	48	324.894	596.671
Micelle OG	7309.3	1200	4725.525	9270.575
Lipolase	29342.7	2071	9381.492	10392.164

Table 8.1: Parameters used to calculate the relative specific increment in ultrasonic velocity, $[u]$, the relative atomic increment in ultrasonic velocity, $[U]_{\text{at}}$, the relative increment in ultrasonic velocity normalized to the solvent accessible surface area, $[U]_{\text{sas}}$, and the relative increment in ultrasonic velocity normalized to the solvent excluded surface area $[U]_{\text{ses}}$ for NaCl, CaCl₂, -CH₂-, OG in free and micelle state and Lipolase. M is the molar mass, N_{at} is the number of atoms in the compound, S_{ses} is the solvent excluded surface area and S_{sas} is the solvent accessible surface area.

8.2 Results

Results of the calculations on the relative specific increment in ultrasonic velocity, $[u]$, the relative atomic increment in ultrasonic velocity, $[U]_{\text{at}}$, the relative increment in ultrasonic velocity normalized to the solvent accessible surface area, $[U]_{\text{sas}}$, and the relative increment in ultrasonic velocity normalized to the solvent excluded surface area $[U]_{\text{ses}}$ for NaCl, CaCl₂, -CH₂-, OG in free state and micelle state and Lipolase are shown in Fig. 8.2.

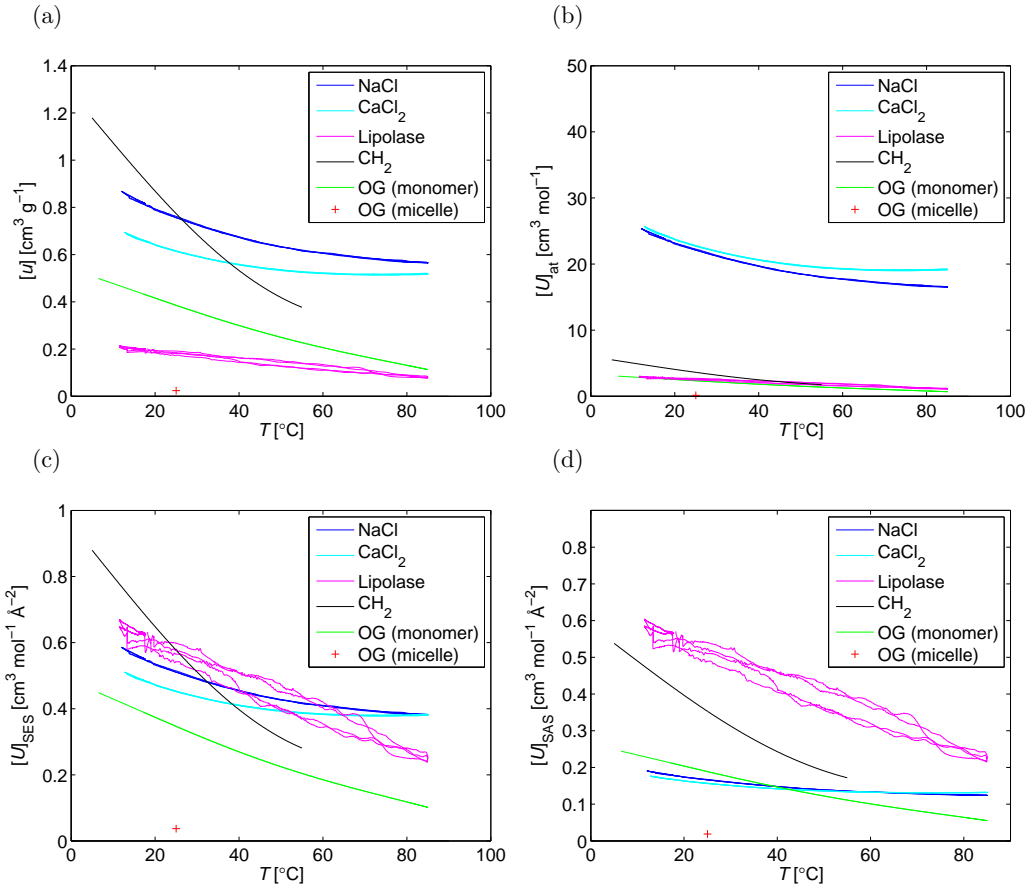


Figure 8.2: Relative molar increment in ultrasonic temperature normalized using the molar mass, M , the number of atoms per solute, N_{at} , the solvent excluded surface area, S_{ses} , and the solvent accessible surface area, S_{sas} , to give the relative specific increment in ultrasonic velocity, $[u]$, the relative atomic increment in ultrasonic velocity, $[U]_{\text{at}}$, relative increment in ultrasonic velocity normalized to the solvent excluded surface area, $[U]_{\text{ses}}$, and the relative increment in ultrasonic velocity normalized to the solvent accessible surface area, $[U]_{\text{sas}}$, respectively, for temperatures, T , between 11 to 85°C.

Fig. 8.2 (a) shows $[u]$ vs. T . In general, the largest changes in $[u]$ are seen for the smallest solutes. Hence the largest changes in $[u]$ are seen for NaCl, CaCl₂ and -CH₂-, whereas the lowest changes in $[u]$ are seen for OG micelles and Lipolase. The larger

changes for the smaller compounds may be related to the increased amount of hydration per mass of these compounds. Note that the magnitude of $[u]$ for $-\text{CH}_2-$ varies more than for NaCl and CaCl_2 . This may be related to the fact that the extent of hydrogen bonding between bulk water molecules diminishes for higher temperatures resulting in an increased hydration entropy of hydrophobic substances [18]. Fig. 8.2 (b) shows $[U]_{\text{at}}$ vs. T . The values of $[U]_{\text{at}}$ for NaCl and CaCl_2 is significantly higher than the values of $[U]_{\text{at}}$ for the other types of considered compounds. Fig. 8.2 (c) shows $[U]_{\text{ses}}$ vs. T . It is seen that normalizing to S_{ses} yields curves qualitatively similar to the curves obtained when normalizing to M . The only real difference between Fig. 8.2(a) and Fig. 8.2(c) is pertaining to the curves for Lipolase. Hence the magnitude of $[u]$ for Lipolase is smaller relative to $[u]$ for the other molecular compounds than the magnitude of $[U]_{\text{ses}}$ for Lipolase relative to $[U]_{\text{ses}}$ for the other molecular compounds. Finally, consider Fig. 8.2 (d) showing $[U]_{\text{sas}}$ as a function of T . The magnitude of the curves pertaining to the smaller molecular compounds decrease relative to the curves of the larger molecular compounds than for the curves normalized to S_{ses} shown in Fig. 8.2(c). Hence the surface area calculated for small molecular compounds is very sensitive to the choice calculational method. In other words, the solvent accessible surface area for the small molecular compounds is much larger than solvent excluded surface area, whereas for large molecular compounds the solvent accessible surface area and the solvent excluded surface area are nearly the same, see Table 8.1.

8.3 Discussion

8.3.1 Normalization of differential ultrasonic velocities

The normalized curves in Fig. 8.2 imply that differential ultrasonic velocities of solutes in aqueous solution do not scale with a single solution parameter. Thus a more elaborate normalization scheme is required to obtain directly compare intrinsic and hydration contributions across the different types of considered model systems.

The first step of developing such an approach is to write the relative molar increment in ultrasonic velocity as

$$[U] = \Gamma_{\text{S}} S_{\text{sxs}} + \Gamma_{\text{M}} V_{\text{M}}, \quad (8.5)$$

where Γ_{S} represent the contribution per surface area, S_{sxs} represent either the solvent excluded surface area or the solvent accessible surface area, Γ_{M} is a coefficient describing the contribution per intrinsic molecular volume and V_{M} represent the intrinsic solute volume, i.e. in this formula V_{M} again represent a real volume and not a molar volume. Unfortunately, preliminary calculations, that not are presented in this thesis, show that it is not straightforward to apply Eq. (8.5) to obtain comparable values of Γ_{S} for proteins and salts. Hence further work on this topic it needed in order to formulate a proper normalization scheme that is readily applicable across different types of model systems. It should be noted that Chalikian *et al.* [15] apparently have performed a calculation on the surface compressibility contribution per surface area from a protein nonpolar surface and a nonbranched chain of $-\text{CH}_2-$ groups in α - ω -aminocarboxylic acid to obtain surface

compressibility contributions that compare reasonably well. Unfortunately no details on the procedure used for these calculations are given in the article not allowing for a reproduction of the calculation.

8.4 Summary

A scheme for normalizing relative molar increments in ultrasonic velocities was presented and applied to the results of the case studies given in Chapters 5, 6 and 7. The outcome of these calculations showed that relative molar increments in ultrasonic velocity are not readily normalized by any single solution parameter. A possible approach for extending the presented normalization scheme was therefore presented. Preliminary calculations on this approach however imply that this approach not sufficient to compare the intrinsic and hydration contributions across different types of model systems.

Chapter 9

Conclusion and outlook

9.1 Conclusion

The objective of this thesis was to examine the capabilities of the ResoScan System as a stand-alone equipment, and especially ultrasonic velocimetry as a stand-alone technique, for characterizing aqueous solutions. In order to pursue this objective, a theoretical framework for interpreting data recorded using ultrasonic velocimetry was introduced in Chapter 2 and the properties of the ResoScan System were investigated in Chapters 3 and 4. The background understanding on ultrasonic velocimetry and the ResoScan System built from these chapters was then used in three case studies in Chapters 5, 6 and 7 that considered three different classes of aqueous solutions containing low-weight molecules, surfactants and proteins, respectively, using a combined theoretical and experimental approach.

The theoretical framework introduced in Chapter 2 was used to treat the results of the three case studies to evaluate the applicability of a number of assumptions simplifying the interpretation of data recorded using ultrasonic velocimetry. Hence it was found that the contributions of dissolved molecules to the differential ultrasonic velocity were additive in the limit of infinite dilution as long as the molecules of the solution do not interact. However, it was also found that the additive assumption could in general not be extended to the individual molecular groups comprising a given molecule. This is due to internal interaction between the molecular groups comprising a given molecule causing contributions from a given molecular group to depend on the chemical properties of the adjacent groups.

Based on the additive assumption ultrasonic velocimetry as a stand-alone method was applicable to investigate a number of molecular phenomena. For aqueous salt solutions it was found that ultrasonic velocimetry potentially can be used to obtain information on ionic hydration. For aqueous surfactant solutions, it was found that ultrasonic velocimetry can be used to detect the critical micelle concentration even though results obtained for sodium dodecyl sulfate was not in agreement with literature values. Furthermore, it was hypothesized that ultrasonic velocimetry can be used to characterize the micelle hydrocarbon core. For aqueous protein solutions it was found that the ultrasonic velocity could be used to detect protein aggregation but that it was hard to distinguish the importance

of intrinsic contributions due to a more compact protein structure from hydration contributions due to altered hydration properties. Moreover, it was shown that ultrasonic velocimetry can not be readily used to characterize the surface of proteins.

The theoretical framework established in Chapter 2 was also used to assess the importance of changes in density and compressibility to the relative molar increment in ultrasonic velocity. Across all considered types of aqueous solutions, it was found that both changes in density and compressibility were important to completely account for the relative molar increment in ultrasonic velocity. However, the decrease in relative molar increment in ultrasonic velocity observed for increasing temperature was for all model systems primarily found to be due to changes in compressibility. From the literature it is known that also changes occurring for the relative molar increment in ultrasonic velocity during protein denaturation and aggregation are primarily due to changes in compressibility. For proteins, it was furthermore found that the magnitude of hydration contribution to the relative molar increment in ultrasonic velocity is much higher than the intrinsic contributions. The decreasing relative molar increment in ultrasonic velocity with increasing temperature is however associated to both changes in the hydration and intrinsic contributions. Unfortunately, it was not possible to conduct a similar analysis for low-weight molecules and micelles.

Finally, the relative molar increment in ultrasonic velocity was normalized with respect to the molar mass, number of atoms per solute, solvent accessible surface area and solvent excluded surface area. The results of the calculations implied that the relative molar increments in ultrasonic velocity can not be normalized to one single parameter. Hence understanding the differential ultrasonic velocity is a complex task requiring knowledge of the contributions from various types of molecular surfaces as well as information on the intrinsic contributions.

Ultrasonic absorption was found to be sensitive to the formation of octyl glucoside micelles as well as for the protein aggregation. However, in general it was found that the ultrasonic absorption is not as sensitive to subtle effects as the ultrasonic velocity.

9.2 Outlook

To further develop the theoretical understanding of ultrasonic velocimetry, it is necessary to develop a theoretical approach that can determine the contributions to increments in ultrasonic velocity per surface area for various types of molecular surfaces appertaining to molecular compounds of varying size and properties. The development of such an approach may also help obtain further information on the concept of hydration that may be highly relevant for the interpretation of ultrasonic velocities as well as help obtain further information on the relative importance of hydration and intrinsic contributions to the differential ultrasonic velocity for various types of model systems. Besides this, the assumption of infinite dilution should be evaluated. Hence the fact that the partial molar volumes for ions added to aqueous solutions is dependent on concentration conflicts with the hypothesis of additive ultrasonic contributions introduced in this thesis.

Appendix A

Derivation of equations

A.1 Governing equations

A.1.1 The Navier–Stokes equation

The dynamical behavior of continuous fluids can be understood through the Navier–Stokes equation. The Navier–Stokes equation is derived in [37] through basic Newtonian mechanics and reprinted here. The starting point of the derivation is the famous Newton’s second law of motion applied on a small volume dV flowing with the ambient flow in a continuous fluid .

$$dM\mathbf{w} = d\mathbf{F}, \quad (\text{A.1})$$

where $dM = \rho dV$ is the mass of the comoving volume, \mathbf{w} is the acceleration of the comoving volume, also denoted the material acceleration, and $d\mathbf{F}$ is the sum of the forces acting on the comoving volume.

The next step of the derivation is then to find the material acceleration \mathbf{w} . The material acceleration can be found by considering the difference in velocity at point \mathbf{r} at time t to the velocity in point $\mathbf{r} + \delta\mathbf{r}$ and time $t + \delta t$

$$\delta\mathbf{v} = \mathbf{v}(\mathbf{r} + \mathbf{v}\delta t, t + \delta t) - \mathbf{v}(\mathbf{r}, t). \quad (\text{A.2})$$

To first order, this velocity difference is given by

$$\delta\mathbf{v} = v_x\delta t \frac{\partial\mathbf{v}(\mathbf{r}, t)}{\partial x} + v_y\delta t \frac{\partial\mathbf{v}(\mathbf{r}, t)}{\partial y} + v_z\delta t \frac{\partial\mathbf{v}(\mathbf{r}, t)}{\partial z} + \delta t \frac{\partial\mathbf{v}(\mathbf{r}, t)}{\partial t} \quad (\text{A.3})$$

$$= \left(\frac{\partial\mathbf{v}}{\partial t} + (\mathbf{v} \cdot \nabla)\mathbf{v} \right) \delta t. \quad (\text{A.4})$$

Dividing by δt and evaluating the expression in the limit where δt approaches zero, the material acceleration is then found

$$\mathbf{w} = \frac{D\mathbf{v}}{Dt} = \left(\frac{\partial\mathbf{v}}{\partial t} + (\mathbf{v} \cdot \nabla)\mathbf{v} \right). \quad (\text{A.5})$$

Inserting the material acceleration in Eq. (A.1) and dividing by dV yields

$$\rho \left(\frac{\partial \mathbf{v}}{\partial t} + (\mathbf{v} \cdot \nabla) \mathbf{v} \right) = \mathbf{f}, \quad (\text{A.6})$$

where \mathbf{f} is the force density of the sum of the forces acting on the small comoving volume. The final step in the derivation of the Navier–Stokes equation is to identify the forces acting on small comoving volume. The Navier–Stokes equation is found in various editions differing by the forces acting on the comoving volume under consideration. The forces could for example arise due to gravity, viscosity and spatial variations in pressure. In the case of a comoving volume affected by these forces, the Navier–Stokes equation is given by

$$\rho \left(\frac{\partial \mathbf{v}}{\partial t} + (\mathbf{v} \cdot \nabla) \mathbf{v} \right) = \mathbf{g} - \nabla p + \eta \nabla^2 \mathbf{v} + \beta \eta \nabla (\nabla \cdot \mathbf{v}), \quad (\text{A.7})$$

where p is the pressure, \mathbf{g} is the gravitational acceleration, η is the dynamic viscosity and β is the ratio between the compressional bulk viscosity and the dynamic viscosity [3]. In this edition of the Navier–Stokes equation, thermal effects are not included.

A.1.2 The equation of continuity

The derivation of the equation of continuity is also given by Lautrup [37] and reprinted here. To derive this equation consider a fixed volume V with mass m . The flux of mass Q_f into this volume is given by

$$Q_f = \int_S \rho \mathbf{v} \cdot d\mathbf{S}, \quad (\text{A.8})$$

where \mathbf{S} is the normal vector of the surface of the volume. To ensure the conservation of mass, the change of the mass of the volume has to equal the flux of mass through the surface of the volume

$$\frac{d}{dt} \int_V \rho dV = - \int_S \rho \mathbf{v} \cdot d\mathbf{S}. \quad (\text{A.9})$$

The surface integral in Eq. (A.9) can be rewritten to a volume integral by applying Gauss' theorem. Hence the equation of continuity is derived

$$\frac{\partial \rho}{\partial t} + \nabla \cdot (\rho \mathbf{v}) = 0. \quad (\text{A.10})$$

A.2 Ultrasonic velocimetry on aqueous solutions

A.2.1 The partial molar volume

The apparent molar volume is given by

$$\phi V = \frac{V - V_0}{CV}. \quad (\text{A.11})$$

This equation can be rewritten to

$$\phi V = \frac{1}{C} - \frac{V_0}{CV} = \frac{\rho_0}{\rho_0 C} - \frac{V_0}{CV}. \quad (\text{A.12})$$

The density of a solution with volume a V containing solutes with a molar mass of M at molar concentration C must be given by

$$\rho = \frac{\rho_0 V_0 + MCV}{V} \quad (\text{A.13})$$

Rewriting this expression yields an expression for the sample volume

$$V = \frac{\rho_0 V_0}{\rho - MC}. \quad (\text{A.14})$$

Inserting Eq. (A.14) in Eq. (A.12) finally yields

$$\phi V = \frac{\rho_0}{\rho_0 C} - \frac{V_0(\rho - MC)}{C\rho_0 V_0} = \quad (\text{A.15})$$

$$\frac{\rho_0}{\rho_0 C} - \frac{\rho V_0}{\rho_0 C V_0} + \frac{MCV_0}{\rho_0 C V_0} = \quad (\text{A.16})$$

$$\frac{M}{\rho_0} - \frac{\rho - \rho_0}{\rho_0 C}. \quad (\text{A.17})$$

Since the sample is considered in the limit of infinite solute dilution, the apparent molar volume and the partial molar volume are the same so

$$V^\circ = \frac{M}{\rho_0} - \frac{\rho - \rho_0}{\rho_0 C}. \quad (\text{A.18})$$

A.2.2 The ultrasonic velocity in aqueous solutions

The first step of this derivation is to differentiate the Newton–Laplace equation. The first step of this differentiation is to rewrite the Newton–Laplace equation to define a function k given by

$$\beta_S U^2 \rho = k = 1. \quad (\text{A.19})$$

It is possible to find a small change for k , denoted δk , given small changes $\delta\beta_S$, δU and $\delta\rho$. Hence

$$\delta k = \frac{\partial k}{\partial \beta_S} \delta \beta_S + \frac{\partial k}{\partial U} \delta U + \frac{\partial k}{\partial \rho} \delta \rho, \quad (\text{A.20})$$

Finding the derivatives in Eq. (A.20), and using Eq. (A.19), δk can then be written as

$$\delta k = \frac{\delta \beta_S}{\beta_S} k + 2 \frac{\delta U}{U} k + \frac{\delta \rho}{\rho} k. \quad (\text{A.21})$$

Since k is a constant it must be true that $\delta k = 0$. Finally the following equation then emerges

$$0 = \frac{\delta \beta_S}{\beta_S} + 2 \frac{\delta U}{U} + \frac{\delta \rho}{\rho}. \quad (\text{A.22})$$

This expression can be used to determine the difference in ultrasonic velocity between a sample containing infinitely diluted solute and a reference sample

$$\frac{\Delta U}{U_0} = -\frac{\Delta \beta_S}{2\beta_{S0}} - \frac{\Delta \rho}{2\rho_0}. \quad (\text{A.23})$$

This equation can now be rewritten by dividing all terms by C

$$\frac{\Delta U}{U_0 C} = -\frac{\Delta \beta_S}{2\beta_{S0} C} - \frac{\Delta \rho}{2\rho_0 C}. \quad (\text{A.24})$$

This equation can in turn be rewritten by straightforward algebra

$$\frac{\Delta U}{U_0 C} = -\frac{\Delta \beta_S}{2\beta_{S0} C} - \frac{\Delta \rho}{2\rho_0 C} = \quad (\text{A.25})$$

$$-\frac{\beta_S - \beta_{S0}}{2\beta_{S0} C} - \frac{\rho - \rho_0}{2\rho_0 C} = \quad (\text{A.26})$$

$$-\frac{\beta_S V}{2\beta_{S0} C V} + \frac{\beta_{S0} V_0 - \beta_{S0}(V_0 - V)}{2C V \beta_{S0}} - \frac{\rho - \rho_0}{2\rho_0 C} = \quad (\text{A.27})$$

$$-\frac{K_S}{2\beta_{S0} C V} + \frac{K_{S0}}{2\beta_{S0} C V} + \frac{V}{2C V} - \frac{V_0}{2C V} - \frac{\rho - \rho_0}{2\rho_0 C}. \quad (\text{A.28})$$

Inserting definition for the apparent molar volume given in Eq. (A.11) and the definition for the apparent molar adiabatic compressibility given by

$$\phi K_S = \frac{K_S - K_{S0}}{C V}, \quad (\text{A.29})$$

in Eq. (A.28) yields

$$\frac{\Delta U}{U_0 C} = -\frac{\phi K_S}{2\beta_{S0}} + \frac{\phi V}{2} - \frac{\rho - \rho_0}{2\rho_0 C}. \quad (\text{A.30})$$

Inserting Eq. (A.18) then yields

$$\frac{\Delta U}{U_0 C} = -\frac{\phi K_S}{2\beta_{S0}} + \frac{\phi V}{2} + \frac{\phi V}{2} - \frac{M}{2\rho_0} \leftrightarrow \quad (\text{A.31})$$

$$\frac{\Delta U}{U_0} = \left(-\frac{\phi K_S}{2\beta_{S0}} + \phi V - \frac{M}{2\rho_0} \right) C. \quad (\text{A.32})$$

Since the solute is in infinite dilution, the apparent molar quantities in Eq. (A.32) can be replaced by partial molar quantities to finally yield

$$\frac{\Delta U}{U_0} = \left(-\frac{K_S^\circ}{2\beta_{S0}} + V^\circ - \frac{M}{2\rho_0} \right) C. \quad (\text{A.33})$$

A.2.3 Multicomponent Systems

The equation for the ultrasonic velocity in multicomponent systems is derived from the basic assumption of infinite dilution so that the contributions from the individual components of the system are additive

$$\frac{\Delta U}{U_0} = \sum_i \frac{\Delta U_i}{U_0}, \quad (\text{A.34})$$

where ΔU_i is the contribution to the ultrasonic velocity from the i th component of the system. Inserting Eq. (A.33) then yields

$$\frac{\Delta U}{U_0} = \sum_i \left(-\frac{K_{S_i}^\circ}{2\beta_{S0}} + V_i^\circ - \frac{M_i}{2\rho_0} \right) C_i. \quad (\text{A.35})$$

Appendix B

Calibration of the ResoScan System

B.1 300 mK per min scan rate

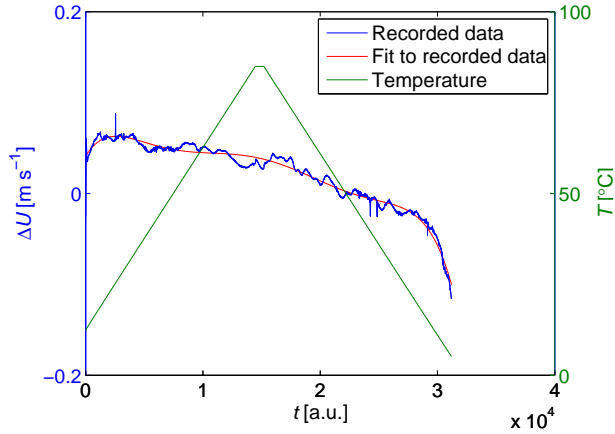


Figure B.1: The temporal course of events for the differential ultrasonic velocity, ΔU , recorded with Milli-Q in both resonator cavities varying temperature, T , for a scan rate of 300 mK min^{-1} . The data is fitted to a single polynomial of degree 6. The time units given by the ResoScan System is in arbitrary units.

The temporal course of events for the differential ultrasonic velocities recorded with Milli-Q water in both resonator cavities for the script utilizing the scan rate of 300 mK min^{-1} is fitted to a single polynomial of degree 6 assuming that the correct difference between the two resonator cavities is $1.7 \times 10^{-2} \text{ m s}^{-1}$, see Fig. B.1. This polynomial is given by $\Delta U_{\text{pol}} = \sum_{i=0}^6 \Delta U_i T^i$ where $\Delta U_0 = 0.0242 \text{ m s}^{-1}$, $\Delta U_1 = 2.0845 \times 10^{-5} \text{ m s}^{-1} \text{ a.u.}^{-1}$, $\Delta U_2 = -6.6964 \times 10^{-9} \text{ m s}^{-1} \text{ a.u.}^{-2}$, $\Delta U_3 = 8.5469 \times 10^{-13} \text{ m s}^{-1} \text{ a.u.}^{-3}$, $\Delta U_4 = -5.2561 \times 10^{-17} \text{ m s}^{-1} \text{ a.u.}^{-4}$, $\Delta U_5 = 1.5275 \times 10^{-21} \text{ m s}^{-1} \text{ a.u.}^{-5}$ and $\Delta U_6 =$

$-1.6898 \times 10^{-26} \text{ m s}^{-1} \text{ a.u.}^{-6}$. Corrected differential ultrasonic velocities, ΔU_{cor} , for temperature scans conducted using the ResoScan System are then obtained using

$$\Delta U_{\text{cor}} = \Delta U - \Delta U_{\text{pol}}, \quad (\text{B.1})$$

where ΔU represent the actual measured differential ultrasonic velocities and ΔU_{pol} are the values of the fitted polynomial. The temporal duration of the conducted temperature scans may vary slightly from experiment to experiment. In these cases the polynomials are stretched or compressed to be applicable to correcting data from all experiments.

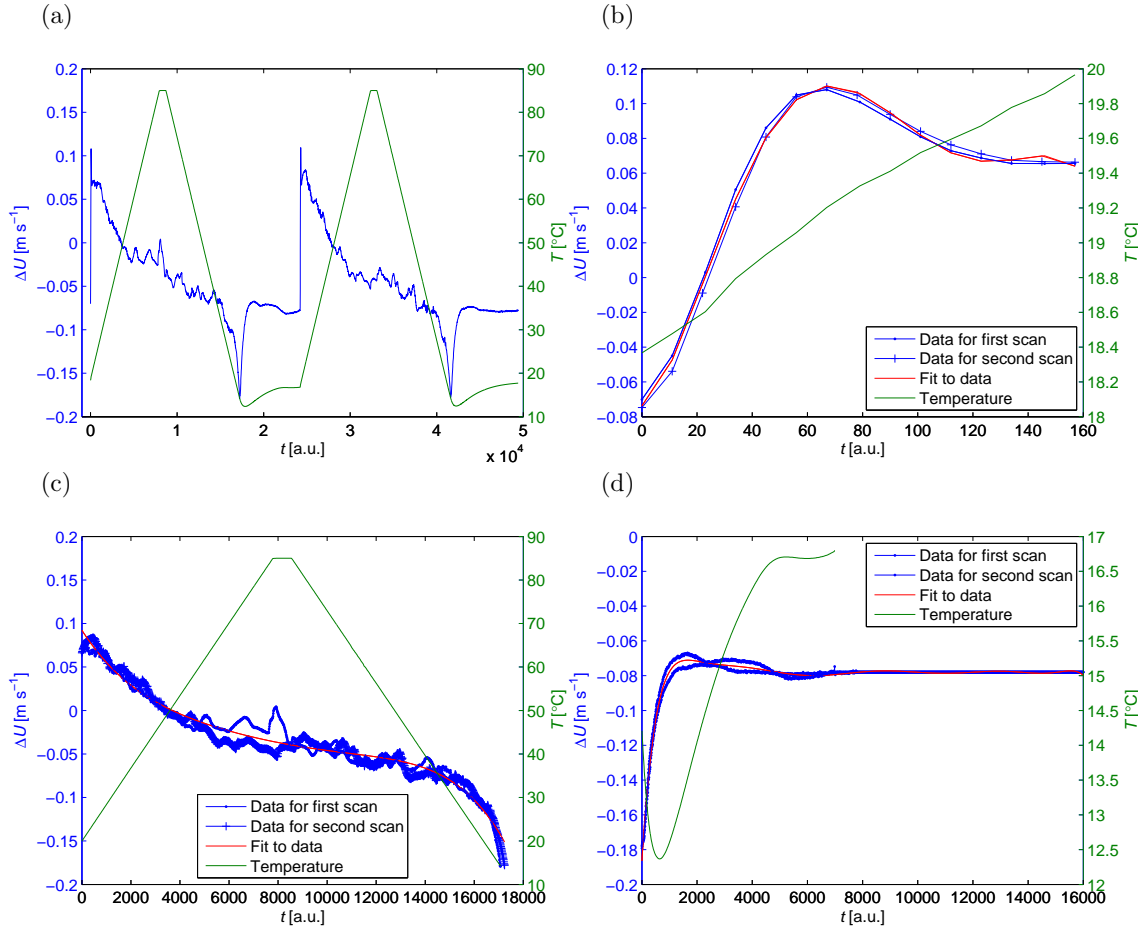


Figure B.2: Overview of the correction procedure of the differential ultrasonic velocities recorded with a temperature scan rate of 500 mK min^{-1} . (a) Overview of temperature scan with Milli-Q water in both resonator cavities. The course of events of the change in ultrasonic velocity shown in this figure can be split into three separate time periods, and a polynomial can be used to fit each of the periods. (b) Fit to the first periods of the curve by a polynomial of degree 5. (c) Fit to the second periods of the curve by a polynomial of degree 5. (d) Fit to the third periods of the curve by a polynomial of degree 10.

B.2 500 mK per min scan rate

In the case of the temperature scan utilizing the scan rate of 500 mK min⁻¹, three distinct polynomials are fitted to the temporal course of events of three distinct identified periods of these temperature scans assuming that the correct difference between the two resonator cavities is -1.5×10^{-2} m s⁻¹, see Fig. B.2.

The first temporal period is fitted to a polynomial of degree 5 given by $\Delta U_{\text{pol}} = \sum_{i=0}^5 \Delta U_i T^i$ where $\Delta U_0 = -0.0587$ m s⁻¹, $\Delta U_1 = 9.4752 \times 10^{-4}$ m s⁻¹ a.u.⁻¹, $\Delta U_2 = 1.6622 \times 10^{-4}$ m s⁻¹ a.u.⁻², $\Delta U_3 = -3.4372 \times 10^{-6}$ m s⁻¹ a.u.⁻³, $\Delta U_4 = 2.4051 \times 10^{-8}$ m s⁻¹ a.u.⁻⁴ and $\Delta U_5 = -5.6816 \times 10^{-11}$ m s⁻¹ a.u.⁻⁵. The second temporal period is also fitted to a polynomial of degree 5 given by $\Delta U_{\text{pol}} = \sum_{i=0}^5 \Delta U_i T^i$ where $\Delta U_0 = 0.1073$ m s⁻¹, $\Delta U_1 = -4.3823 \times 10^{-5}$ m s⁻¹ a.u.⁻¹, $\Delta U_2 = 7.6026 \times 10^{-9}$ m s⁻¹ a.u.⁻², $\Delta U_3 = -8.5322 \times 10^{-13}$ m s⁻¹ a.u.⁻³, $\Delta U_4 = 5.2536 \times 10^{-17}$ m s⁻¹ a.u.⁻⁴ and $\Delta U_5 = -1.3242 \times 10^{-21}$ m s⁻¹ a.u.⁻⁵. The third temporal period is fitted to a polynomial of degree 10 given by $\Delta U_{\text{pol}} = \sum_{i=0}^{10} \Delta U_i T^i$ where $\Delta U_0 = -0.1715$ m s⁻¹, $\Delta U_1 = 2.4912 \times 10^{-4}$ m s⁻¹ a.u.⁻¹, $\Delta U_2 = -2.2035 \times 10^{-7}$ m s⁻¹ a.u.⁻², $\Delta U_3 = 1.0562 \times 10^{-10}$ m s⁻¹ a.u.⁻³, $\Delta U_4 = -3.0696 \times 10^{-14}$ m s⁻¹ a.u.⁻⁴, $\Delta U_5 = 5.6748 \times 10^{-18}$ m s⁻¹ a.u.⁻⁵, $\Delta U_6 = -6.7990 \times 10^{-22}$ m s⁻¹ a.u.⁻⁶, $\Delta U_7 = 5.2506 \times 10^{-26}$ m s⁻¹ a.u.⁻⁷, $\Delta U_8 = -2.5193 \times 10^{-30}$ m s⁻¹ a.u.⁻⁸, $\Delta U_9 = 6.8265 \times 10^{-35}$ m s⁻¹ a.u.⁻⁹ and $\Delta U_{10} = -7.9781 \times 10^{-40}$ m s⁻¹ a.u.⁻¹⁰. Corrected differential ultrasonic velocities are then again obtained using the approach from Eq. (B.1).

Bibliography

- [1] *State of Hydration Shells of Sodium Chloride in Aqueous Solutions in a Wide Concentration Range at 273.15-373.15 K*,
M. L. Antonelli, M. G. Bonicelli, G. Ceccaroni, C. La Mesa, and B. Sesta,
Colloid Polym Sci **272**, 704-711 (1994).
- [2] *Solution properties of octyl- β -D-glucoside. Part 2: Thermodynamics of micelle formation*,
Vladimir N. Afanasiev, Alexandr N. Ustinov, and Irina Yu. Vashurina,
J. Phys. Chem. B **113**, 212-223 (2009).
- [3] *Acoustofluidics in microsystems: investigation of resonances*,
Rune Barnkob,
Master thesis, Technical University of Denmark,
www.nanotech.dtu.dk/microfluidics,
June 2009.
- [4] *Measuring the local pressure amplitude in microchannels acoustophoresis*,
Rune Barnkob, Per Augustsson, Thomas Laurell, and Henrik Bruus,
Lab Chip, **10** (5), 563-570 (2010).
- [5] *Speed of sound in pure water at temperatures between 274 and 394 K and at pressures up to 90 MPa*,
G. Benedetto, R. M. Gavioso, P. A. Giuliano Albo, S. Lago, D. M. Ripa, and R. Spagnolo,
J. Phys. Chem. Ref. Data. **26**, 6, 1667-1680 (2005).
- [6] Jeremy M. Berg, John L. Tymoczko, and Lubert Stryer, *Biochemistry*, W. H. Freeman and Company (New York 2006).
- [7] *The density and compressibility at ultrasound frequencies of suspended particles*,
Henrik Bruus, Technical University of Denmark
Unpublished, (2009).
- [8] *Ultrasonic spectroscopy study relaxation and scattering in whey protein solutions*,
Cory M. Bryant, and D. Julian McClements,
Journal of the Science of Food and Agriculture **79**, 1754-1760 (1999).

- [9] *Hydration of nucleic dilute aqueous solutions: Apparent molar adiabatic and isothermal compressibilities, apparent molar volumes and their temperature slopes at 25 °C*, V. A. Buckin, *Biophysical Chemistry* **29**, 283-292 (1988).
- [10] *Frustrerede molekyler i centrum af vaskeprocessen*, Thomas Callisen, and Ture Damhus, *Dansk Kemi* **87**, 1, 17-20 (2006).
- [11] *Enzymer til vaskemidler - fra bugspytkirtler til gensplejsede mikroorganismer*, Thomas Callisen, Ture Damhus, Vibeke Skovgaard Nielsen, and Peter Skagerlind, *Dansk Kemi* **87**, 3, 25-28 (2006).
- [12] *Solutions properties of alkyl glucosides, alkyl thioglucosides and alkyl maltosides*, Antonio Capalbi, Giacomo Gente, and Camillo La Mesa, *Colloids and Surfaces A: Physicochem. Eng. Aspects* **246**, 99-108 (2004).
- [13] *Cosolvent Effects on the Micellization of Oxyphenyl(copoly)ethylene Oxide Copolymers in Aqueous Solution*, Emilio Catro, Pablo Taboada, and Víctor Mosquera, *J. Phys. Chem. B* **110**, 13113-13123 (2006).
- [14] *Partial Molar Volumes, Expansibilities, and Compressibilities of α,ω -Aminocarboxylic Acids in Aqueous Solutions between 18 and 55 °C*, Tigran V. Chalikian, Armen P. Sarvazyan, and Kenneth Breslauer, *J. Phys. Chem.* **97**, 13017-13026 (1993).
- [15] *The Hydration of Globular Proteins as Derived from Volume and Compressibility Measurements: Cross Correlating Thermodynamic and Structural Data*, Tigran V. Chalikian, Maxim Totrov, Ruben Abagyan, and Kenneth J. Breslauer, *J. Mol. Biol.* **260**, 588-603 (1996).
- [16] *Volumetric Properties of Proteins*, T. V. Chalikian, *Annu. Rev. Biophys. Struct.* **32**, 207-235 (2003).
- [17] *On the Molecular Origins of Volumetric Data*, Tigran V. Chalikian, *J. Phys. Chem. B* **112**, 911-917 (2008).
- [18] *Interfaces and the driving force of hydrophobic assembly*, David Chandler, *Nature* **437**, 640-647 (2005).
- [19] *Physical Stability of Proteins in Aqueous Solution: Mechanism and Driving Forces in Nonnative Protein Aggregation*,

- Eva. Y. Chi, Sampathkumar Krishnan, Theodore W. Randolph, and John F. Carpenter,
Pharmaceutical Research **20**, 9, 1325-1336 (2003).
- [20] *Ions in water: Characterizing the forces that control chemical processes and biological structure*,
Kim D. Collins, George W. Neilson, and John E. Enderby,
Biophysical Chemistry **128**, 95-104 (2007).
- [21] *Heat-Induced Changes in the Ultrasonic Properties of Whey Proteins*,
Milena Corredig, Edita Verespej, and Douglas G. Dalgleish,
J. Agric. Food Chem. **52**, 4465-4471 (2004).
- [22] *NanoElectro Mechanical Systems (NEMS)*,
Zachary Davis,
Course notes for 33321 Nano-2: Nanosystems Engineering, Technical University of Denmark
Unpublished, (2009).
- [23] *Estimation of Critical Micellar Concentration Through Ultrasonic Velocity Measurements*,
S. Durackova, M. Apostolo, S. Canegallo, and M. Morbidelli,
Journal of Applied Polymer Science **57**, 639-644 (1995).
- [24] *Unfolding and Refolding of Bovine Serum Albumin at Acid pH: Ultraosund and Structural Studies*,
N. El Kadi, N. Taulier, J. Y. Huer  rou, M. Gindre, W. Urbach, I. Nwigwe, P. C. Kahn, and M. Waks,
Biophysical Journal **91**, 3397-3404 (2006).
- [25] Alexander T. Florence, and David Attwood, *Physiochemical Principles of Pharmacy*,
PhP (London 2006).
- [26] *Stereochemical aspects of micellar properties of esterified glucoside surfactants in water: apparent molar volume, adiabatic compressibility, and aggregation number*,
K. Fukada, M. Kawasaki, T. Seimiya, Y. Abe, M. Fujiwara, and K. Ohbu,
Colloid Polym. Sci. **278**, 576-580 (2000).
- [27] *Density and Sound Velocity Studies of Aqueous Solutions of Tetracyltrimethylammonium*,
J. J. Gal  n, J. L. Del Castillo, A. Gonz  lez-P  rez, J. Czapkiewicz, and J. R. Rodr  guez,
Journal of Solutions Chemistry **32**, 10, 919-927 (2003).
- [28] *Determination of Electrolyte Apparent Molal Compressibilities at Infinite Dilution Using a High-Precision Ultraosnic Velocimeter*,
R. Garnsey, and R. J. Boe,
The Journal of Chemical Physics **50**, 12, 5222-5228 (1969).

- [29] *Compressibility gives new insight into protein dynamics and enzyme function*,
Kunihiko Gekko,
Biochimica et Biophysica Acta **1595**, 382-386 (2002).
- [30] *Hydration Changes Accompanying Nucleic Acid Intercalation Reactions: Volumetric Characterizations*,
Feixue Han, and Tigran V. Chalikian*,
J. Am. Chem. Soc. **125**, 7219-7229 (2003).
- [31] Richard A. Johnson, *Miller & Freund's Probability and Statistics for Engineers*, Pearson Prentice Hall (New Jersey 2005).
- [32] *Influence of Temperature on the Micellization of Sodium Sodecylsulfate in Water from Speed of Sound Measurements*,
E. Junquera, L. Pena, and E. Aicart,
Journal of Solution Chemistry **23**, 3, 421-430 (1994).
- [33] *Apparent molal volumes and apparent molal compressibilities of some carbohydrates in dilute aqueous solutions at different temperatures*,
M. V. Kaulgud, and S. S. Dhondge,
Indian Journal of Chemistry Section A - Inorganic Bio-Inorganic Physical Theoretical & Analytical Chemistry **72**, 1, 6-11 (1988).
- [34] *Aqueous Solutions of Sodium Methylsulfate by Raman Scattering, NMR, Ultrasound and Density Measurements*,
Shinobu Koda, and Hiroyasu Nomura,
Journal of Solution Chemistry **14**, 355-366 (1985).
- [35] *The Molecular dynamics characterization of n-octyl- β -D-glucopyranoside micelle structure in aqueous solutions*,
Praveen Konidala, Lizhong He, and Bernd Niemeyer,
Journal of Molecular Graphics and Modelling **25**, 77-86 (2006).
- [36] *The Compressibility of Alkylmethylammonium Bromide Micelles*,
Evgeny Kudryashov, Tatiana Kapustina, Siobhan Morrissey, Vitaly Buckin, and Kenneth Dawson,
Journal of Colloid and Interface Science **203**, 59-68 (1998).
- [37] Benny Lautrup, *Physics of Continuous Matter*, IoP (Bristol 2005).
- [38] *Solution properties of octyl β -D glucoside. Part 1: Aggregate size, shape and hydration*,
C. La Mesa, A. Bonincontro, and B. Sesta,
Colloid & Polymer Science **271**, 1165-1171 (1993).
- [39] V. M. M. Lobo, and J. L. Quaresma, *Handbook of electrolyte solution - Part A*, Elsevier (New York 1989).

- [40] V. M. M. Lobo, and J. L. Quaresma, *Handbook of electrolyte solution - Part B*, Elsevier (New York 1989).
- [41] *Protein aggregation: Pathways, Induction Factors and Analysis*, Hanns-Christian Mahler, Wolfgang Friess, Ulla Grauschopf, and Sylvia Kiese, *Journal of Pharmaceutical Sciences* **98**, 9, 2909-2934 (2009).
- [42] *Effects of Ions on the Structure of Water: Structure Making and Breaking*, Yizhak Marcus, *Chem. Rev.* **109**, 1346-1370 (2009).
- [43] *Partial Molal Compressibilities of Salts in Aqueous Solution and Assignment of Ionic Contributions*, J. G. Mathieson, and B. E. Conway, *Journal of Solution Chemistry* **3**, 6, 455-477 (1974).
- [44] *Apparent Molal Volumes and Adiabatic Compressibilities of n-Alkanols and α,ω -Alkane Diols in Dilute Aqueous Solutions at 5, 25, and 45 °C. II. Apparent Molal Adiabatic Compressibilities*, Toshio Nakajima, Tsuyoshi Komatsu, and Tsurutaro Nakagawa, *Bulletin of the Chemical Society of Japan* **48**, 3, 788-790 (1975).
- [45] *Densities of Binary Aqueous Solutions of 306 Inorganic Substances*, P. Novotný, and O. Söhnel, *J. Chem. Eng. Data* **33**, 49-55 (1988).
- [46] *Real-Time Monitoring of Heat-Induced Aggregation of β -Lactoglobulin in Aqueous Solutions Using High-Resolution Ultrasonic Spectroscopy*, Agnieszka Ochendusko, and Vitaly Buckin, *Int. J. Thermophys.* **31**, 113-130 (2010).
- [47] *Ionic hydration in sodium chloride solutions*, G. Onori, *J. Chem. Phys.* **89**, 1, 510-516 (1988).
- [48] *Volumetric properties of aqueous alkali halides and ionic hydration*, G. Onori, A. Santucci, and F. Marchesoni, *Journal of Molecular Liquids* **89**, 1, 209-223 (1991).
- [49] Geoff Rayner-Canham and Tina Overton, *Descriptive Inorganic Chemistry*, W. H. Freeman and Company (New York 2002).
- [50] *Reduced surface: An efficient way to compute molecular surfaces*, Michel F. Sanner, Arthur J. Olson, and Jean-Claude Spehner, *Biopolymers* **38**, 3, 305-320 (1996).
- [51] *Relaxational Contributions to Protein Compressibility from Ultrasonic Data*, A. P. Sarvazyan, *Biopolymers* **18**, 3015-3024 (1979).

- [52] *Ultrasonic Investigation of the pH-Dependent Solute-Solvent Interactions in Aqueous Solutions of Amino Acids*,
A. P. Sarvazyan, D. P. Kharakoz, and Paul Hemmes,
The Journal of Physical Chemistry **83**, 13, 1796-1799 (1979).
- [53] *Ultrasonic velocimetry of biological compounds*,
A. P. Sarvazyan,
Annu. Rev. Biophys. Chem. **20**, 312-342 (1991).
- [54] *The Volume and Compressibility Changes of Lysozyme Associated with Guanidinium Chloride and Pressure-assisted Unfolding*,
K. Sasahara, M. Sakurai, and K. Nitta,
J. Mol. Biol. **291**, 693-701 (1999).
- [55] *Role of calcium as a trigger in the thermal β -lactoglobulin aggregation*,
Jan-Willem F. A. Simons, Hans A. Koster, Ronald W. Visschers, and Harmen H. J. de Jongh,
Archives of Biochemistry and Biophysics **406**, 143-152 (2002).
- [56] *Acoustic forces on particles and liquids in microfluidic systems* ,
Peder Skaft-Pedersen,
Master thesis, Technical University of Denmark,
www.nanotech.dtu.dk/microfluidics,
January 2008.
- [57] *Thermodynamic Properties Underlying the α -Helix-to- β -Sheet Transition, Aggregation and Amyloidogenesis of Polylysine as Probed by Calorimetry, Densimetry, and Ultrasound Velocimetry*,
Vytautas Smirnovas, Roland Winter, Theodor Funck, and Wojciech Dzwolak,
The Journal of Physical Chemistry Letters B **109**, 19043-19045 (2005).
- [58] *Protein Amyloidogenesis in the Context of Volume Fluctuations: A Case Study on Insulin*,
Vytautas Smirnovas, Roland Winter, Theodor Funck, and Wojciech Dzwolak,
ChemPhysChem **7**, 1046-1049 (2006).
- [59] *Revealing Different Aggregation Pathways of Amyloidogenic Proteins by Ultrasound Velocimetry*,
Vytautas Smirnovas, and Roland Winter,
Biophysical Journal **94**, 3241-3246 (2008).
- [60] *Characterization of pH-induced Transitions of β -lactoglobulin: Ultrasonic, Densimetric, and Spectroscopic Studies*,
Nicolas Taulier, and Tigran V. Chalikian,
J. Mol. Biol. **314**, 873-889 (2001).

- [61] *Compressibility of protein transitions*,
Nicolas Taulier, and Tigran V. Chalikian,
Biochimica et Biophysica Acta **1595**, 48-70 (2002).
- [62] *Compressibility Changes Accompanying Conformational Transitions of Apomyoglobin*,
Nicolas Taulier, Irina V. Beletskaya, and Tigran V. Chalikian,
Biopolymers **79**, 218-229 (2005).
- [63] *Hydrophobic Hydration in Cyclodextrin Complexation*,
Nicolas Taulier, and Tigran V. Chalikian,
The Journal of Physical Chemistry Letters B **110**, 12222-12224 (2006).
- [64] *γ -Cyclodextrin Forms a Highly Compressible Complex with 1-Adamantanecarboxylic Acid*,
Nicolas Taulier, and Tigran V. Chalikian,
The Journal of Physical Chemistry Letters B **112**, 9546-9549 (2008).
- [65] John R. Taylor, *An introduction to error analysis*, University Science Books (Sausalito, California 1997).
- [66] *Introduction to the Ultrasonic Resonator Technology of the ResoScan[®] System*,
TF Instruments
- [67] *ResoScanTM-Research System Operations Manual*,
TF Instruments
- [68] *Determination of sound absorption in ultrasonic resonators*,
TF Instruments
- [69] *Quantification of Enzyme Activity by URT*,
TF Instruments
- [70] *Ultrasonic Velocity and Compressibility in Aqueous Solutions of Alkali Metal Chlorides*,
Hisashi Uedaira, and Yasuko Suzuki,
Bulletin of the Chemical Society of Japan **52**, 10, 2787-2790 (1979).
- [71] *The IAPWS Formulation 1995 for the Thermodynamic Properties of Ordinary Water Substance for General and Scientific Uses*,
W. Wagner, and A. Pruss,
J. Phys. Chem. Ref. Data. **31**, 2, 387-535 (2002).
- [72] *Quantitative Assessment of Thermal Denaturation of Bovine α -lactalbumin via Low-Intensity Ultrasound, HPLC, and DSC*,
Qin Wang, Alexander Tolkach, and Ulrich Kulozik,
J. Agric. Food Chem. **54**, 6501-6506 (2006).
- [73] Avogadro molecular editor
http://avogadro.openmolecules.net/wiki/Main_Page, 3/7-2010.

- [74] Inkscape
www.inkscape.org, 10/6-2010.
- [75] Michel Sanner's MSMS program online calculator from Helix Systems, Scientific Supercomputing at the NIH,
<http://molbio.info.nih.gov/structbio/basic.html>, 1/6-2010.
- [76] Homepage of TF Instruments,
www.tf-instruments.com, 17/6-2010.
- [77] Homepage of Martin Chaplin on water structure and science,
<http://www1.lsbu.ac.uk/water/>, 18/6-2010.
- [78] Structural data for *Thermomyces (Humicola) lanuginosa* lipase with pdb ID: 1DT3
www.pdb.org, 1/6-2010.